ABSTRACT

**GUGLIOTTI, LINA ANN.** RNA-Mediated Synthesis of Particles from Organometallic Palladium and Platinum Precursors. (Under the direction of Professor Bruce E. Eaton).

RNA sequences have been discovered that mediate the growth of hexagonal, cubic and spherical palladium and platinum containing particles. *In vitro* selection techniques were used to evolve an initial library of ~ $3 \times 10^{13}$ unique RNA sequences through six to ten cycles of selection to yield several active sequence families. The particle growth occurred in aqueous solution at ambient temperature, without any endogenous reducing agent, and at low concentrations of metal precursor (10 μM – 400 μM). Relative to the metal precursor the RNA concentration was significantly lower (1 μM).

RNA sequences that utilize the organometallic complex tris(dibenzylideneacetone) dipalladium(0) ($[Pd_2(DBA)_3]$) to form palladium containing particles were further characterized for their ability to control particle growth. These RNA sequences (Pdases) were found to form hexagonal and cubic palladium containing particles with a high degree of shape specificity. Replacing the pyridyl-modified RNA sequence with native RNA resulted in a complete loss of RNA function. Removing the 3′-fixed sequence region from the Pdase had little effect on particle growth; however, further truncations into the variable region resulted in a significant loss of activity and particle shape control. Changing the metal center and ligand of the group VIII organometallic precursor complex revealed a strong dependence of particle growth and shape on the DBA ligands.

The Pdases were covalently immobilized on gold surfaces and evaluated for their activity toward particle synthesis. When coupled to gold via oligoethylene glycol linkers, both RNA isolates 17 and 34 were able to mediate the formation of Pd containing particles with the same shape control previously observed in solution. Finally, the use of surface-bound RNA as a tool for directing the orthogonal synthesis of materials on surfaces was demonstrated. Patterning the RNA sequence for hexagons next to the sequence for cubes, followed by incubation in a solution containing $[Pd_2(DBA)_3]$, resulted in the spontaneous formation of spatially distinct spots of Pd containing hexagonal and cubic particles.

**RNA-Mediated Synthesis of Particles from Organometallic Palladium and Platinum Precursors**

by
**Lina Ann Gugliotti**

A dissertation submitted to the Graduate Faculty of
North Carolina State University
In partial fulfillment of the
Requirements for the Degree of
Doctor of Philosophy

**CHEMISTRY**

Raleigh

2006

**APPROVED BY:**

Chair of the Advisory Committee

## DEDICATION

I would like to dedicate this work to my grandmother, Brigida Gugliotti, my late grandmother Maria Carolina Bruno, my late grandfathers, Giambattista Gugliotti and Giuseppe Bruno, and my parents Elio Gugliotti and Grace Gugliotti. Some of the invaluable lessons in life they have taught me were the values of patience and perseverance.

## BIOGRAPHY

Lina A. Gugliotti was born in Waterbury, Connecticut on November 27, 1978 to Elio and Grace Gugliotti. After graduating high school in Watertown, Connecticut she went on to attend Roger Williams University in Bristol, Rhode Island, where she earned a Bachelors of Science in Marine Biology and a Bachelors of Art in Chemistry. In August of 2000, she continued her desire to broaden her education as a Ph. D. student in bioinorganic chemistry under the direction of Dr. Bruce Eaton at North Carolina State University. She has received an Intramural Research Training Postdoctoral Fellowship to continue her studies under the direction of Dr. Robert Crouch at the National Institute of Child Health and Human Development, National Institutes of Health, in Bethesda, Maryland.

## ACKNOWLEDGEMENTS

I would like to start off by thanking my advisor, Dr. Bruce E. Eaton, and my research collaborator, Dr. Daniel L. Feldheim, for their guidance, support and belief in my ability as a chemist throughout my graduate career. They provided me with the knowledge and skills to succeed as a scientist in today's competitive research environment. I would also like to thank my committee members Dr. Kenneth W. Hanck and Dr. Tatyana I. Smirnova for their additional support. In addition, former and current members of both the Eaton and Feldheim research groups are appreciated for all of their assistance.

Likewise, my friends have all been encouraging and patient, and there are several that deserve the added "thank you" for all of their guidance. To Lucas Marks, Christina Marks, Kelly Gillis, Nicole CoWallis, and Steven Hira: we became friends our freshman year at Roger Williams University and have since been there for each other no matter what the circumstances were. The last ten years you have all supported me in your own unique way and I truly appreciate having you in my life. An extra special "thanks" to Lucas Marks. He has been a constant shoulder for me to lean on, no matter what time or day, he was always there for me. We have experienced every aspect of graduate school together: from the stresses of classes, cumulative exams, prelims and research deadlines, to the excitement of accomplishing these tasks. Thanks for being you! To my best-friend, Melissa Knorr, who has been there from high school, to college and graduate school, you are an angel. Thank you for always being there. To Caleb Clark, Dana

DiDonato, Doug Young, Sofi Bin-Salamon, Magda Dolska and Carly Carter, thank you for all of your support and helpful discussions. I am delighted to have had the opportunity to get to know you and work with you. You have made the last six years fun and always exciting!

Finally, I would like to express my gratitude to my family. My parents (Elio and Grace), my sisters (Gina, Tina and Brigitt), my brothers (John and Elio Jr.) and brothers-in-law (George and Joe) have been a constant support throughout my life. Being the "baby girl" in the family they have always been looking out for me, providing me with advice, listening when I have a bad day and supporting me in what ever goals I wanted to achieve. To my beautiful nieces (Sierra, Charlotte, Samantha and Abigail) and god-daughter (Allison): you girls are exceptional and will forever be my little princesses. Without my family's smiles, kind voices and encouragement I would not be where I am today. You have all inspired me to achieve greatness. With all of my heart and love, I thank you!

## TABLE OF CONTENTS

## LIST OF TABLES

## LIST OF FIGURES

## LIST OF SCHEMES

Page

## LIST OF ABBREVIATIONS, SYMBOLS AND TERMS

| Abbreviation, Symbol or Term | Explanation |
|---|---|
| AFM | atomic force microscopy |
| Amp | ampicillin |
| AMV | avian myeloblastosis virus |
| ATP | adenosine 5′-triphosphate |
| bp | base pair |
| cDNA | complementary deoxyribonucleic acid |
| CTP | cytidine 5′-triphosphate |
| dATP | deoxyadenosine 5′-triphosphate |
| dCTP | deoxycytidine 5′-triphosphate |
| ddATP | dideoxyadenosine 5′-triphosphate |
| DBA | dibenzylideneacetone |
| ddCTP | dideoxycytidine 5′-triphosphate |
| ddGTP | dideoxyguanosine 5′-triphosphate |
| ddNTP | dideoxynucleotide 5′-triphosphate |
| ddTTP | dideoxythymidine 5′-triphosphate |
| dGTP | deoxyguanosine 5′-triphosphate |
| DNA | deoxyribonucleic acid |
| dNTP | deoxynucleotide 5′-triphosphate |
| ds | double stranded |

| | |
|---|---|
| dTTP | deoxythymidine 5′-triphosphate |
| EDS | energy dispersive x-ray spectrometry |
| EELS | electron energy loss spectroscopy |
| EG | ethylene glycol |
| f.c.c. | face centered cubic |
| FEG | field emission gun |
| GMP | guanosine 5′-monophosphate |
| GMPS | guanosine 5′-monophosphorothioate |
| GTP | guanosine 5′-triphosphate |
| HR-TEM | high-resolution transmission electron spectroscopy |
| IPTG | isopropyl-β-D-thiogalactopyranoside |
| LB | Luria Bertani |
| MCE | mercaptoethanol |
| MW | molecular weight |
| $[Ni(PPh_3)_4]$ | tetrakis(triphenylphosphine) nickel(0) |
| NTP | nucleotide 5′-triphosphate |
| $NZY^+$ | NZ amine (casein hydrolysate) yeast extract |
| PAGE | polyacrylamide gel electrophoresis |
| $[Pd_2(DBA)_3]$ | tris(dibenyzlideneacetone) dipalladium(0) |
| $[Pd(PPh_3)_4]$ | tetrakis(triphenylphosphine) palladium(0) |
| PCR | polymerase chain reaction |

| | |
|---|---|
| $PPh_3$ | triphenylphosphine |
| ppm | parts per million |
| $[Pt_2(DBA)_3]$ | tris(dibenzylideneacetone) diplatinum(0) |
| $[Pt(PPh_3)_4]$ | tetrakis(triphenylphosphine) platinum(0) |
| rATP | ribosomal adenosine 5′-triphosphate |
| RNA | ribonucleic acid |
| SEM | scanning electron microscopy |
| ss | single stranded |
| TEM | transmission electron microscopy |
| UTP | uridine 5′-triphosphate |
| *UTP | 5-(4-pyridylmethyl)-uridine 5′-triphosphate |
| X-Gal | 5-bromo-4-chloro-3-indolyl-β-D-galactopyranoside |

# INTRODUCTION

Within the biological sciences, natural evolution has created vast functional assemblies of proteins, nucleic acids and other macromolecules that perform valuable, intricate tasks.[1] Biological organisms produce a wide variety of materials with novel properties and structures unmatched to those produced in a laboratory.[2] Biomineralization achieves exquisite control over crystal type and hierarchical materials self-assembly with protein biopolymer templates. Proteins have been demonstrated to not only produce organic molecules with high regioselectivity and sterospecificity, but also inorganic materials such as bone, teeth and shells.[3,4] In addition, some organisms demonstrate the ability to nucleate and sequester free metal ions into crystalline form to reduce cytotoxicity. The malarial parasite, *P. falciparum*, a prime example, sequesters free heme in the erythrocyte to form hemozoin, which is a crystalline and nontoxic form of iron.[5]

In an attempt to emulate these controlled growth processes, research has recently been directed toward understanding how biological systems create the extent of sophisticated material architectures found in nature. An important challenge associated with the preparation of nanoparticles is the ability to control the size and shape of the particles.[6] Conventional methods for controlling metal-metal bond formation and crystal growth primarily utilize synthetic polymers. Archetypical examples are the formation of cubic silver and palladium particles using poly(acrylate)[7] or poly(vinylpyrollidone)[8] templates. Smaller multidentate ligands such as trisodium citrate can be used to control crystal shape as well, for example, in the photoinduced conversion of silver nanospheres to triangular prisms.[9]

However, fundamental polymer structure-templating function relationships are not easily achieved in these experiments. Due to the polydispersity and conformational variability of typical synthetic organic polymers, it would be difficult to predict which polymer(s) would make the best templates.

An alternative to using synthetic polymers in the synthesis of nanoparticles is the use of the biopolymers deoxyribonucleic acid (DNA) and ribonucleic acid (RNA). The use of these polymers, in combination with *in vitro* selection techniques, enables exploration of vast composition space to identify new materials. *In vitro* selection is a method involving multiple cycles of selection and amplification that isolate catalytic molecules from mutagenized or random-sequence pools of RNA or DNA.[10-13] These multiple cycles promote competition between active compounds and eventually result in the purification of those few molecular species that have the highest affinity or efficiency to perform an arbitrary task. Such a selection process begins with a pool of sequence and structural diversity. Each member of the nucleic acid pool has a different sequence and, thus, a unique set of chemical groups that will fold into varying structures that have varying properties or are capable of different functions. This approach relies on the probability that a given pool of random-sequence molecules will include individuals that can perform the function of interest.[10-12]

*In vitro* selection has been used in isolating many nucleic acid binding species, known as aptamers[20], from randomized RNA or DNA pools. Several examples of such RNA binding species include aptamers that bind specifically to organic dyes,[14] Vitamin $B_{12}$,[15] and T4 DNA Polymerase.[16] Several DNA aptamers have been found to catalyze the metallation of mesophorphyrin IX, as well as other related porphyrins.[17-19]

This research aims to explore the functional range of the biopolymer RNA in templating the synthesis of palladium and platinum containing nanoparticles from the zerovalent organometallic complexes tris(dibenzylideneacetone) dipalladium(0), tris(dibenzylideneacetone) diplatinum(0), tetrakis(triphenylphosphine) palladium(0) and tetrakis(triphenylphosphine) platinum(0). RNA mediation in the synthesis of nanomaterials could provide major benefits in the synthesis of well-defined particle shapes, compositions and functions. Some of the potential attributes of RNA *in vitro* selection techniques are:

1. A large library of RNA sequences (~$10^{14}$) can be used to select for new nanoparticle catalysts not readily synthesized by conventional methods;
2. Multiple metal compositions may be tested simultaneously and selected for a desired property;
3. Modification of the RNA to include new functional groups important for catalysis and metal ion binding are easily accomplished. These modifications are compatible with enzymatic processes such as transcription and PCR amplification, thus, a catalytically active modified RNA sequence, even if extremely rare, can be amplified and identified;
4. High selectivity may be achieved for specific structures or properties;
5. A complex mixture of metal ions can be used to discover new materials and nanoparticle catalysts.

Herein we describe the use of *in vitro* selection techniques in exploring modified RNA libraries for sequences which mediate the synthesis of nanoparticles. The goals of this research are:

1. Determine whether RNA can serve as a template for nanoparticle formation;
2. Identify RNA sequence families that template nanoparticle formation;
3. Characterize metal containing particles by examining particles synthesized by individual RNA isolates;
4. Study the effects the metal precursor has on the shape and size of the particles synthesized by individual RNA isolates;
5. Explore surface-immobilized RNA towards synthesizing particles.

## References


1. Niemeyer, C. M. *Angew. Chem. Int. Ed.* **2001**, *40*, 4128-4158.
2. Dewey, T. M.; Mundt, A.; Crouch, G. J.; Zyzniewski, M. C.; Eaton, B. E. *J. Am. Chem. Soc.* **1995**, *117*, 8474-8475.
3. Fincham, A. G.; Moradian-Oldak, J.; Simmer, J. P. *Journal of Structural Biology*. **1999**, *126*, 270-299.
4. Mann, S. *Angew. Chem. Int. Ed.* **2000**, *39*, 3392-3406.
5. Harpstrite, S. E.; Beatty, A. A.; Collins, S. D.; Oksman, A.; Goldberg, D. E.; Sharma, V. *Inorg. Chem.* **2003**, *42*, 2294-2300.
6. Behrens, S.; Rahn, K.; Habicht, W.; Böhm, K.-J.; Rösher, H.; Dinjus, E.; Unger, E. *Adv. Mater.* **2002**, *14*, 1621-1625.
7. Ahmadi, T. S.; Wang, Z. L.; Henglein, A.; El-Sayed, M. A. *Chem. Mater.* **1996**, *8*, 1161-1164.
8. Sun, Y.; Xia, Y. *Science* **2002**, *298*, 2176-2179.
9. Jin, R.; Cao, Y.; Mirkin, C. A.; Kelly, K. L.; Schatz, G. C.; Zheng, J. G. *Science* **2001**, *294*, 1901-1903.
10. Fitzwater, T.; Polisky, B. *Methods in Enzymology, v. 267*, Academic Press, Inc., California, **1996**, 275-301.
11. Breaker, R. *Chem. Rev.* **1997**, *97*, 371-390.
12. Osborne, S. E.; Ellington, A. D. *Chem. Rev.* **1997**, *97*, 349-370.
13. Bittker, J. A.; Le, B. L.; Lin, D. R. *Nature Biotechnology*. **2002**, *20*, 1024-1029.
14. Ellington, A. D.; Szostak, J. W. *Nature*. **1990**, *346*, 818-822.
15. Lorsch, J. R.; Szostak, J. W. *Biochemistry*. **1994**, *33*, 973-982.

16. Tuerk, C.; Gold, L. *Science*. **1990**, *249*, 505-510.

17. Li, Y.; Sen, D. *Biochemistry*. **1997**, *36*, 5589-5599.

18. Li, Y.; Geyer, C. R.; Sen, D. *Biochemistry*. **1996**, *35*, 6911-6922.

19. Li, Y.; Sen, D. *Nature Structural Biology*. **1996**, *3*, 743-747.

20. Ellington, A. D.; Szostak, J. W. *Nature*. **1990**, *346*, 818-822.

# CHAPTER 1: RNA-MEDIATED SYNTHESIS OF PALLADIUM AND PLATINUM CONTAINING PARTICLES

## 1.1. Introduction

Biomineralization achieves exquisite control over crystal type and hierarchical materials self-assembly with protein biopolymer templates. In attempts to mimic natural biomineralization, proteins and polypeptides have been studied extensively as templates for materials synthesis.[1-4] Belcher *et al.* have used phage display techniques to mine for peptides that can bind selectively to various semiconductor crystal faces.[5] Knowledge of peptide-surface binding affinity was then used to engineer a virus that could bind and organize semiconductor nanocrystals into well-ordered thin film assemblies.[6] Much less research has been focused on the interactions between materials and nucleic acids. The thermodynamics of double-stranded DNA (dsDNA)-CdSe nanocrystal association have been investigated,[7] and DNA hybridization has been used to assemble network structures of gold nanoparticles.[8,9] In addition, several studies have described deposition of solid-state materials over dsDNA.[10]

We posited that RNA could act as a template for inorganic particle formation because it is a highly structured biopolymer that can reproducibly fold into intricate three-dimensional structures as dictated by primary sequence. In addition, the ability to tailor the functionality of this biopolymer by using modified nucleotides makes RNA especially attractive.[11,12] Herein we describe the use of modified RNA libraries with enhanced metal binding affinities.

## 1.2. Results and Discussion

### 1.2.1 Synthesis of Pd Containing Particles using [$Pd_2(DBA)_3$] as the Metal Precursor

The selection cycle used for discovering RNA-mediated crystal growth using [$Pd_2(DBA)_3$] as the metal precursor is shown in Scheme 1.1 (p. 10). The selection began with a chemically synthesized (Applied Biosystems ABI 391) library of single-stranded DNA sequences, 87 base pairs (bp) in length, containing a center region of 40 bp, random in sequence. Two-cycle polymerase chain reaction (PCR) was used to generate a dsDNA library of ~ $3 \times 10^{13}$ unique sequences from the chemically synthesized ssDNA pool. In step 1, T7 RNA Polymerase was used to transcribe the dsDNA library into a single-stranded RNA library containing ~$10^{14}$ sequences. During step 1, 5-(4-pyridylmethyl)-uridine 5′-triphosphate (*UTP) was used to provide additional metal coordination sites beyond the heterocyclic nitrogens present in native RNA. In step 2, the RNA library (1 μM) was incubated in two parallel selection experiments with the metal complex tris(dibenzylideneacetone) dipalladium(0) ([$Pd_2(DBA)_3$]), at 100 or 400 μM to provide a source of $Pd^0$ atoms (Scheme 1.1, p. 9). The incubation was performed in aqueous solution for 2 hours at ambient temperature. For selection step 3 to be successful, RNA sequences were required to either mediate the formation of Pd containing particles and remain bound to those particles, or simply bind to particles formed spontaneously or by other RNA sequences. Size-exclusion membranes (Microcon 100, 100-kD cutoff) were used to select for particles that were formed in the presence of RNA.[13] The selected RNA was reverse transcribed [step 4, AMV (avian myeloblastosis virus) reverse transcriptase] to give a cDNA copy of the "winning" sequences. PCR amplification completed the selection cycle providing a dsDNA

template enriched in the winning sequences ready for T7 RNA polymerase transcription and the beginning of the next cycle.[14]

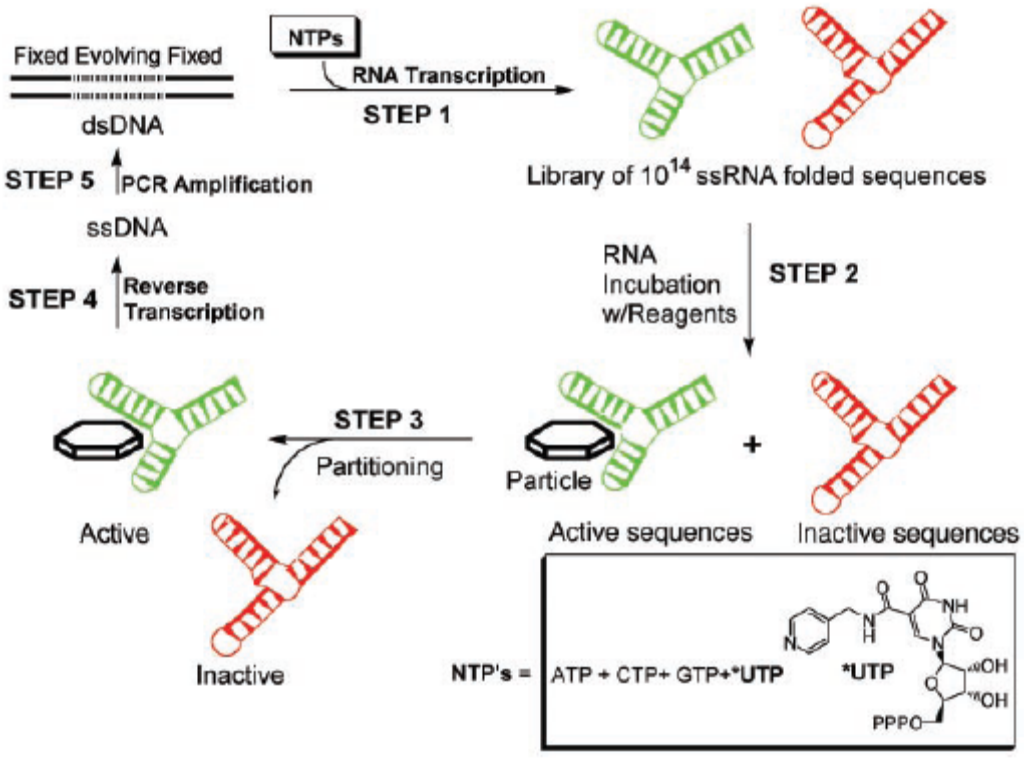


**Scheme 1.1.** Steps of the RNA *in vitro* selection cycle. [17]

Initially (cycles 1 through 3), partitioning (step 3) was accomplished by a 100-kD cutoff filter. The percentage of RNA retained following partitioning was monitored throughout the selection. Due to the rapid increases in RNA retention during cycles 2 and 3 (Figure 1.1, p. 11) it was necessary to subject the RNA to additional selection pressure. In cycles 4 to 8, the 100-kD molecular size cutoff filter was followed by native polyacrylamide

gel (6%) electrophoresis gel (PAGE) mobility shift-dependent partitioning. Slowly migrating bands, relative to the starting RNA transcript, that showed a dependence on both RNA and Pd were isolated (Figure 1.2, p. 11).[17] Particle formation was not dependent on the 100-kD cutoff filter as demonstrated by the observance of gel-shifted bands with similar migrating rates from incubation products purified with and without the filter. In addition, both the crude and purified materials resulting from the metal incubations were analyzed by TEM. From the TEM analysis, particles were observed for both the filter-purified sample and the sample not purified on the filter. However, residual amorphous organic material was also present for the crude sample and thus purification is recommended for sensitive analyses (e.g. electron diffraction, EDS, etc.) where high sample purity is required. As would be expected from the added pressure there was a sharp decrease in the amount of RNA being retained at the end of cycle 4, thus eliminating the weakly bound RNA from the evolving pool. As the selection continues, the more strongly bound RNA populations begin to increase in numbers as they become amplified in subsequent cycles.

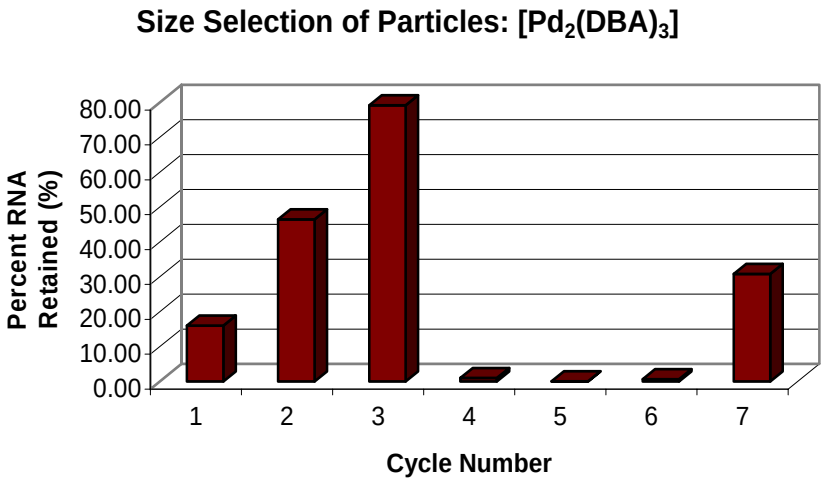


**Figure 1.1.** Percentage of RNA retained following partitioning of active sequences. In cycles 1-3, partitioning was accomplished using a 100-kD cutoff filter. In cycles 4-8, the 100-kD cutoff filter was followed by 6% native PAGE.

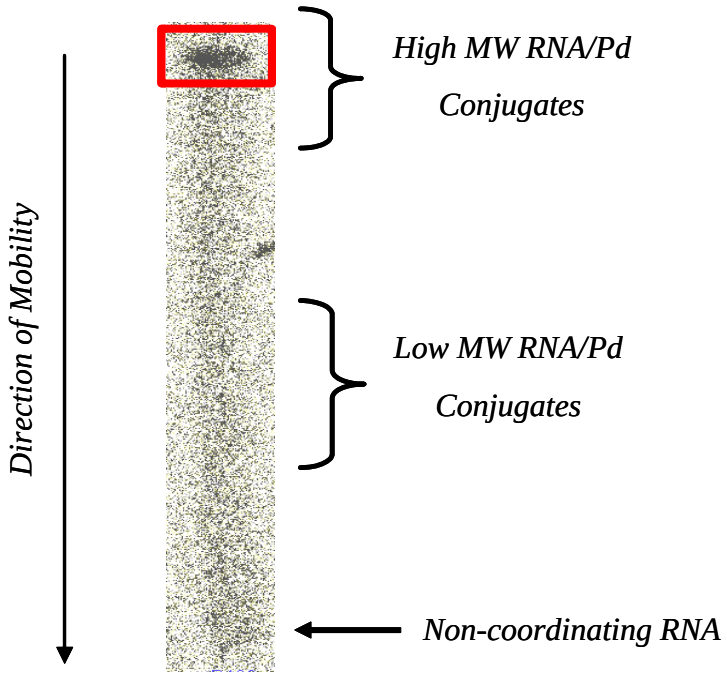


**Figure 1.2.** Representative gel phosphorimage of the 6% native PAGE partitioning of active RNA sequences following the 100-kD cutoff filter. RNA that was isolated and brought forward into subsequent cycles is highlighted in red.

Transmission electron microscopy (TEM) analysis of the Pd containing particles produced in 2 hours by the starting random RNA library revealed mostly small (5 nm diameter) particles of undefined shape (Figure 1.3A). TEM analysis of the Pd containing particles created by the evolved RNA cycle 8 pool after 2 hours were markedly different. The dominant particle shape observed was thin hexagonal plates (Figure 1.3, B and C). Also observed at lower frequency (~ 1%) were cubes and rods. A combination of scanning electron microscopy (SEM) and energy dispersion x-ray spectroscopy (EDS) (Figure 1.4, p. 13) showed that the hexagonal particles contained Pd. Further characterization by atomic force microscopy showed the hexagonal particles to be ca. 20-50 nm in thickness (Figure 1.5, p. 13). Control experiments in which poly(vinylpyridine) was used under identical incubation and isolation conditions gave no particle growth. From the analyses of the evolved RNA pool, it was unclear whether a single RNA sequence was sufficient to create these particles or whether multiple RNA sequences in the pool conspired to mediate particle growth.[17]

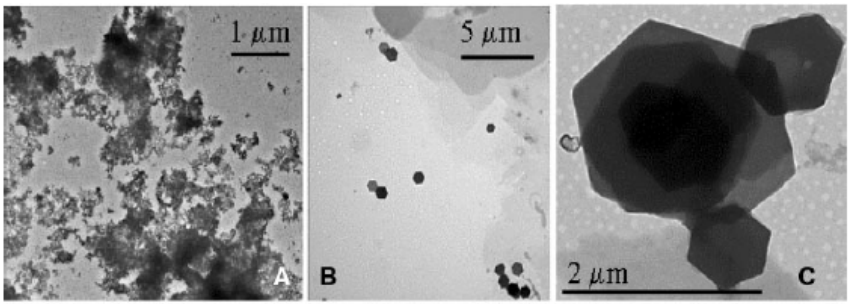


**Figure 1.3.** Transmission electron micrograph images of palladium containing particles formed in the presence of cycle 0 pool modified RNA (A) and the cycle 8 RNA pool (B and C).[17]

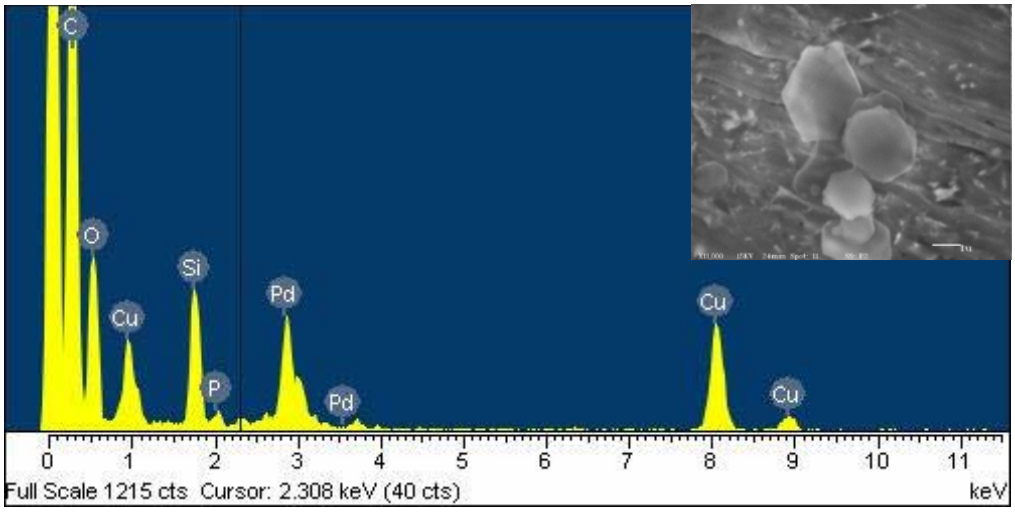


**Figure 1.4.** EDS spectrum of hexagonal particles formed in the presence of the cycle 8 RNA pool at 400 μM [$Pd_2(DBA)_3$], exhibiting characteristic Pd peaks. The particles were cast onto carbon-coated copper TEM grids. Insert: SEM image of hexagons.

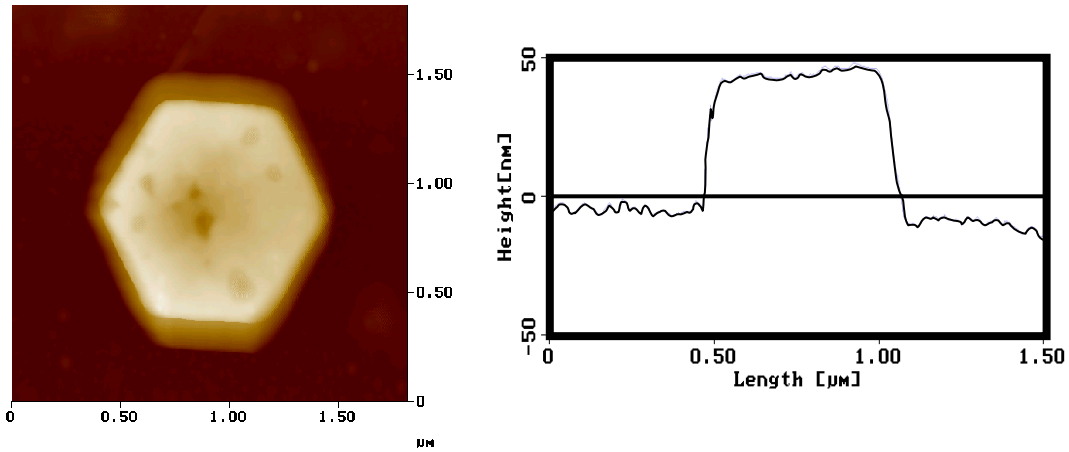


**Figure 1.5.** AFM image of hexagonal Pd containing particle (A) and respective height analysis (B).

To investigate individual sequences, we cloned and sequenced the RNA pool to yield individual RNA isolates. The isolates could be grouped into families, supporting the notion that an RNA biopolymer can evolve in response to an inorganic materials synthesis pressure. A total of 27 RNA sequences have been obtained to date (Figure 1.6, p. 15, Appendix A.1, p. 90) and have been grouped into families on the basis of conserved sequence regions. Members of families 1 and 2 are most probably the result of mutations or deletions/insertions of individual sequences present in the starting pool. Families 3 and 4, and the orphan sequences appear to be discrete isolates based on the relatively long regions of nonhomologous sequence flanking the conserved regions. Interestingly, family 4 sequences are related by their 5′-end conserved region and show sequence similarity to both families 1 and 2.[17]

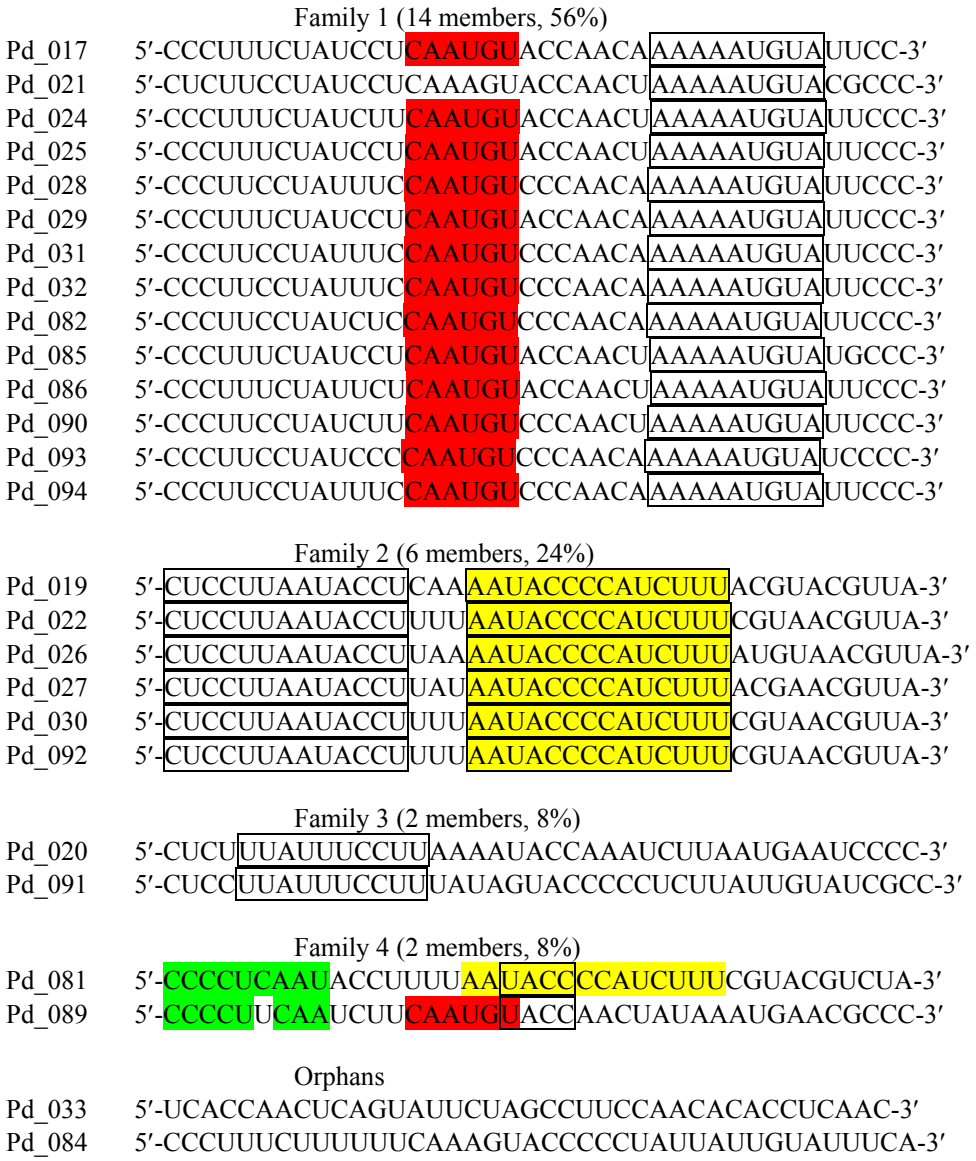


**Figure 1.6.** Representative RNA sequences that can mediate the formation of hexagonal palladium containing particles. Conserved regions are outlined in boxes. Regions in common between families are highlighted in color.[17]

Isolates 17, 19, 20, 81 and 84 were chosen as representatives of the different families, and their ability to form particles was investigated by TEM. All isolates mediated the formation of hexagonal particles of similar structure to those shown in Figure 1.1 (p. 11).

Each of the above RNA family representatives, in contrast to the cycle 8 evolved pool, only form hexagonal particles by TEM analysis. For this form of modified RNA and this selection procedure, hexagonal plates are the dominant Pd containing particle form to evolve. This is an important result since to date, few methods exist for growing thin hexagonal particles.[15] In addition, the hexagonal particles grown by these RNA isolates are distinctive in their large size and shape uniformity. Figure 1.7 shows the distribution of Pd containing hexagonal particles measured by TEM for the evolved pool and isolate 17 after 2 hours incubation with $[Pd_2(DBA)_3]$ (400 μM). The average particle size was similar for both the evolved pool and isolate 17 (1.3 μm ± 0.9 μm versus 1.2 μm ± 0.6 μm, respectively); however, the distribution of the particles was significantly narrower for isolate 17. This result suggests that although each family member directs the formation of the same final particle product, they do so at different rates. Further detailed kinetic analysis will be required to determine if this is indeed true.

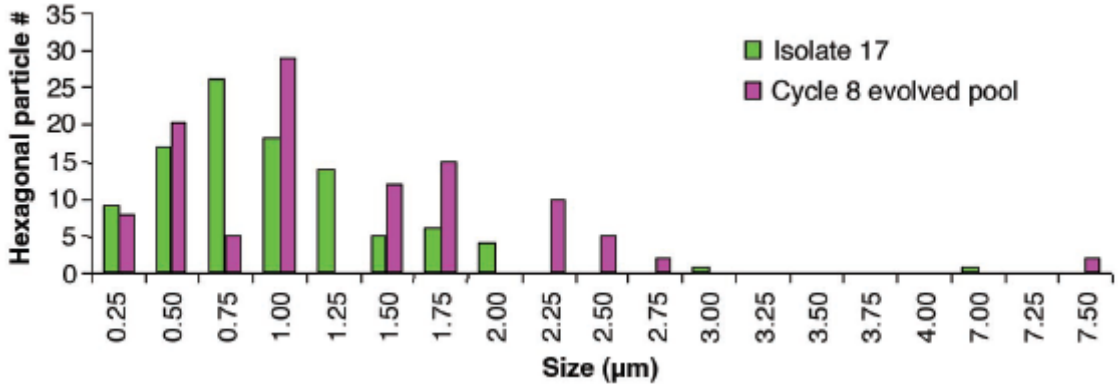


**Figure 1.7.** Particle size histograms of Pd containing hexagons created by isolate 17 and the cycle 8 evolved pool in 2 hours.[17]

Given that individual RNA isolates can mediate hexagonal particle growth, we sought to determine how rapidly the particles formed. For comparison, when synthetic polymers are used to direct crystal type and size, the concentration of polymer is typically in excess of inorganic precursor, and the reaction is performed at elevated temperature. Further, the concentration of the metal precursors is typically several orders of magnitude higher than that reported here. The cycle 8 pool and isolate 17 were tested for their ability to mediate Pd containing particle growth at times ranging from 2 hours down to 1 minute. Surprisingly, hexagonal particles 0.32 μm ± 0.27 μm wide were formed by the RNA pool at 1 μM and $[Pd_2(DBA)_3]$ at 400 μM in 7.5 minutes. To determine if this rapid rate of particle growth required multiple sequences, we tested isolate 17 alone for its ability to mediate particle growth. Under identical conditions, isolate 17 could grow hexagonal particles 1.3 μm ± 0.6 μm wide in 1 minute.[17]

### 1.2.2. Synthesis of Pt Containing Particles using $[Pt_2(DBA)_3]$ as the Metal Precursor

The selection cycle used for discovering RNA-mediated crystal growth using $[Pt_2(DBA)_3]$ as the metal precursor is similar to the design shown in Scheme 1.1 (p. 9). In step 2, the RNA library was incubated with the metal complex tris(dibenzylideneacetone) diplatinum(0) ($[Pt_2(DBA)_3]$), at 400 μM to provide a source of $Pt^0$ atoms. The incubation was performed in aqueous solution for 2 hours at ambient temperature. Size-exclusion membranes (Microcon 100, 100-kD cutoff) were used to select for particles that were formed in the presence of RNA. Initially (cycles 1-2), 1 μM RNA was utilized in the RNA-metal incubation (step 2). In cycles 3-6, the RNA concentration was decreased to 0.5 μM to

increase the selectivity pressure of the selection. Particle formation was not dependent on the 100-kD cutoff filter as demonstrated by analyzing both the crude and purified materials resulting from the metal incubations. As determined by TEM analysis, particles were observed for both the filter-purified sample and the sample not purified on the filter. However, residual amorphous organic material was also present for the crude sample and thus purification is recommended for sensitive analyses (e.g. electron diffraction, EDS, etc.) where high sample purity is required. Similar to the previous selection, the percentage of RNA retained following partitioning was also monitored throughout the course of the selection (Figure 1.8).

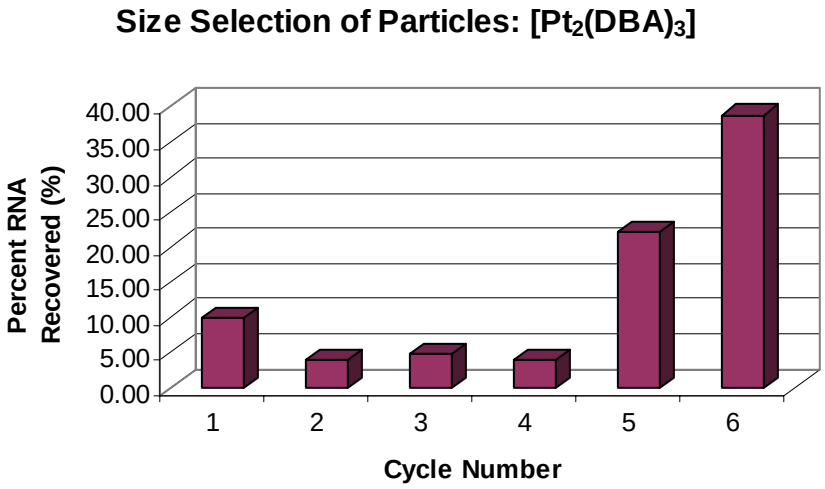


**Figure 1.8.** Percentage of RNA retained following partitioning of active sequences. In cycles 1-2, [RNA library] = 1.0 μM; in cycles 3-6, [RNA library] = 0.5 μM.

TEM analysis of the Pt containing particles produced in 2 hours by the starting random RNA library revealed mostly small (5 nm diameter) particles of undefined shape

(Figure 1.9A). TEM analysis of the Pt containing particles created by the evolved RNA cycle 6 pool after 2 hours was markedly different. The dominant particle shape observed was thin hexagonal plates, representing 46% of the population (Table 1.1, Figure 1.9B). Also observed were cubes and spheres representing 23% and 31% of the population, respectively (Table 1.1, Figure 1.9C). EDS analysis showed that the hexagonal, cubic and spherical particles contained platinum (Figure 1.10, p. 20).

**Table 1.1.** Pt Containing Particles Formed in the Presence of the Cycle 6 RNA Pool

| Particle Shape | Particle Size (μm) | % Population* |
|---|---|---|
| hexagonal | 0.09 ± 0.04 | 46 |
| cubic | 0.05 ± 0.03 × 0.07 ± 0.02 | 23 |
| spherical | 0.07 ± 0.04 | 31 |
| | *total no. particles:* 290 | |

* The entire TEM grid was examined for all types of materials formed. Percentages represent the amount of these materials observed on the grid from the total population.

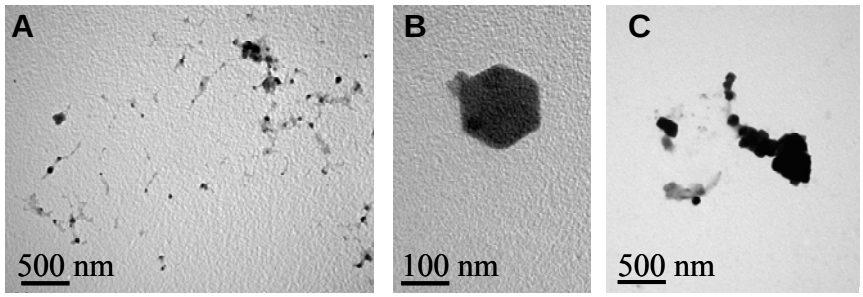


**Figure 1.9.** Transmission electron micrograph images of platinum containing particles formed in the presence of the cycle 0 modified RNA pool (A) and cycle 6 RNA pool (B and C).

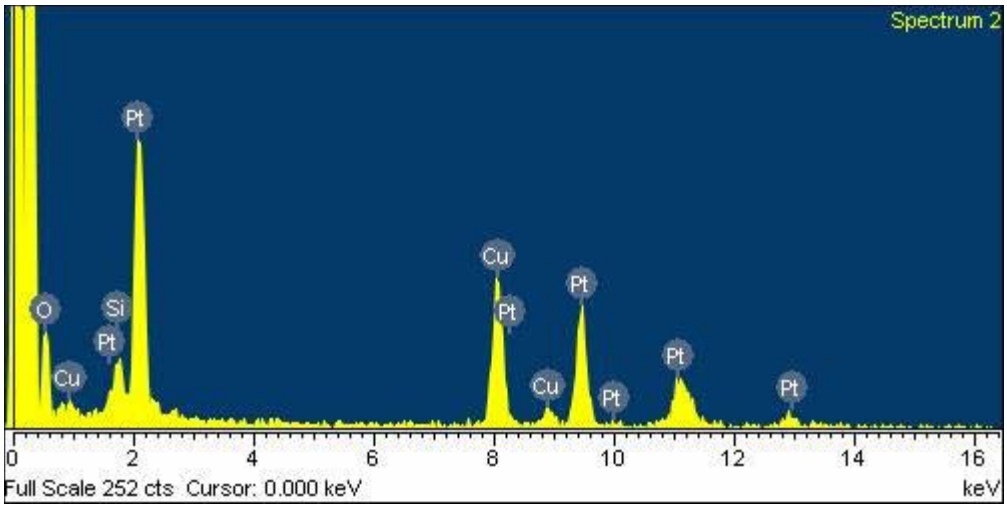


**Figure 1.10.** EDS spectrum of hexagonal particles, formed in the presence of the cycle 6 RNA pool at 400 μM [$Pt_2(DBA)_3$], exhibiting characteristic Pt peaks. The particles were cast onto carbon-coated copper TEM grids.

To investigate individual sequences, the RNA pool was cloned and sequenced to yield individual RNA isolates. To date, 106 RNA sequences have been identified and these isolates could be grouped into families on the basis of conserved sequence regions (Figure 1.11, p. 21, Appendix A.2, p. 92). Members of families 1 and 3 are most probably the result of mutations or deletions/insertions of individual sequences present in the starting pool. Families 2, 4-10, and the orphan sequences appear to be discrete isolates based on the relatively long regions of nonhomologous sequence flanking the conserved regions.

Family 2 (3 members, 3 %)

Pt_002 5′-CUCAAGGUUCUAGCGUUCUAUGGGUAUGUCGCUGCCGUCG-3′

Family 6 (6 members, 6 %)

Pt_012 5′-GAUUACGUACAACCGUGUACCUUCCCAGCCCACCAAGAUC-3′

Subfamily 6a

Pt_018 5′-UAGGCGAUGGUAACCGUUCCCCCGAGUUAACGUCCGCGGC-3′

Family 7 (5 members, 8 %)

Pt_032 5′-CGCAAUGCAUAGGGUUUAGGGUUGGAAAUCGUGGUGAACCU-3′

Orphan

Pt_021 5′-CACCCACUAGGACCCAUGUAGUGNCUACCUUUUNGCCAGA-3′

**Figure 1.11.** Representative RNA sequences that can mediate the formation of hexagonal, cubic and spherical platinum particles. Conserved regions are outlined in boxes. Regions in common between families are highlighted in color.

Isolates 2, 12, 18, 21 and 32 were chosen as representatives of the different families, and their ability to form particles was investigated by TEM. All isolates mediated the formation of hexagonal particles of similar structure to those shown in Figure 1.9B (p. 19). Interestingly, in addition to hexagonal particles, cubic and spherical particles were also observed to be formed in the presence of isolate 18. This observation could be a result of the multiple conserved regions found within isolate 18, but further analysis of this hypothesis is warranted. With the exception of isolate 18, each of the RNA family representatives studied, in contrast to the cycle 6 evolved pool, formed hexagonal particles exclusively. Similar to the $[Pd_2(DBA)_3]$ isolates discovered, for this form of modified RNA and this selection procedure, hexagonal plates are the dominant Pt containing particle form to evolve. In comparison to the hexagonal Pd containing particles grown by the $[Pd_2(DBA)_3]$ RNA isolates, these hexagonal Pt containing particles are smaller on average (Table 1.2, p. 22).

**Table 1.2.** Shape and Size Distribution of Pt Containing Particles Formed by Individual Cycle 6 RNA Isolates

| RNA Isolate | Particle Shape | No. Particles Counted | Size (μm) | % Population* |
|---|---|---|---|---|
| 2 | hexagonal | 121 | 0.14 ± 0.05 | 100 |
| 12 | hexagonal | 113 | 0.16 ± 0.08 | 100 |
| 18 | spherical | 282 | 0.023 ± 0.008 | 73 |
| | hexagonal | 65 | 0.22 ± 0.14 | 17 |
| | cubic | 39 | 0.07 ± 0.02 × 0.10 ± 0.03 | 10 |
| 21 | hexagonal | 118 | 0.13 ± 0.04 | 100 |
| 32 | hexagonal | 129 | 0.18 ± 0.09 | 100 |

* The entire TEM grid was examined for all types of materials formed. Percentages represent the amount of these materials observed on the grid from the total population.

### 1.2.3. Synthesis of Pd Containing Particles using [$Pd(PPh_3)_4$] as the Metal Precursor

The selection cycle used for discovering RNA-mediated crystal growth using [$Pd(PPh_3)_4$] as the metal precursor is similar to the design shown in Scheme 1.1 (p. 9). In step 2, the RNA library was incubated with the metal complex tetrakis(triphenylphosphine) palladium(0) ([$Pd(PPh_3)_4$]), at 400 μM to provide a source of $Pd^0$ atoms. The incubation was performed in aqueous solution for 2 hours at ambient temperature. Size-exclusion membranes (Microcon 100, 100-kD cutoff) were used to select for particles that were formed in the presence of RNA. Initially (cycles 1-2), 1 μM RNA was utilized in the RNA-metal incubation (step 2). In cycles 3-10, the RNA concentration was decreased to 0.5 μM to increase the selectivity pressure of the selection. Particle formation was not dependent on the 100-kD cutoff filter as demonstrated by analyzing both the crude and purified materials resulting from the metal incubations. As determined by TEM analysis, particles were

observed for both the filter-purified sample and the sample not purified on the filter. However, residual amorphous organic material was also present for the crude sample and thus purification is recommended for sensitive analyses (e.g. electron diffraction, EDS, etc.) where high sample purity is required. Similar to the previous selections, the percentage of RNA retained following partitioning was monitored (Figure 1.12).

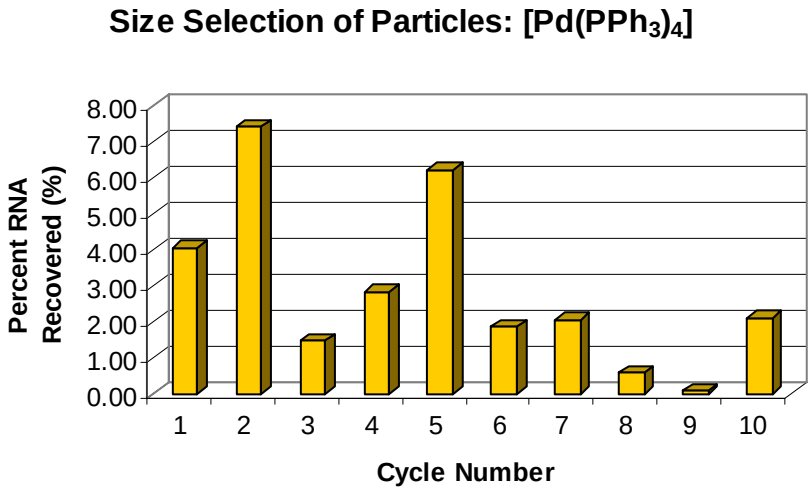


**Figure 1.12.** Percentage of RNA retained following partitioning of active sequences. In cycles 1-2, [RNA library] = 1.0 μM; in cycles 3-10, [RNA library] = 0.5 μM.

TEM analysis of the Pd containing particles produced in 2 hours by the starting random RNA library revealed mostly small (5 nm diameter) particles of undefined shape (Figure 1.13A, p.24). TEM analysis of the Pd containing particles created by the evolved RNA cycle 10 pool after 2 hours were markedly different. The only particles observed were small, spherical shapes (Figure 1.13B, p. 24). EDS analysis showed the spherical particles to contain palladium (Figure 1.14, p. 24).

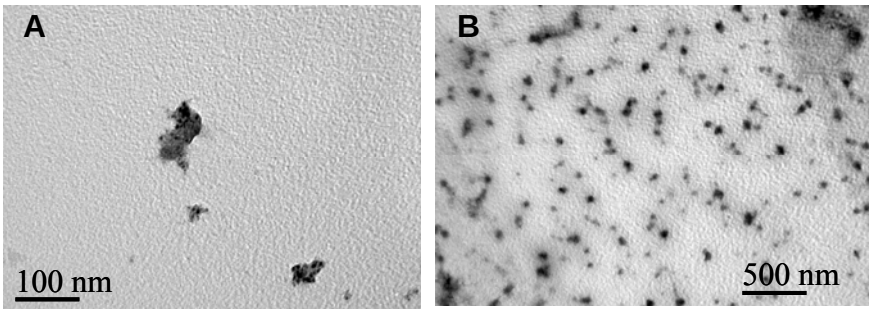


**Figure 1.13.** Transmission electron micrograph images of palladium containing particles formed in the presence of the cycle 0 modified RNA pool (A) and cycle 10 RNA pool (B).

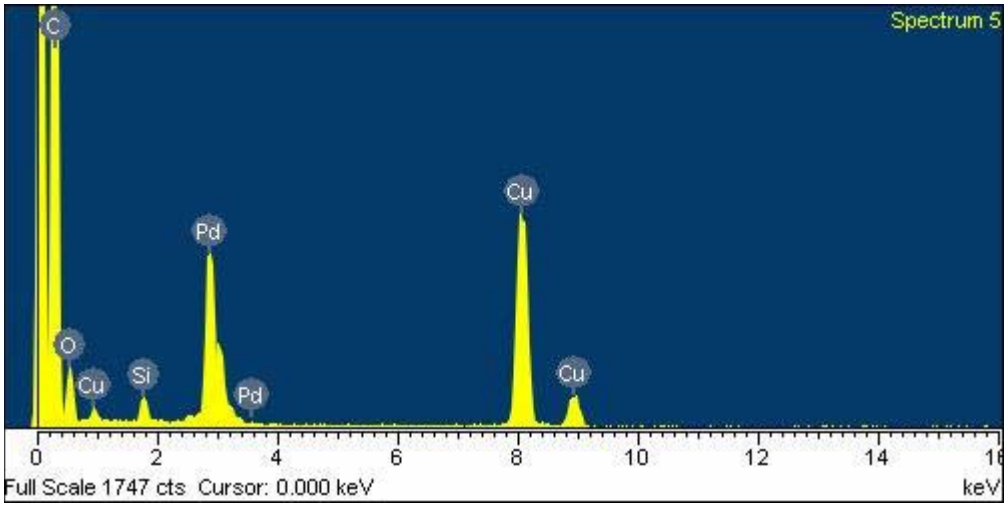


**Figure 1.14.** EDS spectrum of spherical particles, formed in the presence of the cycle 10 RNA pool at 400 μM [$Pd(PPh_3)_4$], exhibiting characteristic Pd peaks. The particles were cast onto carbon-coated copper TEM grids.

To investigate individual sequences, the RNA pool was cloned and sequenced to yield individual RNA isolates. To date, 38 RNA isolates were identified and these isolates could be grouped into families on the basis of conserved sequence regions (Figure 1.15, p. 25, Appendix A.3, p. 95). Members of families 1 and 2 are most probably the result of mutations or deletions/insertions of individual sequences present in the starting pool.

Families 3 and 4, and the orphan sequences appear to be discrete isolates based on the relatively long regions of nonhomologous sequence flanking the conserved regions.

Family 1 (4 members, 16 %)
Pd_S002 5′-AAGCAGUAGGUGGAUUUCAGGCAGACGAUGCUGACUCCUU-3′

Family 2 (2 members, 13 %)
Pd_S008 5′-GAUGCCUGUCGAGCAUGCUGUAGAGAUGCCUGUCGAGCAUGCUGUAA-3′

Family 3 (2 members, 13 %)
Pd_S031 5′-UCUCAACGGUGUCACGUAGCGCGAAAGACGCCUGCAACCC-3′

Family 4 (2 members, 13 %)
Pd_S032 5′-GCAUCUAGCUACAAAGCUUUUUUCUAUUUGAUUCCUUCU-3′

Orphans
Pd_S010 5′-CGGUGUGUGGCCGCAUGCGUACAAACGCGCUGCAAGGUUA-3′

**Figure 1.15.** Representative RNA sequences that can mediate the formation of spherical palladium containing particles. Conserved regions are outlined in boxes.

Isolates 2 and 31 were chosen as representatives of the different families, and their ability to form particles was investigated by TEM. Both isolates mediated the formation of spherical particles of similar structure to those shown in Figure 1.13 (p. 24). The average particle size was similar for both the evolved pool and isolates 2 and 31 (Table 1.3, p. 6).

**Table 1.3.** Shape and Size Distribution of Pd Containing Particles Formed by the Evolved Cycle 10 Modified RNA Pool and Individual Cycle 10 RNA Isolates

| Sample | Particle Shape* | No. Particles Counted | Size (μm) |
|---|---|---|---|
| Cycle 10 Pool | Spherical | 286 | 0.028 μm ± 0.009 μm |
| Isolate Pd_S002 | Spherical | 179 | 0.025 μm ± 0.008 μm |
| Isolate Pd_S031 | Spherical | 194 | 0.027 μm ± 0.009 μm |

* The entire TEM grid was examined for all types of materials formed.

### 1.2.4. Synthesis of Pt Containing Particles using [$Pt(PPh_3)_4$] as the Metal Precursor

The selection cycle used for discovering RNA-mediated crystal growth using [$Pt(PPh_3)_4$] as the metal precursor is similar to the design shown in Scheme 1.1 (p. 9). In step 2, the RNA library was incubated in two parallel selection experiments with the metal complex tetrakis(triphenylphosphine) platinum(0) ([$Pt(PPh_3)_4$]), at 10 or 100 μM to provide a source of $Pt^0$ atoms. The metal precursor concentration for this selection is considerably less than the metal concentrations used in the previous three selections. This decrease in concentration was necessary to increase the selection pressure. The incubation was performed in aqueous solution for 2 hours at ambient temperature. Size-exclusion membranes (Microcon 100, 100-kD cutoff) were used to select for particles that were formed in the presence of RNA. Initially (cycle 1), 1 μM RNA was utilized in the RNA-metal incubation (step 2). In cycles 2-8, the RNA concentration was decreased to 0.5 μM to increase the selectivity pressure of the selection. Pt containing particle formation was not dependent on the 100-kD cutoff filter as demonstrated by analyzing both the crude and purified materials resulting from the metal incubations. As determined by TEM analysis, particles were observed for both the filter-purified sample and the sample not purified on the filter. However, residual amorphous organic material was also present for the crude sample and thus purification is recommended for sensitive analyses (e.g. electron diffraction, EDS, etc.) where high sample purity is required. Similar to the previous selections, the percentage of RNA retained following partitioning was also monitored throughout the selection (Figure 1.16, p. 27).

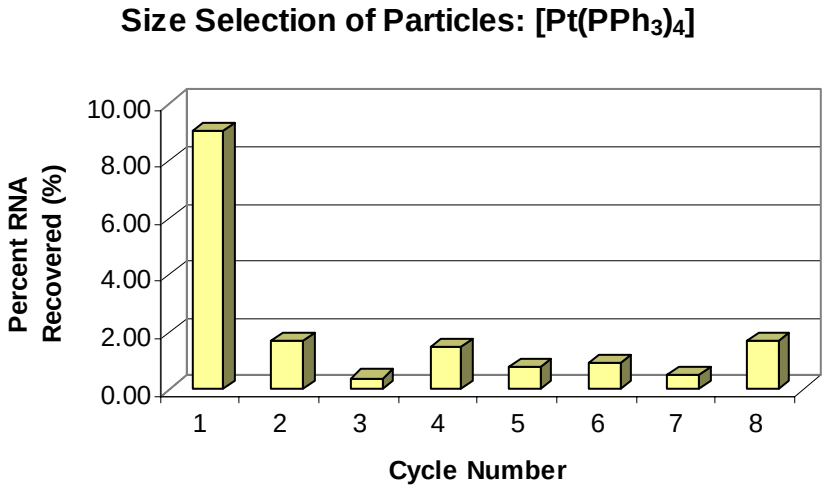


**Figure 1.16.** Percentage of RNA retained following partitioning of active sequences. In cycle 1, [RNA library] = 1.0 μM; in cycles 2-8, [RNA library] = 0.5 μM.

TEM analysis of the Pt containing particles produced in 2 hours by the starting random RNA library revealed mostly small (5 nm diameter) particles of undefined shape (Figure 1.17A, p. 28). TEM analysis of the Pt containing particles created by the evolved RNA cycle 8 pool after 2 hours were markedly different. The only particles observed were small, spherical shapes (Figure 1.17B, p. 28). EDS analysis showed that the spherical particles contained platinum (Figure 1.18, p. 28).

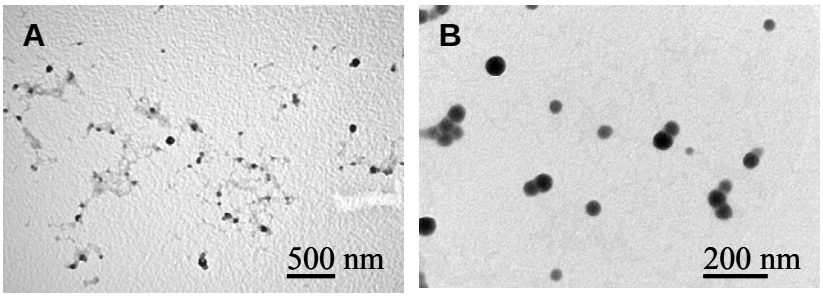


**Figure 1.17.** Transmission electron micrograph images of platinum containing particles formed in the presence of the cycle 0 modified RNA pool (A) and cycle 8 RNA pool (B).

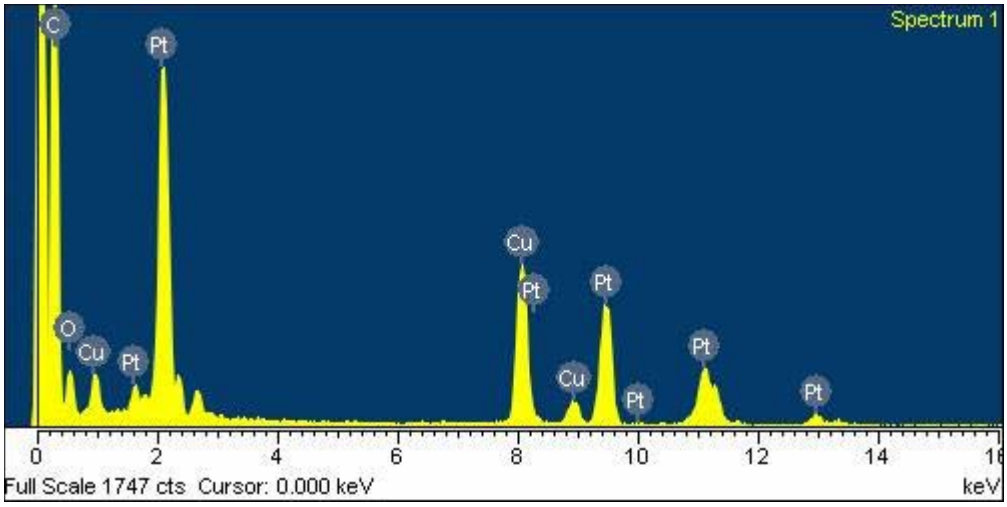


**Figure 1.18.** EDS spectrum of spherical particles, formed in the presence of the cycle 8 RNA pool at 100 μM [$Pt(PPh_3)_4$], exhibiting characteristic Pt peaks. The particles were cast onto carbon-coated copper TEM grids.

To investigate individual sequences, the RNA pool was cloned and sequenced to yield individual RNA isolates. To date, a total of 11 RNA isolates were identified and these isolates could be grouped into families on the basis of conserved sequence regions (Figure 1.19, p. 29, Appendix A.4, p. 97). Members of family1 are most probably the result of mutations or deletions/insertions of individual sequences present in the starting pool. The

orphan sequences appear to be discrete isolates based on the relatively long regions of nonhomologous sequence flanking the conserved regions.

Family 1 (3 members, 27 %)
Pt_S049 5′-UCCCAUCGCUACUUAUUCUAUUUUGAUACCUCGUUAUCUA-3′

Orphans
Pt_S069 5′-UCAUCAUCACUUACCCAUUCAACACCCCUCCUCAAAAAAC-3′

**Figure 1.19.** Representative RNA sequences that can mediate the formation of spherical platinum containing particles. Conserved regions are outlined in boxes.

Isolates 49 and 69 were chosen as representatives of the different families, and their ability to form particles was investigated by TEM. Both isolates mediated the formation of spherical particles of similar structure to those shown in Figure 1.17 (p. 28). The average particle size was similar for both the evolved pool and isolates 49 and 69 (Table 1.4).

**Table 1.4.** Shape and Size Distribution of Pt Containing Particles Formed by the Evolved Cycle 8 Modified RNA Pool and Individual Cycle 8 RNA Isolates

| Sample | Particle Shape* | No. Particles Counted | Size (μm) |
|---|---|---|---|
| Cycle 8 Pool | Spherical | 346 | 0.07 μm ± 0.05 μm |
| Isolate Pt_S049 | Spherical | 263 | 0.04 μm ± 0.02 μm |
| Isolate Pt_S069 | Spherical | 218 | 0.06 μm ± 0.03 μm |

* The entire TEM grid was examined for all types of materials formed.

## 1.3. Conclusion

We now know that RNA can mediate the formation of novel inorganic materials. The hexagonal Pd containing and Pt containing plates evolved over 8 cycles and 6 cycles,

respectively, of *in vitro* selection. These particle shapes and sizes cannot easily be reproduced by any other known methods. The presence of multiple RNA sequence families that mediate this novel particle growth supports the notion that this biopolymer can be an active participant in inorganic materials evolution. It is interesting to note that upon comparison of the modified RNA pools resulting from these four separate selections, there are isolates found containing regions of sequence similarity that are shared among the pools (Figure 1.20, p. 30; Figure 1.21, p. 31; Figure 1.22, p. 31).

| | |
|---|---|
| Pt_083 | 5′-CUAUUCGUCAUAGUUGCAAACCCAUCUUUCUUCAUC-3′ |
| Pd_019 | 5′-CUCCUUAAUACCUCAAAAUACCCCAUCUUUACGUACGUUA-3′ |
| Pd_084 | 5′-CCCUUUCUUUUUUCAAAGUACCCCCUAUUAUUGUAUUUCA-3′ |
| Pd_022 | 5′-CUCCUUAAUACCUUUUAAUACCCCAUCUUUCGUAACGUUA-3′ |
| Pd_026 | 5′-CUCCUUAAUACCUUAAAAUACCCCAUCUUUAUGUAACGUUA-3′ |
| Pd_020 | 5′-CUCUUUAUUUCCUUAAAAUACCAAAUCUUAAUGAAUCCCC-3′ |
| Pd_081 | 5′-CCCCUCAAUACCUUUUAAUACCCCAUCUUUCGUACGUCUA-3′ |
| | |
| Pt_095 | 5′-CGCAUGCUCAGAUUACAGCCGAAGUCCUAGCCUCACGGAA-3′ |
| Pd_017 | 5′-CCCUUUCUAUCCUCAAUGUACCAACAAAAAAUGUAUUCC-3′ |
| Pd_021 | 5′-CUCUUCCUAUCCUCAAAGUCCAACUAAAAAUGUACGCCC-3′ |
| Pd_029 | 5′-CCCUUUCUAUCCUCAAUGUACCAACAAAAAAUGUAUUCCC-3′ |
| Pd_090 | 5′-CCCUUCCUAUCUUCAAUGUCCCAACUAAAAAUGUAUUCCC-3′ |
| Pd_093 | 5′-CCCUUCCUAUCCCCAAUGUCCCAACAAAAAAUGUAUCCCC-3′ |
| | |
| Pt_033 | 5′-UGGCCUGCCAAUGGACGUGUGCUAAGAUUCCACUCGAUAU-3′ |
| Pt_035 [3] | 5′-GCAAAGCAUAACGCGUACGCAAUGAACGCGGACAUUCAUC-3′ |
| Pt_037 | 5′-GCAAAGCAUAACGCGUUACGCAAUGAACGCGGACAUUCAUC-3′ |
| Pt_043 [2] | 5′-UACGGUUAUGGCUGCCGCGUAACGAAGGCCAAAACGAAUU-3′ |
| Pt_057 | 5′-AGUAAAACUGAAUGCCACUGCGUUGGGGAUCGUGUGAUUG-3′ |
| Pt_074 | 5′-CCAUGAUGGCGCAUUGAGACCACAUCGAGAUUGAGCGCAU-3′ |
| Pd_089 | 5′-CCCCUUCAAUCUUCAAUGUACCAACUAUAAAUGAACGCCC-3′ |

**Figure 1.20.** Comparison of RNA isolates selected to mediate the formation of palladium and platinum containing particles from the organometallic precursors $[Pd_2(DBA)_3]$ and $[Pt_2(DBA)_3]$, respectively. Regions of sequence similarity are marked by boxes. Isolates that mediate the formation of particles from $[Pd_2(DBA)_3]$ are highlighted in red. Isolates that mediate the formation of particles from $[Pt_2(DBA)_3]$ are highlighted in green.

Pd_S017 [2] 5′-UAACUAGUCGCGAAGAGAAGCGUAUUAUUCUCAUCGGUUC-3′
Pd_S032 5′-GCAUCUAGCUACAAAGCUUUUUUCUAUUUGAUUCCUUCU-3′
Pt_S049 5′-UCCCAUCGCUACUUAUUCUAUUUUGAUACCUCGUUAUCUA-3′
Pt_S060 5′-UCCCAUCGAAUACUUAUUCUAUUUUUGAUCCUCGCCCUC-3′
Pt_S004 5′-UACCUACAAACAAUCUUAUUGUAUCUUACCUCCACCUCC-3′
Pt_S058 5′-AUUUUUCAUACAUCACUCUAGCUGCUAUUAUUCUUAAUUG-3′

**Figure 1.21.** Comparison of RNA isolates selected to mediate the formation of palladium and platinum containing particles from the organometallic precursors [$Pd(PPh_3)_4$] and [$Pt(PPh_3)_4$], respectively. Regions of sequence similarity are marked by boxes. Isolates that mediate the formation of particles from [$Pd(PPh_3)_4$] are highlighted in orange. Isolates that mediate the formation of particles from [$Pt(PPh_3)_4$] are highlighted in blue.

Pt_S074 5′-GUGGAAUAAGCCUAUGAGUAGCCCUUUGGAGCCCGACGC-3′
Pt_001 5′-GGGACUAGGAUCUAUGGGUAUGUCGCGGCCGUCGAGAUGCC-3′
Pt_002 5′-UCAAGGUUCUAGCGUUCUAUGGGUAUGUCGCUGCCGUCG-3′
Pt_013 5′-UGCAAAGGGGCAAUACGGCAACCGUUGUCUAUGGGUAAC-3′

Pd_S019 5′-CGCUACGACUCGGGAAGGGGUCCGUCGUGACAGUCGCUAUGUUC-3′
Pd_S021 5′-CGCACGACUCGGAAGGGGUCCGUCAGUGACGAGCGCAUGUUC-3′
Pt_041 5′-GUAAGGCGAAGGGGGCAGGGAUUACCUUCAUCCGCUUAGG-3′
Pt_044 5′-ACUGCCGGAAGGGGUCUGUGCACCGAAGGCGGGGGGGUA-3′

Pd_089 5′-CCCCUUCAAUCUUCAAUGUACCAACUAUAAAUGAACGCCC-3′
Pt_S090 5′-AUAGAUACACAUCCUCUAUCAUCCAUUAUCACAAAACAU-3′

**Figure 1.22.** Comparison of RNA isolates selected to mediate the formation of palladium and platinum containing particles from the organometallic precursors [$Pd_2(DBA)_3$], [$Pd(PPh_3)_4$], [$Pt_2(DBA)_3$] and [$Pt(PPh_3)_4$], respectively. Regions of sequence similarity are marked by boxes. Isolates that mediate the formation of particles from [$Pd_2(DBA)_3$] are highlighted in red. Isolates that mediate the formation of particles from [$Pd(PPh_3)_4$] are highlighted in orange. Isolates that mediate the formation of particles from [$Pt_2(DBA)_3$] are highlighted in green. Isolates that mediate the formation of particles from [$Pt(PPh_3)_4$] are highlighted in blue.

Further examination into the ability of individual RNA isolates to synthesize these unique palladium and platinum containing particles will provide additional information on such biomolecule-inorganic materials interactions.

## 1.4. Experimental Section

**Reagents.** All reagents were used without further purification. Tris(dibenzylideneacetone) dipalladium(0), tetrakis(triphenylphosphine) palladium(0), and tetrakis(triphenylphosphine) platinum(0) were purchased from Strem. Tris(dibenzylideneacetone) diplatinum(0) was purchased from Lancaster. Milli-Q water was treated with diethylpyrocarbonate (depc) prior to use to ensure nuclease- and protease-free water.

**Amplification of DNA Templates.** 5′-primer (5′-TAATACGACTCAC-TATAGGGAGACAAGAATAAACGCTCAA-3′) and 3′-primer (5′-GCCTGTTGT-GAGCCTCCTGTCGAA-3′) were purchased from Midland Certified, Inc. for use with the $[Pd_2(DBA)_3]$ and $[Pt(PPh_3)_4]$ selections. The above 5′-primer was used in conjunction with 3′-primer(LAG) (5′-CTACAGCATGCTCGACAGGCATCT-3′) purchased from Midland Certified, Inc. for use with the $[Pt_2(DBA)_3]$ and $[Pd(PPh_3)_4]$ selections. 1× *Taq* DNA Polymerase buffer (New England Biolabs, 10 mM KCl, 10 mM $(NH_4)_2SO_4$, 20 mM Tris-HCl, pH 8.8, 2 mM $MgSO_4$, 0.1% Triton X-100), 0.12 mM each of dATP, dCTP, dGTP, and dTTP, 2 mM $MgCl_2$, 1 μM each of 5′-primer and 3′-primer, and 0.1 U/μL *Taq* DNA Polymerase (New England Biolabs) were added to 3 nM (ss)dsDNA template. PCR was performed using the following reaction parameters: 95 °C, 2 minutes; multiple cycles of 95 °C, 30 seconds, 60 °C, 30 seconds, 72 °C, 45 seconds; hold at 4 °C. The dsDNA was purified using QIAquick PCR Purification Kit (Qiagen) and quantitated via UV-Vis spectroscopy.

**Generation of RNA Isolates.** RNA isolates were prepared by transcription of dsDNA templates. 5× T7 RNA Polymerase buffer (4% (w/v) PEG 8000, 40 mM Tris-HCl, pH 8.0, 12 mM $MgCl_2$, 5 mM dithiothreitol (DTT), 1 mM spermidine HCl, 0.002% Triton X-100), 0.2 mM each of ATP, CTP, GTP, and 5-(4-pyridymethyl)-uridine 5′-triphosphate (*UTP), 150 nM dsDNA template, 125 nM T7 RNA Polymerase (Promega), 0.8 U/μL RNase inhibitor (Promega) were incubated at 37 °C for 6 hours to yield 5-(4-pyridylmethyl)-uridine modified RNA transcripts (87-mer): 5′-GGGAGACAAGAATAAACGCTCGG-[40N]-TTCGACAGGAGGCTCACAACAGGC-3′ for the $[Pd_2(DBA)_3]$ and $[Pt(PPh_3)_4]$ selections; 5′-GGGAGACAAGAATAAACGCTCGG-[40N]-AGATGCCTGTCGAGCAT-GCTGTAG-3′ for the $[Pt_2(DBA)_3]$ and $[Pd(PPh_3)_4]$ selections. [α-$^{32}$P]-ATP body-labeled RNA was generated using the identical protocol but with the addition of 30 μCi of [α-$^{32}$P]-ATP. Size-exclusion membranes (Microcon 10, 10-kD cutoff) were used to separate the full-length RNA from the reaction buffer and any unincorporated NTPs. The reaction mixture was first concentrated onto the membranes by centrifugation and washed four times with buffer containing NaCl (1 mM), KCl (1 mM), $CaCl_2$ (1 mM), $MgCl_2$ (1 mM), and $Na_3PO_4$ (1 mM, pH 7.2) followed by two water (pH 7) washes to remove excess salts. The purified RNA was recovered from the membranes by resuspension in 50-100 μL of water. Non-radiolabeled RNA was quantitated by UV-Vis spectroscopy while radiolabeled RNA was quantitated by liquid scintillation counting using a Beckman Coulter LS-6500.

**Formation of Nanoparticles.** *$[Pd_2(DBA)_3]$ Selection*: RNA sequences (1 μM) were incubated in the presence of $[Pd_2(DBA)_3]$ (100 or 400 μM). The $[Pd_2(DBA)_3]$ was prepared in a glove box under argon atmosphere ($O_2$ < 1 ppm and $H_2O$ < 1 ppm). All glassware was

flame-dried. The [$Pd_2(DBA)_3$] metal was dissolved in freshly distilled (K, benzophenone) THF to give a concentration of 8 mM. This THF solution was then added to water (pH 7), giving an aqueous solution of 5% THF and 100 or 400 μM [$Pd_2(DBA)_3$]. The incubations were performed in aqueous solution for 2 hours at ambient temperature. For cycles 1-3, size-exclusion membranes (Microcon 100, 100-kD cutoff) were used to separate the RNA-bound particles from free RNA and unincorporated metal precursor. The reaction mixture was first concentrated onto the membranes by centrifugation and washed four times with buffer containing NaCl (1 mM), KCl (1 mM), $CaCl_2$ (1 mM), $MgCl_2$ (1 mM), and $Na_3PO_4$ (1 mM, pH 7.2) followed by two water (pH 7) washes to remove excess salts. The RNA-bound particles were recovered from the membrane by resuspension in 50-100 μL of water. In cycles 4 to 8, the 100-kD molecular size cutoff filter was followed by native polyacrylamide gel (6%) electrophoresis mobility shift-dependent partitioning. Slowly migrating bands, relative to the starting RNA transcript, that showed a dependence on both RNA and Pd were isolated. The RNA was electroeluted from the excised gel bands at a constant 10 W for 4 hours. Following electroelution, the RNA were concentrated onto 10-kD molecular size cutoff filter, desalted with three-column volumes of water and then recovered from the membrane by resuspension in 50-100 μL of water. Non-radiolabeled RNA was quantitated by UV-Vis spectroscopy while radiolabeled RNA was quantitated by liquid scintillation counting using a Beckman Coulter LS-6500. *[$Pt_2(DBA)_3$] Selection*: RNA sequences were incubated in the presence of [$Pt_2(DBA)_3$] (400 μM). The [$Pt_2(DBA)_3$] was prepared in a glove box under argon atmosphere ($O_2$ < 1 ppm and $H_2O$ < 1 ppm). All glassware was flame-dried. The [$Pt_2(DBA)_3$] was dissolved in freshly distilled (K, benzophenone) THF to

give a concentration of 8 mM. This THF solution was then added to water (pH 7), giving an aqueous solution of 5% THF and 400 μM [$Pt_2(DBA)_3$]. The incubations were performed in aqueous solution for 2 hours at ambient temperature. Initially (cycles 1-2), 1 μM RNA was utilized in the RNA-metal incubation (step 2). In cycles 3-6, the RNA concentration was decreased to 0.5 μM to increase the selectivity pressure of the selection. Size-exclusion membranes (Microcon 100, 100-kD cutoff) were used to select for particles that were formed in the presence of RNA. The reaction mixture was first concentrated onto the membranes by centrifugation and washed four times with buffer containing NaCl (1 mM), KCl (1 mM), $CaCl_2$ (1 mM), $MgCl_2$ (1 mM), and $Na_3PO_4$ (1 mM, pH 7.2) followed by two water (pH 7) washes to remove excess salts. The RNA-bound particles were recovered from the membrane by resuspension in 50-100 μL of water. *[$Pd(PPh_3)_4$] Selection*: RNA sequences were incubated in the presence of [$Pd(PPh_3)_4$] (400 μM). The [$Pd(PPh_3)_4$] was prepared in a glove box under argon atmosphere ($O_2$ < 1 ppm and $H_2O$ < 1 ppm). All glassware was flame-dried. The [$Pd(PPh_3)_4$] was dissolved in freshly distilled (K, benzophenone) THF to give a concentration of 8 mM. This THF solution was then added to water (pH 7), giving an aqueous solution of 5% THF and 400 μM [$Pd(PPh_3)_4$]. The incubations were performed in aqueous solution for 2 hours at ambient temperature. Initially (cycles 1-2), 1 μM RNA was utilized in the RNA-metal incubation (step 2). In cycles 3-10, the RNA concentration was decreased to 0.5 μM to increase the selectivity pressure of the selection. Size-exclusion membranes (Microcon 100, 100-kD cutoff) were used to select for particles that were formed in the presence of RNA. The reaction mixture was first concentrated onto the membranes by centrifugation and washed four times with buffer containing NaCl (1 mM), KCl (1 mM),

$CaCl_2$ (1 mM), $MgCl_2$ (1 mM), and $Na_3PO_4$ (1 mM, pH 7.2) followed by two water (pH 7) washes to remove excess salts. The RNA-bound particles were recovered from the membrane by resuspension in 50-100 μL of water. *$[Pt(PPh_3)_4]$ Selection*: RNA sequences were incubated in the presence of $[Pt(PPh_3)_4]$ (10 or 100 μM). The $[Pt(PPh_3)_4]$ was prepared in a glove box under argon atmosphere ($O_2$ < 1 ppm and $H_2O$ < 1 ppm). All glassware was flame-dried. The $[Pt(PPh_3)_4]$ was dissolved in freshly distilled (K, benzophenone) THF to give a concentration of 8 mM. This THF solution was then added to water (pH 7), giving an aqueous solution of 5% THF and 10 or 100 μM $[Pt(PPh_3)_4]$. The incubations were performed in aqueous solution for 2 hours at ambient temperature. Initially (cycle 1), 1 μM RNA was utilized in the RNA-metal incubation (step 2). In cycles 2-8, the RNA concentration was decreased to 0.5 μM to increase the selectivity pressure of the selection. Size-exclusion membranes (Microcon 100, 100-kD cutoff) were used to select for particles that were formed in the presence of RNA. The reaction mixture was first concentrated onto the membranes by centrifugation and washed four times with buffer containing NaCl (1 mM), KCl (1 mM), $CaCl_2$ (1 mM), $MgCl_2$ (1 mM), and $Na_3PO_4$ (1 mM, pH 7.2) followed by two water (pH 7) washes to remove excess salts. The RNA-bound particles were recovered from the membrane by resuspension in 50-100 μL of water.

**Reverse Transcription.** 0.5× 1$^{st}$ Strand Buffer (50 mM Tris-HCl, pH 8.3, 75 mM KCl, and 3 mM $MgCl_2$), 0.5 mM each of dATP, dCTP, dGTP and dTTP, 2 μM 3′ primer (LAG), and 0.4 U/μL AMV Reverse Transcriptase (New England Biolabs) were added to the RNA retained from the metal incubations. The RNA was reverse transcribed at 42 °C for 1

hour. Following reverse transcription, the enzyme was inactivated by heating at 72 °C for 15 minutes. The cDNA was brought forward into amplification without further purification.

**Transmission and Scanning Electron Microscopy.** Bright-field images were obtained using TEM that was performed at the University of North Carolina School of Dentistry using a Philips CM12 transmission electron microscope operating at 100 kV accelerating voltage. To prepare samples for analysis, an aqueous solution of RNA-bound particles was drop-cast onto carbon-coated copper TEM grids (formvar support, 300 mesh, Ted Pella). Bright-field images were captured digitally with Digital Micrograph using a Gatan 780 DualVison camera.

**Atomic Force Microscopy.** AFM images were obtained on a Digital Instruments Nanoscope IIIa in tapping mode. To prepare samples for AFM analysis, an aqueous solution of RNA-bound particles was drop-cast onto poly(lysine)-coated silicon wafers.

**Energy Dispersive X-ray Spectrometry.** EDS was performed at the Shared Materials Instrumentation Facility, Duke University using a Hitachi HF-2000 FEG TEM equipped with an Oxford Instruments Inca Energy 100 energy dispersive x-ray spectrometer. To prepare samples for EDS analysis, an aqueous solution of RNA-bound particles was drop-cast onto carbon-coated copper TEM grids (formvar support, 300 mesh, Ted Pella).

**Dideoxy-Mediated Bulk Sequencing of Evolved Pools.** *End-labeling 5′-primer*: Twenty picomoles of 5′-primer was end-labeled with 1 μM [$\gamma$-$^{32}$P]-ATP in the presence of 0.6 U/μL of bacteriophage T4 Polynucleotide Kinase (New England Biolabs). The reaction mixture was incubated at 37 °C for 30 minutes. Following the reaction, the polynucleotide kinase was inactivated by heating at 90 °C for 2 minutes. A 250 μL aliquot of water was

added and the labeling mixture was concentrated onto a 10-kD molecular size cutoff filter to remove kinase buffer and unincorporated phosphate. The end-labeled primer (*5′-primer) was then recovered from the membrane by resuspension in 25-50 μL of water. *Dideoxy Mediated Cycle Sequencing*: The ddNTP/dNTP terminator mixes were prepared using the following ratios for *Taq* DNA Polymerase: ddATP:dATP, 60:1; ddCTP:dCTP, 40:1; ddGTP:dGTP, 20:1; ddTTP:dTTP, 60:1. A 2 μL aliquot of the appropriate terminator mixture was added to a 4 μL aliquot containing the DNA template, 0.1 U/μL *Taq* DNA Polymerase, 1 μM *5′-primer, and 1× sequencing buffer. Therefore, for one sample, there are four terminator/reaction mixtures, each corresponding to the four deoxynucleotides. The sequencing reaction had undergone 30 cycles of PCR (95 °C, 2 min; 95 °C, 30 sec; 60 °C, 30 sec; 70 °, 30 sec; repeat for 30 cycles; hold at 4 °C). The reaction was quenched by adding an aliquot of stop solution. A 6 μL aliquot of each reaction was then loaded onto a preheated 10 % Native PAGE (2000 V, 50 mA, constant 30 W, ~ 3.5 h). The gel was imaged using a Packard Cyclone Storage Phosphor System and Packard OptiQuant Image Analysis Software.

**Cloning of Evolved Pools.** In preparation of cloning the dsDNA, the sample was amplified using standard PCR conditions (see "Amplification of DNA Templates"), incorporating a custom 5′-primer not previously used in the selection amplifications. The 5′ Cloning Primer (5CP, 5′-GGGAGACAAGAATAAACGCTCAA-3′), was synthesized by Midland Certified, Inc. The amplification product was purified using QIAquick PCR Purification Kit (Qiagen) followed by 6% PAGE purification. The dsDNA product was excised from the gel and electroeluted at a constant 10 W for 4 hours. Following

electroelution, the dsDNA were concentrated onto 30-kD molecular size cutoff filter, desalted with three-column volumes of water and then recovered from the membrane by resuspension in water. The resulting dsDNA were quantitated by UV-Vis spectroscopy. *Polishing dsDNA Templates*: Following the information provided with the PCR-Script™ Amp Cloning Kit (Stratagene) the dsDNA sample was polished using cloned 0.04 U/μL *Pfu* DNA Polymerase, 1× polishing buffer and 0.19 mM each of dATP, dCTP, dGTP, and dTTP. The polishing reaction was mixed gently and then incubated at 72 °C for 30 minutes. *Ligating the Insert to Vector*: The ligation reaction for ligating the sample insert with the vector incorporated 1 ng/μL pPCR Script Amp SK(+) cloning vector (Stratagene), 1× reaction buffer, 0.5 mM rATP, 0.3 μM polished dsDNA, 0.5 U/μL *Srf I* restriction enzyme, 0.4 U/μL T4 DNA Ligase, and water to a final volume of 10 μL. The ligation reaction was mixed gently and then incubated at 25 ºC for 2 hours. Following the incubation, the ligase was inactivated by heating at 65 °C for 10 minutes. *Transformations*: The XL10-Gold Kan® Ultracompetent cells (Stratagene) were thawed on ice and gently mixed by tapping. A 40 μL aliquot of cells was added to a chilled 1.5-mL eppendorf tube and a 1.6 μL aliquot of XL10-Gold β-mercaptoethanol mix (Stratagene) was added to the cells. The cells were swirled gently and incubated on ice for 10 minutes, with swirling every 2 minutes. A 2 μL aliquot of the ligation material was then added to the cells. The cells were incubated on ice for an additional 30 minutes. Following this incubation, the cells were heat pulsed in a 42 °C water bath for 30 seconds (the temperature and length of heat pulse is critical for obtaining the highest efficiencies). Following the heat pulse, the cells were placed on ice for 2 minutes;

then 0.45 mL of preheated (42 °C) $NZY^+$ broth was added to the cells and incubated at 37 °C for 1 hour with shaking at 250 rpm. A sterile spreader was used to plate the transformed cells onto already prepared LB Amp agar plates containing IPTG and X-Gal (Fermentas) for blue and white color screening. The plates were incubated at 37 °C for 15-18 hours. To insure the white colonies plated above do contain the recombinant insert and that only one insert is being incorporated into each of the *E. coli* cells, individual white colonies were picked with sterile toothpicks and streaked onto prepared LB Amp agar plates containing IPTG and X-Gal. These plates were then incubated for 15-18 hours at 37 °C. Following this incubation, the plates were placed at 4 °C to enhance the white color of the colonies.

**Sequencing of Evolved Pools.** *Inoculation of Colonies*: Following the 37 °C incubation of transformations plated on LB Amp Agar containing IPTG and X-Gal, individual white colonies were picked using a sterile toothpick and loaded into a 96-well inoculating plate (plate 1) containing 0.90 mL liquid LB Amp Agar (Fermentas). The samples were incubated overnight (16-18 h) at 37 °C with shaking at 222 rpm for cell enrichment. Following this first overnight inoculation, a 5 μL aliquot of inoculate was transferred to a second inoculating plate containing fresh liquid LB Amp agar for further cell enrichment. The second inoculation (plate 2) was incubated at 37 °C with shaking at 222 rpm overnight (16-18 h) while plate 1 was stored at 4 °C. Following the second set of inoculations, pellet of cells in plate 2 were formed by centrifuging the inoculation plate at 2700 rpm for 15 minutes. The liquid media was poured from the sample wells and the sample plate was inverted and gently tapped to remove excess media with careful attention not to loosen and dump the pellets. The plate 1 inoculations were transferred to plate 2, plate

2 was centrifuged once more to concentrate and pellet the cells, and the liquid media was removed. *Alkaline Lysis of Cells*: The bacterial alkaline lysates were prepared using the Bio Robot 9600 (Qiagen) courtesy of the Genome Research Laboratory (GRL), Centennial Campus, NC State University. The following protocol was performed: Each bacterial pellet was resuspended in 0.3 mL Buffer R1 containing RNase I enzyme and mixed by vortexing the 96-well sample block for 10 minutes. A 0.3 mL aliquot of Buffer R2 was added to each well and the block was vortexed for 2 minutes and incubated at room temperature for 5 minutes. Following the room temperature incubation, a 0.3 mL aliquot of Buffer R3 was added to each well and the block was vortexed for an additional 2 minutes. A QIAfilter 96-well plate (Qiagen) was placed in position on the QIAvac 96 manifold while a collection block was placed into the base of the manifold. The lysates were then transferred from the sample block to the wells of the QIAfilter 96-well plate. Vacuum was applied (-200 to –300 mbar) until the lysates were completely transferred to the collection block in the base of the manifold. To desalt and concentrate the dsDNA, 0.7-volumes of room temperature isopropanol was added to each well, the block was taped and mixed immediately by inverting three times. The collection block was centrifuged at 2800 rpm for 15 minutes at room temperature to pellet the plasmid DNA. The supernatant was removed by quickly inverting the collection block followed by tapping to remove residual supernatant. Each pellet was then washed with 0.5 mL of 70% ethanol and centrifuged at 2800 rpm for 2 minutes to re-concentrate the pellets. The wash solution was removed using the same technique mentioned previously and the pellets were dried under vacuum. The dsDNA pellets were redissolved in 35 μL of 10 mM Tris-Cl, pH 8.5 and quantitated by UV-Vis spectroscopy. *BigDye*

*Terminator Cycle Sequencing*: To each well of a 96-well PCR plate the following material was added: 4 μL of BigDye Terminator Mix (containing $MgCl_2$, dNTPs, enzyme and reaction buffer), 0.32 μM of 5′ Sequencing Primer (5SP, 5′- GTAATACGACTCACTATA-GGGC-3′), 200-500 ng of dsDNA template and water to a final volume of 10 μL. Cycle sequencing was performed using a GeneAmp 9700 thermocycler: 96 °C, 10 sec; 50 °C, 30 sec, 60 °C, 4 min, repeat for 30 cycles; hold at 4 °C. *Purification of Cycle Sequencing*: A 96-well short plate (Edge BioSystems Performa® DTR) was centrifuged at 1141 rpm for 8 minutes to remove storage buffer; the eluate was discarded. The sequencing reaction samples were brought up to 20 μL with water and were then transferred to the center of each purification column in the 96-well short plate. The short plate was then centrifuged at 1141 rpm for 5 minutes and the eluate containing the purified dsDNA product retained. The sequences were identified on an Applied Biosystems ABI 3700#1 sequencer (Genome Research Laboratory, NC State University).

## 1.5. References


1. Cha, J. N.; Stucky, G. D.; Morse, D. E.; Deming, T. J. *Nature* **2001**, *403*, 289.
2. Belcher, A. M.; Wu, X. H. *Nature* **1996**, *381*, 56.
3. Hartgerink, J. D.; Beniash, E.; Stupp, S. I. *Science* **2001**, ***294***, 1684.
4. Whitling, J. M.; Spreitzer, G.; Wright, D. W. *Adv. Mater.* **2000**, *12*, 1377.
5. Whaley, S. R.; English, D. S.; Hu, E. L.; Barbara, P. F.; Belcher, A. M. *Nature* **2000**, *405*, 665.
6. Mao, C. B.; Flynn, C. E.; Hayhurst, A.; Sweeney, R.; Qi, J.; Georgiou, G.; Iverson, B.; Belcher, A. M. *Proc. Natl. Acad. Sci. U.S.A.* **2003**, *100*, 6946.
7. Mahtab, R.; Harden, H. H.; Murphy, C. J. *J. Am. Chem. Soc.* **2000**, *122*, 14.
8. Cao, Y.; Jin, R.; Mirkin, C. A. *J. Am. Chem. Soc.* **2001**, *123*, 7961.
9. Loweth, C. J.; Caldwell, W. B.; Peng, X. G.; Alivisatos, A. P.; Schultz, P. G. *Angew. Chem. Int. Ed. Engl.* **1999**, *38*, 1808.
10. Mertig, M.; Ciacchi, L. C.; Seidel, R.; Pompe, W.; De Vita, A. *Nano Lett.* **2002**, *2*, 841.
11. Dewey, T. M.; Mundt, A. A.; Crouch, G. J.; Zyzniewski, M. C.; Eaton, B. E. *J. Am. Chem. Soc.* **1995**, *117*, 8474.
12. Dewey, T. M.; Zyzniewski, M. C.; Eaton, B. E. *Nucleosides Nucleotides* **1996**, *15*, 1611.
13. Initial partitioning rounds gave ~0.5% RNA retained by the Microcon filter as determined by scintillation counting of [$\alpha$-$^{32}$P]-ATP body–labeled RNA.
14. If the partitioning of step 3was 100% effective at separating the active from the inactive RNA sequences, this would be a one-cycle technique. However, only a small fraction (~hundreds) of the starting $10^{14}$ RNA sequences are active, making it likely that a small

amount of inactive RNA sequences are carried along in step 3. Consequently, the cycle must be repeated several times.

15. Walter, J. *Adv. Mater.* **2000**, *12*, 31.

16. Joyce, G. F. *Nature* **2002**, *420*, 278.

17. Gugliotti, L. A.; Feldheim, D. L.; Eaton, B. E. *Science* **2004**, *304*, 850.

# CHAPTER 2: RNA-MEDIATED CONTROL OF NANOPARTICLE SHAPE

## 2.1. Introduction

The size, shape and crystal structure of a solid-state material can have a profound impact on its chemical and physical properties. The optical properties and catalytic activities of metals,[1,2] the magnetic moments of metal oxides,[3] and the electron transport characteristics of semiconductors,[4] for example, all change dramatically with crystal size, polymorph, and macroscopic morphology. Despite the importance of controlling the crystal morphology, modern crystal engineering remains largely an empirical discipline with few exceptions. Crystal size and shape are typically manipulated by controlling growth kinetics. This can be accomplished by adjusting monomer concentration and temperature and by adding small molecules, surfactants, or polymeric capping reagents.[5-7] While the molecular-level interactions between capping reagents and a growing crystal are currently unknown for many systems, it is generally postulated that an additive binds to the crystal in a face-selective fashion. This can slow the growth of that face relative to other growth directions, resulting in highly anisotropic crystal shapes.[8] Choosing the correct additive is crucial and largely a trial-and-error process. If the binding interactions between the capping reagent and a crystal are too strong, only very small crystal nuclei will form. If they are too weak, face-selective growth will not occur.

Nature has provided some of the best examples of selective materials crystal growth. Numerous bacteria, viruses and other living organisms on earth synthesize a solid-state material, some for structural integrity or protection, others for biosphere function such as

light focusing[9] or magnetotaxis.[10] Many of these functions have now been mimicked in the lab. Proteins, peptides and ampiphilic monolayers that closely resemble nature's ability to form materials have been isolated. Biomimetic methods have been used to prepare oriented hydroxyapatite crystal similar to human bone, silica fibrils reminiscent of marine sponges, and porous calcium carbonate networks such as those found in marine brittlestars.[11-13] These methods have been extended to the formation of other materials not found in nature such as metallized DNA wires[14] and viral-templated liquid crystals.[15] Many of these biomimetic syntheses utilize protein or peptide fragments. Given recent developments in RNA catalysis, it was of interest to determine if selected sequences[16] of this highly structured biopolymer could also control materials crystal growth.

A new approach to the discovery of unique RNA sequences that can mediate crystal growth and direct crystal shape was previously described in Chapter 1.[16] Modified (4-pyridyl-uridine) RNA libraries[17,18] were used and *in vitro* selection based on particle size was performed until a small subset of sequences was found that mediated the formation of thin (ca. 20 nm) hexagonal palladium containing plates from the zerovalent metal complex tris(dibenzylideneacetone) dipalladium(0) ($[Pd_2(DBA)_3]$). RNA *in vitro* selection[19-25] has a number of attributes as an alternative materials synthesis tool. A large number of sequences and crystals can be screened simultaneously and selected for a desired size or shape. In addition, RNA-mediated evolution is performed in a cyclic process, multiple times until the selected property emerges. During this process, mutations can occur that alter the interactions between a pool of RNA sequences and their concomitant growing crystal. When successful, this materials evolution process ultimately converges on RNA structures that

reproducibly fold into intricate 3D structures dictated by their sequence. This leads to the questions we pose herein: Do all evolved sequences in a given family (Figure 2.1, p. 48) yield the same particle shape? Is the metal, ligand or both important in the growth process, or is the particle shape controlled exclusively by the folded RNA acting as a template? Is the entire RNA molecule required or will truncated sequences maintain activity toward particle shape control? Is the pyridyl-modified uridine used to discover the RNA sequences required, or can native uridine be used in its place?

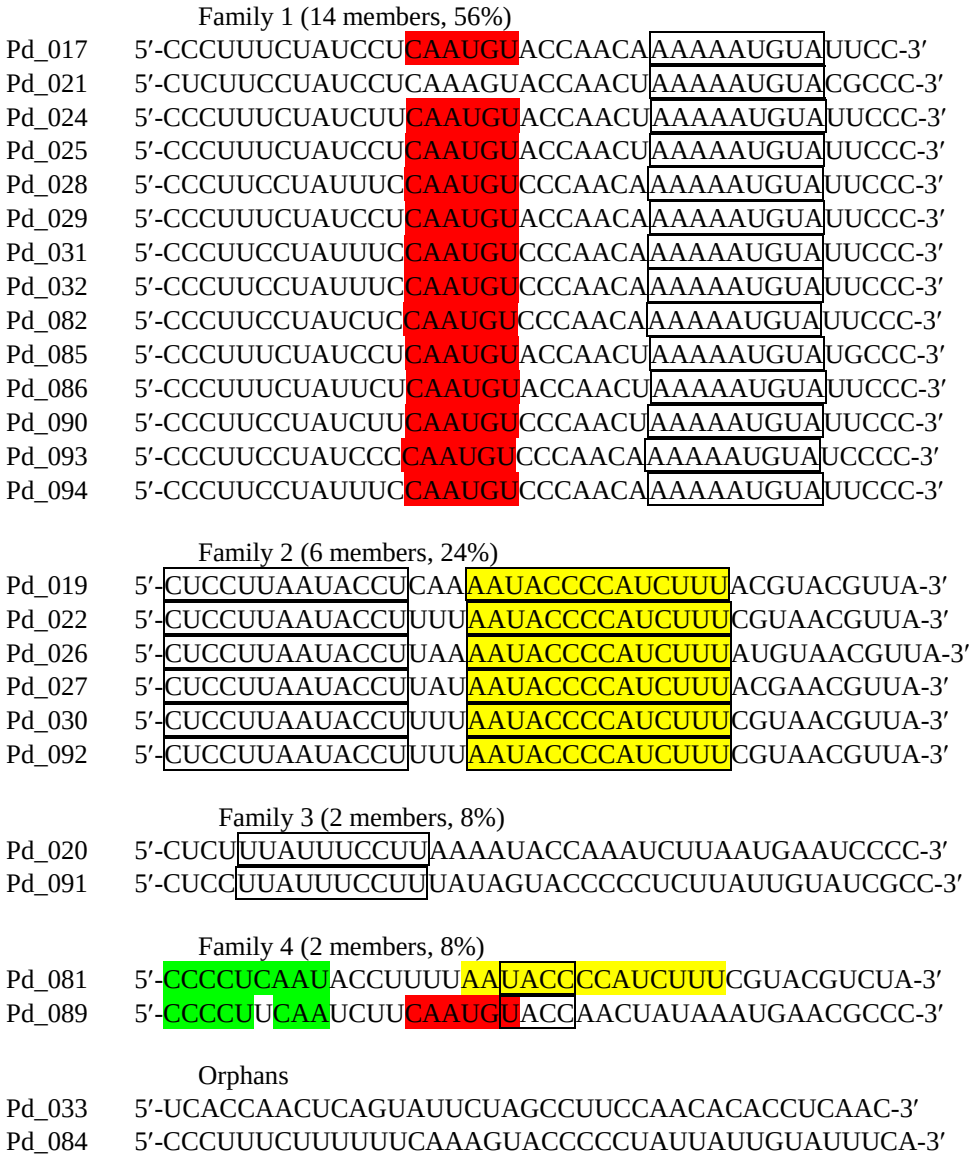


**Figure 2.1.** Evolved RNA sequences capable of mediating the formation of hexagonal Pd containing platelets. The sequences are grouped into families related by highly conserved regions (shown in color).[16]

## 2.2. Results and Discussion

The RNA *in vitro* selection that gave the sequences capable of synthesizing hexagonal Pd containing particles (Pdases) was previously reported (refer to Chapter 1, p. 9, for experimental scheme).[16]

### 2.2.1. Sequence-dependent Pd Containing Particle Growth

From Figure 2.1 (p. 48) it is clear that the selection converged on highly conserved sequences. It was of interest to determine if all of these sequences in fact assembled the same shape and size Pd containing particle. However, significant sequence variability was found outside the conserved region, and this portion of the molecule might play an important role in dictating crystal growth and shape. When representative sequences from each respective family were incubated with $[Pd_2(DBA)_3]$ individually (isolates 17, 19, 20, 81 and 84), each was found to yield hexagonal Pd containing plates exclusively, consistent with crystal shape being correlated with the conserved sequence motif (Figure 2.2).

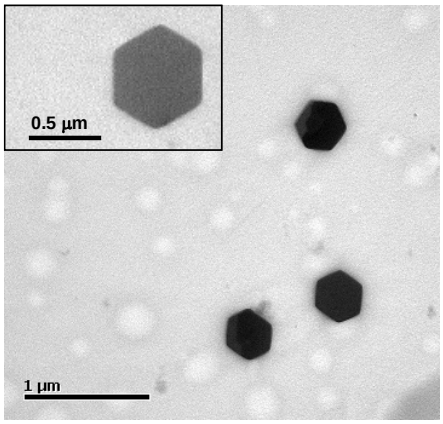


**Figure 2.2.** TEM micrograph of hexagonal palladium containing particles formed in the presence of Pdase 17.[26]

As previously discussed in Chapter 1, EDS analysis revealed that these hexagonal particles do contain palladium. For a more quantitative analysis to determine the chemical composition of these particles, electron energy loss spectroscopy (EELS) was performed. Results from the EELS spectrum (data not shown) show the hexagonal particles to contain palladium, in addition to a high content of carbon. It should be noted that the sample used for the aforementioned EELS analysis, relative to the well-shaped hexagons used in previous experiments, was of poor quality: the corners of the hexagons were rounded in shape rather than sharply defined and a film-like material was observed along the particle surface.

There are a number of possibilities, or a combination thereof, that may contribute to the high carbon content observed. Several sources of such carbon include hydrocarbon contamination, carbon associated with the RNA molecules, the dibenzylideneacetone ligands and the molecular [$Pd_2(DBA)_3$] complex. Hydrocarbon contamination can be introduced into a sample during TEM grid preparation and grid transfer and insertion into the sample chamber. It is probably that this contamination contributes in some way to the carbon source. A second possibility is that the high carbon content is a result of the RNA bound to the particle. While definitive conclusions cannot be made at this time on the location and number of RNA molecules bound to each particle, it is not probable that the RNA is the main source of this result. Additional nitrogen and phosphorous electron energy loss peaks corresponding to the RNA bound molecules should be observed; these nitrogen and phosphorous peaks were absent in the spectrum. Another probable source of this carbon content may be a result of the dibenzylideneacetone ligands themselves. To date, the mechanism of particle formation is not known. As the dibenzylideneacetone ligands are

displaced from the organometallic precursor it is possible that they become incorporated either between or within layers and/or clusters of palladium atoms during particle growth. Also, free ligand may not be effectively purified from the incubation reactions and thus becomes deposited on the sample grids along with the particles. These free ligands may result in the amorphous film that is observed along the particle surface. Lastly, there is the possibility that the RNA is templating the crystallization of molecular $[Pd_2(DBA)_3]$. It does not seem probable that this carbon source is due to $[Pd_2(DBA)_3]$ crystals as the observed peak height ratio of oxygen to palladium from the EDS results (Figure 1.4, p. 13) should reflect an approximate 3:2 mole ratio. Further analysis on well-shaped hexagonal particles is necessary to accurately define the chemical composition of these particles.

A combination of high-resolution TEM (HR-TEM) and electron diffraction was used to determine whether these hexagonal palladium containing particles were crystalline. Lattice fringes are observed in the HR-TEM image, albeit not uniformly throughout the particle surface, but rather present in localized areas (Figure 2.3A, p.52). These areas may be a result of the particle surface being heated by the electron beam and thus forming domains of crystalline material. Additional diffraction data needs to be obtained over a time-course to determine whether the beam is indeed heating the particles and forming these fringes.

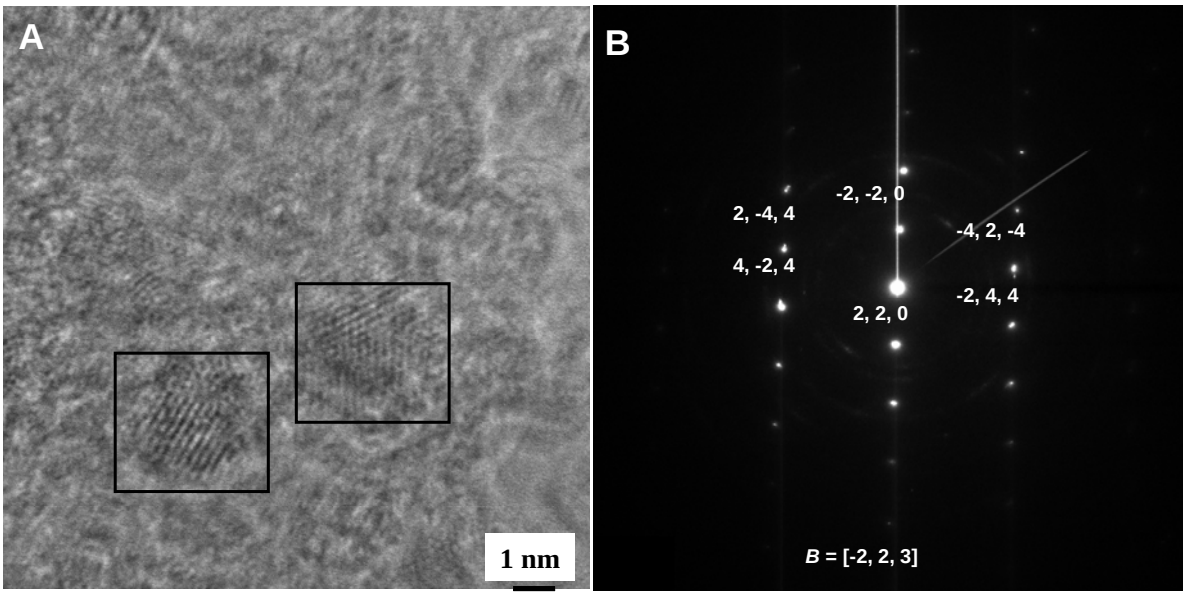


**Figure 2.3.** (A) High-resolution TEM image obtained from a single hexagonal palladium containing particle. Localized areas of observed lattice fringes are marked in boxes. Accelerating voltage: 200 kV; Magnification: 1,500,000×. (B) Electron diffraction obtained from a single hexagonal palladium containing particle. Accelerating voltage: 80 kV; Camera length: 60 cm; Tilt (x/y): 21.5 °, 2.4 °.

Initial electron diffraction studies performed on the hexagonal particles were achieved using an accelerating voltage of 200 kV. Radiation damage to the hexagonal particles, as observed by the formation of holes in the particle surface, was occurring as a result of the particle being exposed for an extended period of time to the electron beam. Decreasing the accelerating voltage to 80 kV eliminated this radiation damage and allowed for diffraction to be obtained at various tilt angles. A representative diffraction spot pattern from a single hexagonal particle resembles one that would be expected from a face-centered cubic crystal (Figure 2.3B). A lattice constant for this pattern was found experimentally to be 10.9 Å, approximately 2.8-fold larger than the theoretical lattice constant of 3.9 Å for face-centered cubic palladium metal. The idea of the RNA templating the formation of these

particles along an extended unit cell has not been explored; however, additional studies are required to determine the exact packing structure of the hexagonal particles.

In contrast to the RNA Pdases of the sequences families, orphan sequence Pdase 34 (5′-UCCAACAUCUUUUAAUUUUGUGGCGUCCACAUAUCAUCCA-3′) yielded cubic shaped particles exclusively (Figure 2.4). The average size ($w \times l$) of cubic particles formed in 2 hours was 0.10 μm ± 0.05 μm × 0.07 μm ± 0.02 μm. EDS analysis was performed on these particles and the results show these particles to contain palladium (data not shown).

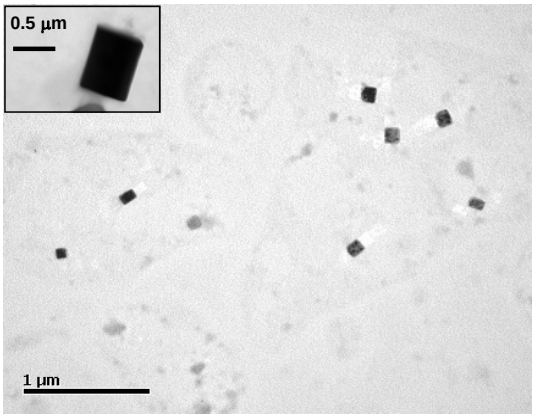


**Figure 2.4.** TEM micrograph of cubic palladium containing particles formed in the presence of Pdase 34.[26]

To determine the crystalline nature of these cubic palladium containing particles, electron diffraction was performed using an accelerating voltage of 200 kV. Figure 2.5 (p. 54) displays two representative diffraction patterns obtained from a cubic particle: a ring pattern, obtained near the edge of the particle, characteristic of a polycrystalline material; a spot pattern, obtained in the center of the particle, characteristic of a single crystalline material. Several experimental d-spacings for the ring pattern were calculated and found to

be in close agreement to reported values for face-centered cubic palladium metal (Table 2.1, p. 55). Additionally, the spot pattern obtained resembles a pattern to be expected from a face-centered cubic crystal. The lattice constant for this pattern was found experimentally to be 4.4 Å, slightly larger (by 0.5 Å) than what would be expected for face-centered cubic palladium metal. To explore the possibility that these particles are crystalline $[Pd_2(DBA)_3]$, the experimental d-spacings for the cubic particles were compared to theoretical d-spacings for molecular $[Pd_2(DBA)_3]\bullet CHCl_3$ (Table 2.2, p. 55). These results, in conjunction with the EDS and EELS data for the hexagonal particles, are not the results that would be expected for crystals of molecular $[Pd_2(DBA)_3]$.

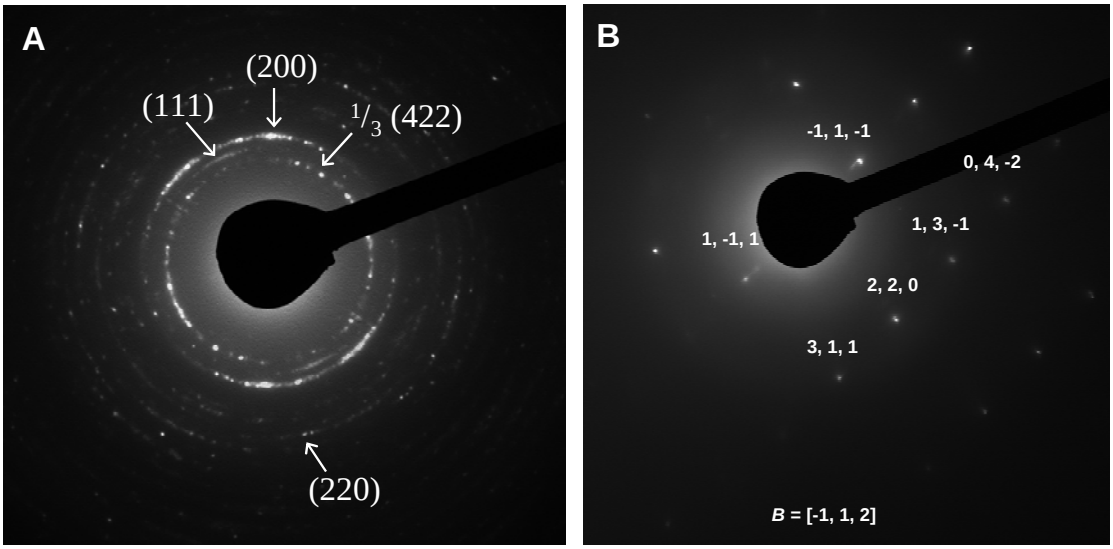


**Figure 2.5.** Electron diffraction obtained from a single cubic palladium containing particle (A) near the edge and (B) in the center of the particle. Accelerating voltage: 200 kV; Camera length: 40 cm; Tilt (x/y): 0 °, 0 °.

**Table 2.1.** Comparison of Experimental d-spacings for Cubic Palladium Containing Particles and Reported d-spacings for Face-centered Cubic Palladium Metal

| (*h, k, l*) | Expt. d-spacings (Å) *(cubic particles)* | Reported d-spacings (Å) *(f.c.c. palladium metal)* |
|---|---|---|
| $^1/_3$ (4 2 2) | 2.46 | 2.38 |
| (1 1 1) | 2.18 | 2.24 |
| (2 0 0) | 2.00 | 1.94 |
| (2 2 0) | 1.40 | 1.37 |

**Table 2.2.** Theoretical d-spacings[27] for Molecular $[Pd_2(DBA)_3]$ ]•$CHCl_3$

| (*h, k, l*) | Theor. d-spacings (Å) |
|---|---|
| (0 1 0) | 13.49 |
| (1 0 0) | 12.14 |
| (0 0 1) | 11.58 |
| (1 1 1) | 5.78 |
| (2 0 0) | 6.07 |
| (2 2 2) | 4.15 |
| (3 1 1) | 3.28 |

It seemed reasonable that Pdase sequence families made related palladium containing particle shapes and that the conserved motif was essential in determining particle shape, but it was unclear what role the more variable parts of the sequence played. To investigate the importance of these more variable sequence regions on particle formation, two new truncated RNA sequences were enzymatically synthesized from chemically prepared DNA templates (Figure 2.6, p. 56). In one sequence (truncate 1), the 3′-fixed region was removed from the full-length Pdase 17 template, leaving only the conserved sequence and variable portion. In the second sequence (truncate 2), the 3′-fixed region and four nucleotides of the variable region were removed from the original Pdase 17 template. Both truncates were subjected to the $[Pd_2(DBA)_3]$ precursor under identical incubation and partitioning conditions used in the

selection (e.g., ambient temperature for 2 hours), and the resulting material was analyzed by TEM. Both hexagonal and spherical particles were observed with truncate 1, while particles of undefined shape were observed with truncate 2.[26] The estimated yield as determined by TEM of particles generated with truncates 1 and 2 was relatively poor in comparison with the full-length Pdase 17. These results suggest that the fixed region of the sequence must function in the structural context of the variable region in maintaining the required 3D structure for creating the hexagonal Pd containing particles.

5′--23 Fixed--CCCUUUCUAUCCUCAAUGUACCAACAAAAAAUGUAUUCC---24 Fixed--3′

5′--23 Fixed—CCCUUUCUAUCCUCAAUGUACCAACAAAAAAUGUAUUCC--3′

5′--23 Fixed—CCCUUUCUAUCCUCAAUGUACCAACAAAAAAUGUA--3′

**Figure 2.6.** Full-length 87-mer Pdase 17 sequence (top) and the 3′-truncated sequences examined for the ability to mediate the formation of Pd containing hexagons. Truncate 1 (middle) was a 62-mer, and truncate 2 (bottom) was a 58-mer. Conserved region is underlined.[26]

### 2.2.2. Modified-UTP Dependence

In the original selection experiments it was postulated that pyridyl modification could provide added diversity in Pd-ligand interactions and that expanding the chemical diversity of the RNA would be advantageous. However, it remained to be tested if in fact the pyridyl modification provided any benefit at all in these sequences. The importance of the pyridyl modification was examined by replacing pyridyl-modified UTP with native UTP for both Pdase 17 and 34 and examining the particle formation for the resulting RNA molecules. In both cases, no examples of hexagonal or cubic Pd containing particles were observed and

only a low yield of spherical particles was found by TEM.[26] As positive controls, both hexagonal and cubic palladium containing particles were formed using the pyridyl-modified Pdase 17 and 34. Knowing that the pyridyl group was important for Pdase activity and that this was a good ligand for $Pd^0$, it was of interest to determine how the Pd precursor ligands might influence particle growth.

### 2.2.3. Metal and Ligand Dependence

The RNA Pdase sequences showed rapid kinetics in particle growth (> 1 μm in 1 minute). An essential part of any Pd metal particle growth mechanism requires the elimination of ligands. This elimination process could occur by associative or dissociative processes where the RNA played a role in displacing the ligands or stabilizing coordinatively unsaturated Pd intermediates. If Pd-ligand bonds were important, then studying other metal-ligand combinations in the group VIII triad (Ni, Pd and Pt) as precursors for the Pdases might reveal differences in metal particle size and shape. It is well-known that metal-ligand bond strengths increase moving down this triad in the periodic table. It was of interest to determine if the Pdases were capable of discriminating different metal precursors, either Pd with different ligands or the transition metals of the same triad (Pt and Ni). The effects of changing the group VIII metal precursor on particle shape and size were studied both with isolates 17 and 34. Pyridyl-modified Pdases 17 and 34 (1 μM) were incubated in the presence of various metal precursors (400 μM) for 2 hours at ambient temperature, and the resulting particles were examined by TEM. Focusing first on the results for Pdase 17, changing the metal center to Pt, while retaining the DBA ligands, resulted in a 4.9:1.1:1 ratio

of hexagonal:cubic:spherical Pt containing particles (Figure 2.7, Table 2.3, p. 59). Growth of hexagonal particles was 0.22 μm in 2 hours compared to 1.24 μm ± 0.57 μm for the same sequence with $[Pd_2(DBA)_3]$. Changing the ligand to triphenylphosphine ($PPh_3$) resulted in formation of spherical particles only, independent of the metal center (Pd, Pt or Ni). When $[Pt(PPh_3)_4]$ was used as a precursor, particles only reached a size of ca. 7 nm, compared to > 200 nm for all other precursors.[26]

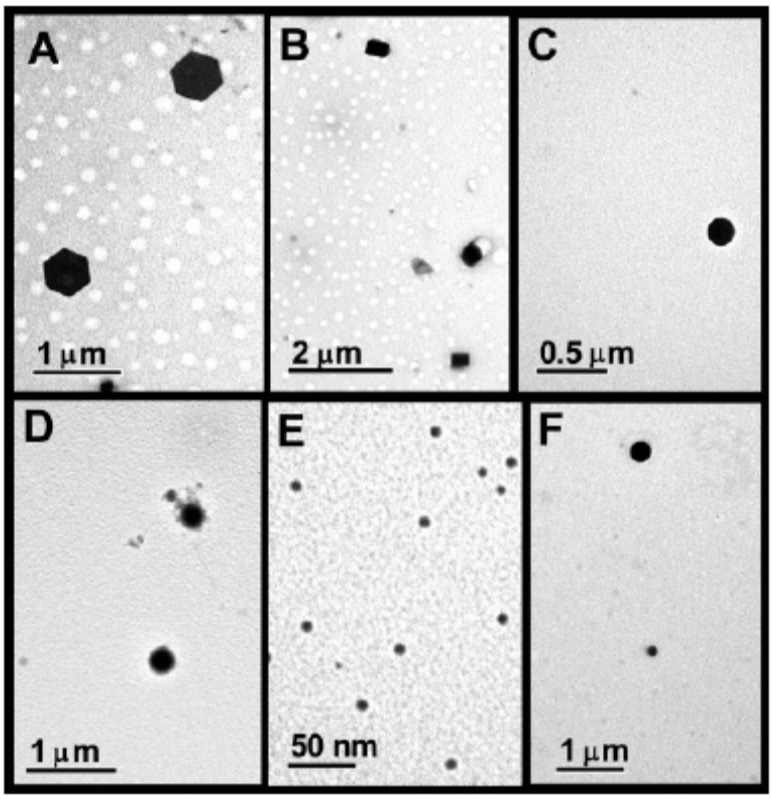


**Figure 2.7.** TEM images of particles formed with Pdase 17 and (A-C) $[Pt_2(DBA)_3]$, (D) $[Pd(PPh_3)_4]$, (E) $[Pt(PPh_3)_4]$ and (F) $[Ni(PPh_3)_4]$.[26]

**Table 2.3.** Metal Precursor Effects on Particle Shape and Size

| RNA Isolate | Metal Precursor | Particle Shape | Size (μm) | % Population* |
|---|---|---|---|---|
| 17 | $[Pd_2(DBA)_3]$ | hexagonal | 1.24 ± 0.57 | 100 |
| | $[Pt_2(DBA)_3]$ | spherical | 0.10 ± 0.06 | 14 |
| | | cubic | 0.22 ± 0.13 | 16 |
| | | hexagonal | 0.46 ± 0.22 | 69 |
| | $[Pd(PPh_3)_4]$ | spherical | 0.27 ± 0.16 | 100 |
| | $[Pt(PPh_3)_4]$ | spherical | 0.007 ± 0.003 | 100 |
| | $[Ni(PPh_3)_4]$ | spherical | 0.27 ± 0.10 | 100 |
| 34 | $[Pd_2(DBA)_3]$ | cubic | 0.10 ± 0.05 × 0.07 ± 0.02 | 100 |
| | $[Pt_2(DBA)_3]$ | spherical | 0.16 ± 0.05 | 2 |
| | | cubic | 0.14 ± 0.07 | 29 |
| | | hexagonal | 0.37 ± 0.16 | 68 |
| | $[Pd(PPh_3)_4]$ | spherical | 0.31 ± 0.29 | 100 |
| | $[Pt(PPh_3)_4]$ | spherical | 0.009 ± 0.007 | 100 |
| | $[Ni(PPh_3)_4]$ | spherical | 0.24 ± 0.10 | 100 |

* The entire TEM grid was examined for all types of materials formed. Percentages represent the amount of these materials observed on the grid from the total population.

When $[Pt_2(DBA)_3]$ was incubated with Pdase 34, hexagonal and cubic particles were the major shapes observed. Changing the ligand to $PPh_3$, however, again resulted in spherical shaped particles by the RNA for all metals examined. Taken together, these results imply a correlation between Pd or Pt ligand-metal bond strength and shape control of the RNA Pdase to create hexagonal particles. The weaker $\sigma$ donor ligands DBA as compared to triphenylphosphine gave consistently higher yields of hexagonal particles for both Pd and Pt.

## 2.3. Conclusion

The goals of this study were to better understand the effects of RNA primary sequence and metal precursor on RNA-mediated growth of metal particles. Perhaps the most

surprising result was the discovery of a sequence (Pdase 34) that codes for Pd containing cubes rather than hexagonal platelets, the exclusive product of all other sequences studied to date. Though sharing the same 5′- and 3′-fixed sequence regions, Pdases 17 and 34 are individually unique by way of their evolved sequence regions and do not share a common conserved region (Figure 2.1, p. 48). While the deeper fundamental structural origins for the observed differences are not known at this time, the implication of the result is that a single *in vitro* selection can result in multiple catalytic RNA sequences, which, depending on their structure, assemble discrete crystal shapes with high degree of specificity.

The results obtained from Pdase 17 sequence truncates 1 and 2 provide information regarding the length of RNA template required to mediate the formation of hexagonal Pd containing particles. It appears that the four nucleotide bases between the conserved region and the fixed 3′-region, or a portion thereof, are somehow critical to the structure of the Pdase and its ability to direct particle shape with a high degree of specificity. Removing these regions likely disrupts a critical folding motif necessary for proper interaction with the precursor complex and juxtaposition of the growing particle with incoming $Pd^0$ fragments. The precise length of the fixed 3′-region that is necessary to exclusively form hexagons has yet to be determined.

Replacing the pyridyl-modified uridine with native uridine resulted in a complete loss of RNA catalytic activity. This loss of activity could be a combination of changes in the 3D structure or the absence of an essential function group at the catalytic site. The metal-ligand dependence on both the rate of particle formation as well as the specificity of crystal shape might suggest that ligand elimination is an important aspect of the particle growth

mechanism. It remains to be determined if the pyridyl modification plays an active role in either the associative or dissociative elimination of DBA ligands from the Pd precursor organometallic complex.

In addition to sequence-dependent shape control, it is apparent that formation of Pd containing particles is highly dependent upon the ligand of the precursor complex. Changing the metal from Pd to Pt, while keeping the DBA ligand constant, did not compromise the ability of Pdases 17 and 34 to form particles, but did result in a slight decrease in shape specificity with a wider range of products being observed (cubes, hexagons and spheres). However, in the case of Pdase 17, changing the ligand from DBA to the more tightly bound triphenylphosphine was detrimental to size of the particles produced as observed by TEM.

Taken together, the results show that the full-length Pdases 17 and 34 evolved through the course of the *in vitro* selection to recognize a specific metal-ligand set, $[Pd_2(DBA)_3]$. Changes in sequence length, base composition, metal and ligand all affect the ability of these RNA sequences to mediate the formation of metal particles. These results suggest highly structured catalytic sites in these Pdases that can discriminate between metal precursors and their associated ligands. Interestingly, for the Pd and Pt DBA complexes, shape specificity was largely preserved favoring the formation of previously unknown hexagonal Pt particle plates. Consistent with increased metal-ligand bond strength and Pdase 17 playing an active role in elimination of ligand, the Pt particles were significantly smaller than the Pd particles under the same incubation conditions.

## 2.4. Experimental Section

**Reagents.** All reagents were used without further purification. Tris(dibenzylideneacetone) dipalladium(0), tetrakis(triphenylphosphine) palladium(0), and tetrakis(triphenylphosphine) platinum(0) were purchased from Strem. Tetrakis(triphenylphosphine) nickel(0) was purchased from Acros. Tris(dibenzylideneacetone) diplatinum(0) was purchased from Lancaster. Milli-Q water was treated with diethylpyrocarbonate (depc) prior to use to ensure nuclease- and protease-free water.

**Amplification of DNA Templates.** 5′-primer (5′-TAATACGACTCACTATA-GGGAGACAAGAATAAACGCTCAA-3′) and 3′-primer (5′-GCCTGTTGTGAG-CCTCCTGTCGAA-3′) were purchased from Midland Certified, Inc. for use with Pdases 17 and 34. The above 5′-primer was used in conjunction with 3′-primer truncate 1 (5′-GGAATACATTTTTTGTT-3′) and with 3′-primer truncate 2 (5′-TACATTTTTTGTTGGT-3′) when amplifying Pdase 17 truncates 1 and 2, respectively. Both sets of truncate 3′-primers were purchased from Midland Certified, Inc. ssDNA templates for truncates 1 and 2 were synthesized and purified by SomaLogic, Inc. 1× *Taq* DNA Polymerase buffer (New England Biolabs, 10 mM KCl, 10 mM $(NH_4)_2SO_4$, 20 mM Tris-HCl, pH 8.8, 2 mM $MgSO_4$, 0.1% Triton X-100), 0.12 mM each of dATP, dCTP, dGTP, and dTTP, 2 mM $MgCl_2$, 1 μM each of 5′-primer and 3′-primer, and 0.1 U/μL *Taq* DNA Polymerase (New England Biolabs) were added to 3 nM (ss)dsDNA template. PCR was performed using the following reaction parameters: 95 °C, 2 minutes; multiple cycles of 95 °C, 30 seconds, 60 °C, 30 seconds, 72

°C, 45 seconds; hold at 4 °C. The dsDNA was purified using QIAquick PCR Purification Kit (Qiagen) and quantitated via UV-Vis spectroscopy.

**Generation of RNA Isolates.** RNA isolates were prepared by transcription of dsDNA templates. 1× T7 RNA Polymerase buffer (Promega, 4% (w/v) PEG 8000, 40 mM Tris-HCl, pH 8.0, 12 mM $MgCl_2$, 5 mM dithiothreitol (DTT), 1 mM spermidine HCl, 0.002% Triton X-100), 0.2 mM each of ATP, CTP, GTP, and 5-(4-pyridymethyl)-uridine 5′-triphosphate (*UTP), 150 nM dsDNA template, 125 nM T7 RNA Polymerase (Promega), and 0.8 U/μL RNase inhibitor (Promega) were incubated at 37 °C for 6 hours to yield 5-(4-pyridylmethyl)-uridine modified RNA transcripts (87-mer): 5′-GGGAGACAA-GAATAAACGCTCGG-[40N]-TTCGACAGGAGGCTCACAACAGGC-3′. Size-exclusion membranes (Microcon 10, 10-kD cutoff) were used to separate the full-length RNA from the reaction buffer and any unincorporated NTPs. The reaction mixture was first concentrated onto the membranes by centrifugation and washed four times with buffer containing NaCl (1 mM), KCl (1 mM), $CaCl_2$ (1 mM), $MgCl_2$ (1 mM), and $Na_3PO_4$ (1 mM, pH 7.2) followed by two water (pH 7) washes to remove excess salts. The purified RNA was recovered from the membranes by resuspension in 50-100 μL of water and quantitated by UV-Vis spectroscopy.

**Formation of Nanoparticles.** RNA sequences (1 μM) were incubated in the presence of the metal complex precursor (400 μM). The following metal precursors were investigated: tris(dibenzylideneacetone) dipalladium(0) ($[Pd_2(DBA)_3]$), tris(dibenzylideneacetone) diplatinum(0) ($[Pt_2(DBA)_3]$), tetrakis(triphenylphosphine) palladium(0) ($[Pd(PPh_3)_4]$), tetrakis(triphenylphosphine) platinum(0) ($[Pt(PPh_3)_4]$), and tetrakis(triphenylphosphine) nickel(0) ($[Ni(PPh_3)_4]$). The organometallic complexes were

prepared in a glove box under argon atmosphere ($O_2$ < 1 ppm and $H_2O$ < 1 ppm). All glassware was flame-dried. The metals were each dissolved in freshly distilled (K, benzophenone) THF to give a concentration of 8 mM. This THF solution was then added to water (pH 7), giving an aqueous solution of 5% THF and 400 μM organometallic precursor. The incubations were performed in aqueous solution for 2 hours at ambient temperature. Size-exclusion membranes (Microcon 100, 100-kD cutoff) were used to separate the RNA-bound metal containing particles from free RNA and unincorporated metal precursor. The reaction mixture was first concentrated onto the membranes by centrifugation and washed four times with buffer containing NaCl (1 mM), KCl (1 mM), $CaCl_2$ (1 mM), $MgCl_2$ (1 mM), and $Na_3PO_4$ (1 mM, pH 7.2) followed by two water (pH 7) washes to remove excess salts. The RNA-bound particles were recovered from the membrane by resuspension in 50-100 μL of water.

**Electron Microscopy.** Bright-field images were obtained using TEM that was performed at the University of North Carolina School of Dentistry using a Philips CM12 transmission electron microscope operating at 100 kV accelerating voltage. To prepare samples for analysis, an aqueous solution of RNA-bound particles was drop-cast onto carbon-coated copper TEM grids (Formvar support, 300 mesh, Ted Pella). Bright-field images were captured digitally with Digital Micrograph using a Gatan 780 DualVison camera. Diffraction analysis of hexagonal Pd containing particles generated by RNA Pdase 17 was performed at the W. M. Keck Laboratory for Atomic Imaging and Manipulation, Department of Physics and Astronomy, University of North Carolina at Chapel Hill using a JEM 2010F-FasTEM (point resolution of 0.23 nm and lattice resolution of 0.10 nm)

operating at 80 kV accelerating voltage. Diffraction analysis of cubic Pd contaning particles generated by Pdase 34 was performed at the Shared Materials Instrumentation Facility, Duke University using a Hitachi HF-2000 FEG TEM (point resolution of 0.23 nm and lattice resolution of 0.10 nm) operating at 200 kV. To prepare samples for diffraction analysis, an aqueous solution of RNA-bound particles was drop-cast onto lacey carbon-coated copper TEM grids (formvar support, 200 mesh, Ted Pella).

## 2.5. References


1. Tam, F.; Moran, C.; Halas, N. *J. Phys. Chem. B* **2004**, *108*, 17290-17294.
2. Jin, R.; Cao, Y.; Mirkin, C. A.; Kelly, K.; Schatz, G.; Zheng, J. *Science* **2001**, *294*, 1901-1903.
3. Liu, C.; Zhang, Z. J. *Chem. Mater.* **2001**, *13*, 2092-2096.
4. Huynh, W. U.; Dittmer, J. J.; Alivisatos, A. P. *Science* **2002**, *295*, 2425-2427.
5. Kirkland, A. I.; Jefferson, D. A.; Duff, D. G.; Edwards, P. P.; Gameson, I.; Johnson, B. F. G.; Smith, D. J. *Proc. R. Soc. London, Ser. A* **1993**, *440*, 589-609.
6. Busbee, B. D.; Obare, S. O.; Murphy, C. J. *Adv. Mater.* **2003**, *15*, 414-416.
7. Ahmadi, T. S.; Wang, Z. L.; Henglein, A.; El-Sayed, M. A. *Chem. Mater.* **1996**, *8*, 1161-1164.
8. Puntes, V. F.; Krishnan, K.; Alivisatos, A. P. *Top. Catal.* **2002**, *19*, 145-148.
9. Vukusic, P.; Sambles, J. R. *Nature* **2003**, *424*, 852-855.
10. Matsunaga, T.; Okamura, Y. *Trends Microbiol.* **2003**, *11*, 536-541.
11. Aizenberg, J.; Muller, D. A.; Grazul, J. L.; Hamann, D. R. *Science* **2003**, *299*, 1205-1208.
12. Cha, J. N.; Shimizu, K.; Zhou, Y.; Christiansen, S. C.; Chmelka, B. F.; Stucky, G. D.; Morse, D. E. *Proc. Natl. Acad. Sci. U.S.A.* **1999**, *96*, 361-365.
13. Hartgerink, J. D.; Beniash, E.; Stupp, S. I. *Science* **2001**, *294*, 1684-1688.
14. Yan, H.; Park, S. H.; Finkelstein, G.; Reif, J. H.; Labean, T. H. *Science* **2003**, *301*, 1882-1884.
15. Lee, S. W.; Lee, S. K.; Belcher, A. M. *Adv. Mater.* **2003**, *15*, 689-692.
16. Gugliotti, L. A.; Feldheim, D. L.; Eaton, B. E. *Science* **2004**, *304*, 850-852.

17. Dewey, T. M.; Zyzniewski, M. C.; Eaton, B. E. *Nucleosides Nucleotides* **1996**, *15*, 1611-1617.

18. Vaught, J.; Dewey, T. M.; Eaton, B. *J. Am. Chem. Soc.* **2004**, *126*, 11231-11237.

19. Eaton, B. E. *Curr. Opin. Chem. Biol.* **1997**, *1*, 10-16.

20. Nieuwlandt, D.; West, M.; Cheng, X. Q.; Kirshenheuter, G.; Eaton, B. E. *ChemBioChem* **2003**, *4*, 651-654.

21. Tarasow, T. M.; Tarasow, S. L.; Eaton, B. E. *J. Am. Chem. Soc.* **2000**, *122*, 1015-1021.

22. Kuhne, H.; Joyce, G. F. *J. Mol. Evol.* **2003**, *57*, 292-298.

23. Tuerk, C.; Gold, L. *Science* **1990**, *249*, 505-510.

24. Ellington, A. D.; Szostak, J. W. *Nature* **1992**, *355*, 850-852.

25. Eaton, B. E.; Holley, B. In *Evolutionary Methods in Biotechnology*; Brakmann, S., Schwienhorst, A., Eds.; Wiley-VCH: Weinheim, Germany, 2004; pp 87-111.

26. Gugliotti, L. A.; Feldheim, D. L.; Eaton, B. E. *J. Am. Chem. Soc.* **2005**, *127*, 17814-17818.

27. (a) The following website was used in calculating theoretical d-spacings for molecular $[Pd_2(DBA)_3]$•$CHCl_3$: www.ruppweb.org/new_comp/reciprocal_cell.htm. The unit cell parameters used for molecular $[Pd_2(DBA)_3]$ •$CHCl_3$ were a = 12.400 Å, b = 15.149 Å, c = 12.956 Å, $\alpha$ = 115.04 °, $\beta$ = 95.23 ° and $\gamma$ = 97.30 °. (b) Selvakumar, K.; Valentini, M.; Wörle, M.; Pregosin, P. S. *Organometallics* **1999**, *18*, 1207-1215.

# CHAPTER 3: RNA-MEDIATED SYNTHESIS OF PALLADIUM CONTAINING NANOPARTICLES ON GOLD SURFACES

## 3.1. Introduction

RNA *in vitro* selection[1-7] is a powerful technique for discovering nucleotide sequences with highly binding affinities (aptamers) and catalytic activities (ribozymes). Numerous examples of oligonucleotide (RNA or DNA) sequences are now known to bind to small molecules[8-16] and protein targets.[17-25] Reactions now known to be catalyzed by oligonucleotides include forming amide carbon-nitrogen,[26] urea carbon-nitrogen,[27] Diels-Alder carbon-carbon,[28] Aldol carbon-carbon,[29] Michael carbon-carbon,[30] and alkylation/substitution.[31,32] The discovery of these aptamer and ribozyme sequences has enhanced our fundamental understanding of oligonucleotide structure-function relationships. An expanding view is emerging on how oligonucleotides may be used commercially as therapeutic and diagnostic agents.[33-41]

As previously stated in Chapters 1 and 2, we have applied RNA *in vitro* selection to the discovery of RNA sequences that mediate solid-state inorganic reactions. In that work, RNA sequences were found to mediate the formation of metal-metal bonds, resulting in the rapid and shape-controlled synthesis of Pd containing nanoparticles (RNA "Pdases").[42] These RNA sequences could be grouped into "families" related by highly conserved sequence regions. Closer examination of Pdase families is beginning to reveal the dependence of particle growth on RNA sequence. When placed in aqueous solution and incubated with the zerovalent Pd precursor complex $[Pd_2(DBA)_3]$ (DBA =

dibenzylideneacetone), Pdase 17 (Table 3.1) was found to mediate the formation of hexagonal plates. In contrast, incubation of $[Pd_2(DBA)_3]$ with Pdase 34 resulted in the formation of cubes.[43] Thus, we are beginning to find that *in vitro* selection not only uncovers RNA sequences capable of mediating the formation of materials under unprecedented reaction conditions but that a single *in vitro* selection experiment can result in templates for different particle sizes and morphologies.

**Table 3.1.** RNA Pdase Sequence Codes for Hexagonal (17) and Cubic (34) Pd Containing Particles

| |
|---|
| Isolate 17: 5′-CCCUUUCUAUCCUCAAUGUACCAACAAAAAAUGUAUUCC-3′ |
| Isolate 34: 5′-UCCAACAUCUUUUAAUUUUGUGGCGUCCACAUAUCAUCCA-3′ |

One application of RNA-mediated materials synthesis would be the generation of spatially well-defined architectures of chemically distinct nanoscale materials on surfaces. It can be envisaged that new devices and sensors will require precise positioning of large numbers of functionally distinct nanoscale materials ("orthogonal" assembly as first described by Wrighton and Whitesides).[44-51] An elegant solution to the large scale integration of nanomaterials is to program their assembly using the exquisite complementary base pairing rules of DNA. Once the materials of interest are synthesized and coated with the appropriate ssDNA sequence they can be combined and assembled via DNA hybridization. Early demonstrations of this strategy are seen in work by Mirkin, Seeman and LaBean.[48,52-57]

A complementary materials integration strategy would be to put catalytic RNA sequences on a surface positioned as required for device function. From RNA *in vitro* selection, it may be possible to find sequences and concomitant structures that can be pre-organized on a scaffold surface and subsequently treated with metal precursors to generate *in situ* the desired materials. This would require that each RNA catalysts synthesize its corresponding material with high specificity, and remain active under the conditions used to organize or pattern the RNA.

For this surface materials integration strategy to be viable, maintaining the RNA folded structure would be a necessary requirement for catalytic activity. It is well-known that many metal surfaces can interact with RNA, sometimes irreversibly, and this would result in denaturing the active structure. For example, previous reports of DNA bound to Au substrates suggest that binding to the surface by the DNA nucleobases[58-60] can be significant making it uncertain if in fact active folded RNA sequences found from solution *in vitro* selection experiments would perform when attached to an Au surface. Herein we describe using Pdases as a prototype RNA template bound to an Au surface.

In addition to the concerns over RNA folded structure when surface bound, the reactivity of the metal substrates utilized by the RNA (e.g., $[Pd_2(DBA)_3]$ in the case of Pdases) toward an Au surface was uncertain, and if the rates of Pdase activity were severely compromised, particle formation could be dominated by the spontaneous deposition of Pd on the Au surface. Our first attempts to define some of the working parameters that could lead to the success of an "on chip" RNA-mediated materials synthesis and integration strategy are described herein.

### 3.2. Results and Discussion

To explore the possibility of synthesizing metal particles on a surface using pre-organized RNA, Pdases that assemble hexagonal and cubic Pd containing nanoparticles were covalently attached to Au substrates. Two attachment strategies were investigated (Figure 3.1, p. 72). First, the linker 12-thioacetic-3,6,9,12-tetraoxadodecane-1-maleimide was assembled onto gold, followed by covalent coupling of 5′-phosphorothioate-modified RNA to the maleimide moiety of the monolayer. In the second strategy, *O*-[*ω*-thioacetyl tetra(ethyleneglycol)]-*O*-(5′-guanosine) monophosphate (TA-$(EG)_4$-GMP) was used during DNA transcription to generate the 5′-TA-$(EG)_4$-GMP modified RNA. The modified RNA was then combined in aqueous solution with mercaptoethanol, and the two were coadsorbed onto Au substrates.[69]

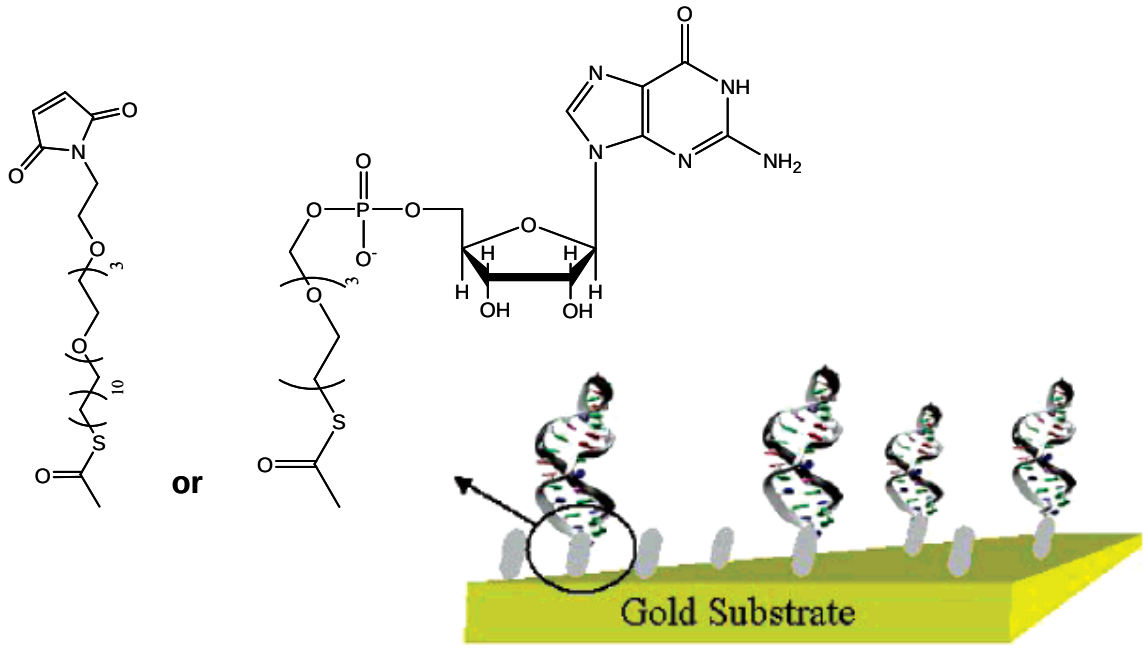


**Figure 3.1.** Schematic illustration of surface-bound Pdase sequence.

Of initial interest was whether the RNA sequences would remain active when attached to a solid support. It was found that both sequences were active in particle growth when attached to a solid Au support through the EG and that exclusive shape control was maintained (Figure 3.2, p. 73). Pd containing hexagons grown with RNA Pdase 17 and 400 μM [$Pd_2(DBA)_3$] reached a width of ca. 700 nm in 40 minutes. As was found previously for solution-phase synthesis by Pdase 17,[43] the Pd containing particles were only ca. 20 nm thick as determined with atomic force microscopy. Pd containing cubes grown by Pdase 34 and 400 μM [$Pd_2(DBA)_3$] grew to an average dimension of approximately 500 nm × 500 nm × 200 nm in 40 minutes.[69] It should be noted that while the overall shape of the particles created by Pdases 17 and 34 were the same as observed previously for solution-phase synthesis, the apparent rates of particle formation were reduced. From these results, it was

unclear if the reduction in the observed rate of formation was a consequence of slow metal substrate ($[Pd_2(DBA)_3]$) diffusion to the surface bound Pdases or if their structures had been compromised by the surface.

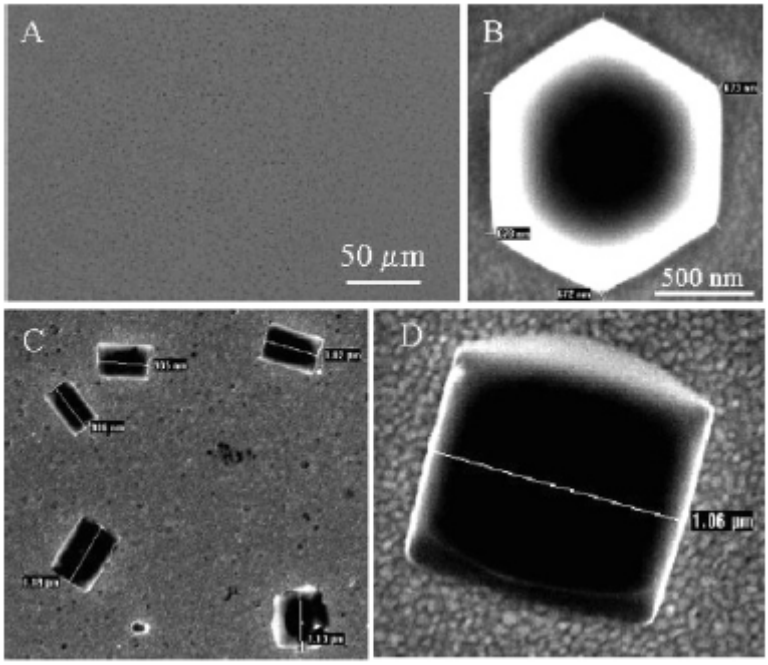


**Figure 3.2.** SEM images of Pd containing particles synthesized with RNA Pdase sequence 17 (A and B) and sequence 34 (C and D).[69]

Two experiments were performed to determine the importance of RNA folded structure and how proximity to the Au surface was impacting particle growth. First, Pdase 17 was attached to Au directly through a 5′-phosphorothioate moiety. In the absence of the EG linker, particle shape control was completely lost, and the yield of any solid Pd was qualitatively lower as judged by SEM. This is likely the result of strong interactions between the RNA nucleobases and the Au surface.[61,62] In a second experiment designed to test if RNA denaturation was a problem, Pdase 17 was bound to Au through a EG linker, and the

substrate was heated at 55 °C for 5 minutes in neat THF followed by slow cooling to ambient temperature to deliberately denature the RNA. Again, only a low yield of amorphous Pd was observed on the surface with no hexagons observed (Figure 3.3A). Surprisingly, when the same Au surfaces with THF-denatured Pdase 17 attached were transferred to water at 55 °C, and then slowly cooled to ambient temperature, treatment of these surfaces with 400 μM [$Pd_2(DBA)_3$] gave hexagonal Pd containing particle growth (Figure 3.3B), consistent with reversible denaturation of the RNA and refolding to the active structure.[69] It now appears that RNA bound to an Au surface can reversibly denature and fold into its active structure. What remained uncertain is how many RNA molecules were required to form a particle.

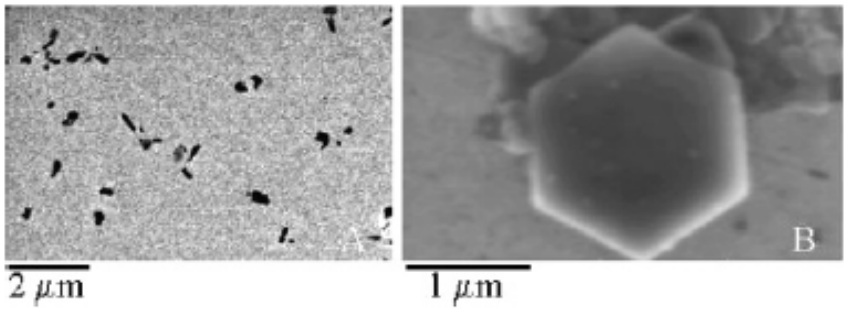


**Figure 3.3.** SEM images of Pd containing particles grown with RNA sequence 17 following melting at 55 °C in neat THF (A) and reannealing in water (B).[69]

From all of our previous results, it was unknown how many RNA molecules were required to synthesize a Pd containing particle. Ideally, an orthogonal synthesis strategy for fabrication of integrated nanoscale materials on surfaces would require only one RNA molecule per particle of defined composition. However, controlling the shape of metal nanoparticles typically involves addition of an excess of capping ligand, usually a polymer,

surfactant or small molecule.[63,64] In these previously published examples, these ligands bind selectively to certain faces of the growing particle, speeding or slowing growth along specific faces relative to other growth directions.[65-67] Although we had demonstrated that RNA confined to a surface could still dictate particle shape, it was of interest to determine if a relatively low surface coverage would result in successful particle growth and still control particle shape.

To estimate the number of RNA molecules required to maintain control over particle shape, TA-$(EG)_4$-RNA 17 was attached to Au substrates along with the diluent molecule mercaptoethanol (MCE). As the mole ratio of RNA in solution was decreased, RNA surface coverage and particle coverage also decreased (Figure 3.4, p. 76). Solution mole ratios of 1 RNA:64 MCE yielded surface densities of $2.0 \times 10^9$ RNAs $cm^{-1}$ as determined by [$\alpha$-$^{32}$P]-ATP radiolabeling and scintillation counting. At this coverage, the distance between RNA molecules is ca. 300 nm assuming a uniform, closest-packed arrangement with no aggregation. RNA aggregation in solution prior to deposition on the surface was ruled out by native PAGE, which revealed a single band for sequences 17 and 34. It can be estimated that folded RNA structures of this molecular weight will be on order of 10-20 nm in diameter.[69] Despite the low RNA density, large Pd containing hexagons were observed to grow on the surface, a result that suggests that a single RNA molecule may be able to nucleate a Pd containing hexagon and control its morphology at least within the first approximately 300 nm of growth. What happens during later stages of the growth when the growing particle encounters additional RNA sequences is unclear. At the RNA coverage used in this experiment, there are between 10 and 100 molecules underneath each 1 μm hexagonal

particle at the end of the reaction. However, for Pdase 34, many cubic particles less than 50 nm were observed making it likely that a single RNA molecule was able to mediate their formation. How each molecule contributes to the growth of a particle is an open question, but the data suggest that at a minimum a large excess of RNA is not required to nucleate and grow these large hexagonal and cubic particles. To be useful in the RNA synthesis and integration of materials on surfaces, it would be necessary that the Pdases not migrate on the surface. From the above experiments, it cannot be determined if Pdases were surface mobile either prior to treatment with metal precursor or during particle growth.

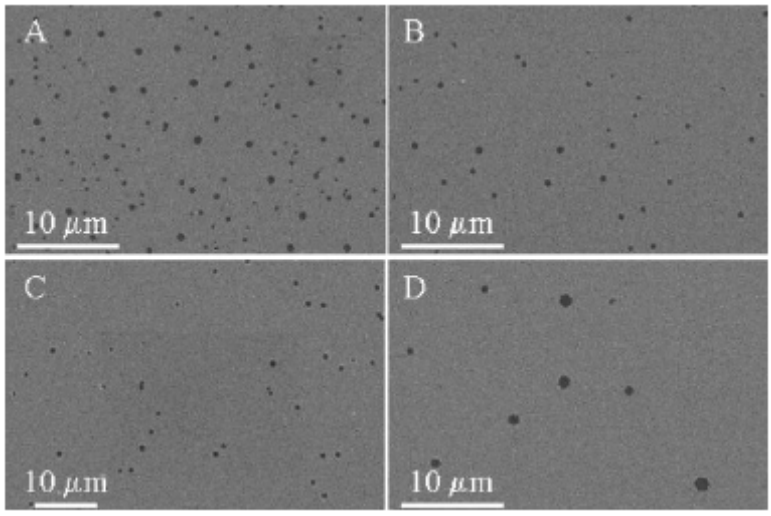


**Figure 3.4.** SEM images of Pd containing particles grown from TA-$(EG)_4$-RNA 17 and mercaptoethanol mixed monolayers on Au. RNA:mercaptoethanol mole ratio in the monolayer deposition solution was 1:1 (A), 1:4 (B), 1:16 (C), and 1:64 (D) with resulting densities of $3.2 \times 10^{10}$ (A), $1.2 \times 10^{10}$ (B), $5.8 \times 10^{9}$ (C), and $2.0 \times 10^{9}$ $cm^{-2}$ (D).[69]

To demonstrate the one-pot, simultaneous synthesis of differently shaped nanoparticles on surfaces and probe Pdase surface mobility over the time course of particle synthesis, Pdases 17 and 34 attached to a 12-thioacetic-3,6,9,12-tetraoxadodecane-1-

maleimide linker were deposited on a Au surface by microcontact printing. Rows of ca. 100 μm spots (ca. 100 pL) were printed side-by-side on an Au surface. It should be noted that unlike the previously described examples of Pdase mediated growth of particles from the surface, where ample liquid was present to help preserve the RNA structure, the small volumes deposited during contact printing rapidly evaporated. The printed sides were incubated in a solution containing $[Pd_2(DBA)_3]$, and the formation of particles examined by optical microscopy and SEM. No attempt was made to renature these printed Pdases after the printing process. Nevertheless, optical microscopy showed that particles were indeed formed exclusively in the printed rows of Pdase 17, whereas cubes and rectangles were found in the printed rows of Pdase 34 (Figure 3.5, p. 78). No migration beyond the printed spots was observed, which suggests that surface-bound RNA is immobile on the time scale of the experiment.[69] These initial results are encouraging since the printing parameters had not been optimized and no attempt was made to renature the RNA.

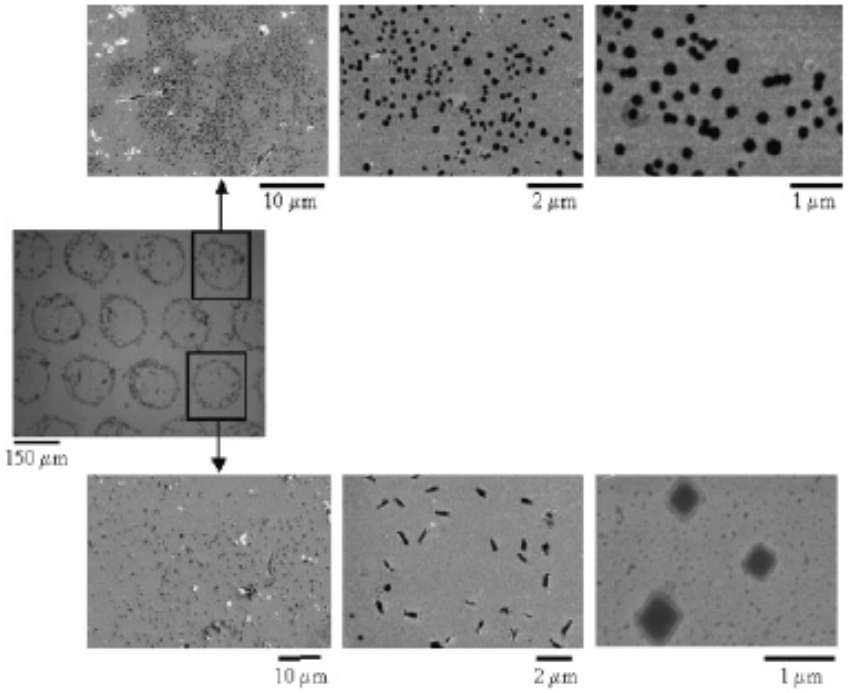


**Figure 3.5.** Far left: Optical microscope image of Pd containing hexagons and cubes grown by patterning RNA sequences 17 and 34 on a gold slide. Shown at higher magnification SEM images of individual circles of Pd containing hexagons (top) and cubes (bottom), respectively.[69]

### 3.3. Conclusion

We have shown that Pd containing particles can be formed by surface-bound RNA Pdases. Furthermore, the shape of the particles can be dictated by the sequence of RNA immobilized on an Au surface. Both hexagonal and cubic shaped Pd containing particles can be assembled simultaneously from the same metal precursor with a high degree of specificity. A linker of sufficient length is required to allow the folded RNA to maintain activity. Denaturation of the folded RNA does result in complete loss of Pdase activity, consistent with a 3D structure being required. The fact that Pdase activity could be recovered from these denatured surfaces indicated that RNA folding was in fact reversible and the

denatured sequences were not irreversibly bound to the Au surface. The ability to recover RNA templating activity on surfaces may be important as we attempt to construct new molecular architectures.

The minimum number of Pdase molecules required to assemble a particle appears to be one. However, we note that Pd containing particles grown from surfaces with sequence 34 are consistently longer in one dimension than their more cubic counterparts grown from solution. It is possible that particle growth is being transferred from one RNA to another in these examples. For Pdase 17, the exact number required to grow hexagonal particles is unclear because growth is fast and we have yet to find size distributions of Pd containing hexagons smaller than the average RNA spacing. Although these RNA sequences do not form aggregates in solution and they appear to be immobile when deposited on a surface, it is possible that they phase separate to yield small RNA islands that conspire to control crystal growth. It is clear, however, that in contrast to many methods of particle shape control, an excess of RNA ligand is not required to control the final shape of these Pd containing particles.

### 3.4. Experimental Section

**Reagents.** All reagents were used without further purification. Tris(dibenzylideneacetone) dipalladium(0) was purchased from Strem. Milli-Q water was treated with diethylpyrocarbonate (depc) prior to use to ensure nuclease- and protease-free water. The 12-thioacetic-3,6,9,12-tetraoxadodecane-1-maleimide linker was synthesized by

the Feldheim Group. The *O*-[$\omega$-thioacetyl tetra(ethyleneglycol)]-*O*-(5′-guanosine) monophosphate (TA-$(EG)_4$-GMP) was synthesized by the Eaton Group.

**Electron and Optical Microscopy.** Scanning electron microscopy (SEM) was performed at Duke University with a Philips FEI XL30 Thermal Field Emitter SEM operating at 5 kV accelerating voltage. AZeiss Axioplan 2 upright microscope equipped with high-resolution optics (50×/0.9NA Epiplan-Apochromat, 100×/0.9NA Epiplan-Neofluar), Sutter Lambda LS Xenon light source, Ludl Biopoint 2 motorized stage, Hamamatsu Orca ER CCD camera, Andor Ixon 8285 EMCCD camera, CRI MicroColor tunable color LCD filter, and IQ software from Andor Bioimaging was used for control of microscope and accessories, image analysis, 3D-rendering, and deconvolution.

**Amplification of DNA Templates.** 5′-primer (5′-TAATACGACTCACTATA-GGGAGACAAGAATAAACGCTCAA-3′) and 3′-primer (5′-GCCTGTTGTGAG-CCTCCTGTCGAA-3′) were purchased from Midland Certified, Inc. 1× *Taq* DNA Polymerase buffer (New England Biolabs, 10 mM KCl, 10 mM $(NH_4)_2SO_4$, 20 mM Tris-HCl, pH 8.8, 2 mM $MgSO_4$, 0.1% Triton X-100), 0.12 mM each of dATP, dCTP, dGTP, and dTTP, 2 mM $MgCl_2$, and 0.1 U/μL *Taq* DNA Polymerase (New England Biolabs) were added to 3 nM (ss)dsDNA template. PCR was performed using the following reaction parameters: 95 °C, 2 minutes; multiple cycles of 95 °C, 30 seconds, 60 °C, 30 seconds, 72 °C, 45 seconds; hold at 4 °C. The dsDNA was purified using QIAquick PCR Purification Kit (Qiagen) and quantitated via UV-Vis spectroscopy.

**Preparation of TA-(EG4)-RNA 17.** TA-$(EG_4)$-RNA 17 was prepared by transcription of RNA isolate 17 dsDNA template. 4% (w/v) PEG 8000, 40 mM Tris-HCl, pH

8.0, 12 mM $MgCl_2$, 5 mM dithiothreitol (DTT), 1 mM spermidine HCl, 0.002% Triton X-100, 0.2 mM ATP, 0.2 mM CTP, 0.15 mM GTP, 1.5 mM TA-$(EG)_4$-GMP, 0.2 mM 5-(4-pyridymethyl)-uridine 5′-triphosphate (*UTP), 150 nM dsDNA template, 125 nM T7 RNA Polymerase (Promega), 0.8 U/μL RNase inhibitor (Promega) were incubated at 37 °C for 6 hours to yield TA-$(EG)_4$-RNA 17. Size-exclusion membranes (Microcon 10, 10-kD cutoff) were used to separate the full-length RNA from the reaction buffer and any unincorporated NTPs. The reaction mixture was first concentrated onto the membranes by centrifugation and washed four times with buffer containing NaCl (1 mM), KCl (1 mM), $CaCl_2$ (1 mM), $MgCl_2$ (1 mM), and $Na_3PO_4$ (1 mM, pH 7.2) followed by two water (pH 7) washes to remove excess salts. The purified RNA was recovered from the membranes by resuspension in 50-100 μL of water and quantitated by UV-Vis spectroscopy.

**Generation of RNA Isolates.** The RNA isolates were prepared by transcription of dsDNA templates. 4% (w/v) PEG 8000, 40 mM Tris-HCl, pH 8.0, 12 mM $MgCl_2$, 5 mM dithiothreitol (DTT), 1 mM spermidine HCl, 0.002% Triton X-100, 0.2 mM each of ATP, CTP, GTP, and 5-(4-pyridymethyl)-uridine 5′-triphosphate (*UTP), 150 nM dsDNA template, 125 nM T7 RNA Polymerase (Promega), 0.8 U/μL RNase inhibitor (Promega) were incubated at 37 °C for 6 hours to yield 5-(4-pyridylmethyl)-uridine modified RNA transcripts (87-mer): 5′-GGGAGACAAGAATAAACGCTCGG-[40N]-TTCGACAGG-AGGCTCACAACAGGC-3′. 5′-phosphorothioate-modified RNA was generated using the identical protocol but with 0.15 mM GTP and 1.5 mM guanosine monophosphorothiate (GMPS). Size-exclusion membranes (Microcon 10, 10-kD cutoff) were used to separate the full-length RNA from the reaction buffer and any unincorporated NTPs. The reaction

mixture was first concentrated onto the membranes by centrifugation and washed four times with buffer containing NaCl (1 mM), KCl (1 mM), $CaCl_2$ (1 mM), $MgCl_2$ (1 mM), and $Na_3PO_4$ (1 mM, pH 7.2) followed by two water (pH 7) washes to remove excess salts. The purified RNA was recovered from the membranes by resuspension in 50-100 μL of water and quantitated by UV-Vis spectroscopy.

**Preparation of 12-Thioacetic-3,6,9,12-tetraoxadodecan-1-maleimide Monolayers on Gold.** Au slides were treated with UVozonolysis for 20 minutes, followed by soaking in 100% ethanol for 15 minutes. The cleaned Au slides were incubated in 1 mM 12-thioacetic-3,6,9,12-tetraoxadodecan-1-maleimide in ethanol solvent overnight at 4 °C, followed by rinsing in ethanol for 10 minutes. RNA, modified at the 5′ end with a guanosine monophosphorothioate (GMPS), was covalently linked to the substrate by soaking the substrate in 1 μM RNA for 2-4 hours. The substrate was then rinsed with diethylpyrocarbonate-treated autoclaved double distilled water for 30 minutes before use. Oligonucleotides were spotted on surfaces using an instrument by GeneMachines.

### 3.5. References


1. Ellington, A. D.; Szostak, J. W. *Nature* **1990**, *346*, 818-822.
2. Tuerk, C.; Gold, L. *Science* **1990**, *249*, 505-510.
3. Chapman, K. B.; Szostak, J. W. *Curr. Opin. Struct. Biol.* **1994**, *4*, 618-622.
4. Lorsch, J. R.; Szostak, J. W. *Acc. Chem. Res.* **1996**, *29*, 103-110.
5. Robertson, D. L.; Joyce, G. F. *Nature* **1990**, *344*, 467-468.
6. Beaudry, A. A.; Joyce, G. F. *Science* **1992**, *257*, 635-641.
7. Wright, M. C.; Joyce, G. F. *Mol. Biol. Cell* **1996**, *7*, 1950.
8. Lorsch, J. R.; Szostak, J. W. *Biochemistry* **1994**, *33*, 973-982.
9. Ellington, A. D. *Curr. Biol.* **1994**, *4*, 427-429.
10. Burgstaller, P.; Famulok, M. *Angew. Chem.-Int. Ed. Engl.* **1994**, *33*, 1084-1087.
11. Famulok, M. *J. Am. Chem. Soc.* **1994**, *116*, 1698-1706.
12. Lauhon, C. T.; Szostak, J. W. *FASEB J.* **1995**, *9*, A1422.
13. Lauhon, C. T.; Szostak, J. W. *J. Am. Chem. Soc.* **1995**, *117*, 1246-1257.
14. Huizenga, D. E.; Szostak, J. W. *Biochemistry* **1995**, *34*, 656-665.
15. Burgstaller, P.; Famulok, M. *Bioorg. Med. Chem. Lett.* **1996**, *6*, 1157-1162.
16. Burke, D. H. et al. *Chem. Biol.* **1997**, *4*, 833-843.
17. Schneider, D.; Tuerk, C.; Gold, L. *J. Mol. Biol.* **1992**, *228*, 862-869.
18. Jensen, K. B.; Atkinson, B. L.; Willis, M. C.; Koch, T. H.; Gold, L. *Proc. Natl. Acad. Sci. U.S.A.* **1995**, *92*, 12220-12224.
19. Burke, D. H.; Scates, L.; Andrews, K.; Gold, L. *J. Mol. Biol.* **1996**, *264*, 650-666.
20. Kumar, P. K. R.; Lai, M.; Ellington, A. D. *J. Cell. Biochem.* **1995**, *34*, 6.

21. Conrad, R. C.; Giver, L.; Tian, Y.; Ellington, A. D. *Comb. Chem.* **1996**, *267*, 336-367.

22. Conrad, R.; Ellington, A. D. *Anal. Biochem.* **1996**, *35*, 261-265.

23. Klug, S. J.; Huttenhofer, A.; Famulok, M. *RNA* **1999**, *5*, 1180-1190.

24. Weiss, S.; et al. *J. Virol.* **1997**, *71*, 8790-8797.

25. Cox, J. C.; et al. *Nucleic Acids Res.* **2002**, 30.

26. Wiegand, T. W.; Janssen, R. C.; Eaton, B. E. *Chem. Biol.* **1997**, *4*, 675-683.

27. Nieuwlandt, D.; West, M.; Cheng, X. Q.; Kirshenheuter, G.; Eaton, B. E. *ChemBioChem* **2003**, *4*, 651-654.

28. Tarasow, T. M.; Tarasow, S. L.; Eaton, B. E. *Nature* **1997**, *389*, 54-57.

29. Fusz, S.; Eisenfuhr, A.; Srivatsan, S. G.; Heckel, A.; Famulok, M. *Chem.Biol.* **2005**, *12*, 941-950.

30. Sengle, G.; Eisenfuhr, A.; Arora, P. S.; Nowick, J. S.; Famulok, M. *Chem. Biol.* **2001**, *8*, 459-473.

31. Wecker, M.; Smith, D.; Gold, L. *RNA* **1996**, *2*, 982-994.

32. Wilson, C.; Szostak, J. W. *Nature* **1995**, *374*, 777-782.

33. Osborne, S. E.; Matsumura, I.; Ellington, A. D. *Curr. Opin. Chem. Biol.* **1997**, *1*, 5-9.

34. Potyrailo, R. A.; Conrad, R. C.; Ellington, A. D.; Hieftje, G. M. *Anal. Chem.* **1998**, *70*, 3419-3425.

35. Fahlman, R. P.; Sen, D. *J. Am. Chem. Soc.* **2002**, *124*, 4610-4616.

36. Brody, E. N.; et al. *Mol. Diagn.* **1999**, *4*, 381-388.

37. Collett, J. R.; Cho, E. J.; Ellington, A. D. *Methods* **2005**, *37*, 4-15.

38. Levy, M.; Cater, S. F.; Ellington, A. D. *ChemBioChem* **2005**, *6*, 2163-2166.

39. Yan, A. C.; Bell, K. M.; Breeden, M. M.; Ellington, A. D. *Front. Biosci.* **2005**, *10*, 1802-1827.

40. Bock, C.; et al. *Proteomics* **2004**, *4*, 609-618.

41. Guhlke, S.; Famulok, M.; Biersack, H. J. *Eur. J. Nuclear Med. Mol. Imaging* **2003**, *30*, 1441-1443.

42. Gugliotti, L. A.; Feldheim, D. L.; Eaton, B. E. *Science* **2004**, *304*, 850-852.

43. Gugliotti, L. A.; Feldheim, D. L.; Eaton, B. E. *J. Am. Chem. Soc.* **2005**, *127*, 17814-17818.

44. Naito, K. *Chaos* **2005**, *15*.

45. Laibinis, P. E.; Hickman, J. J.; Wrighton, M. S.; Whitesides, G. M. *Science* **1989**, *245*, 845-847.

46. Gardner, T. J.; Frisbie, C. D.; Wrighton, M. S. *J. Am. Chem. Soc.* **1995**, *117*, 6927-6933.

47. Chung, S. W.; et al. *Small* **2005**, *1*, 64-69.

48. Demers, L.; et al. *Science* **2002**, *296*, 1836-1838.

49. Gates, B. D.; Xu, Q.; Stewart, M.; Ryan, D.; Willson, C. G.; Whitesides, G. M. *Chem. Rev.* **2005**, *105*, 1171-1196.

50. Love, J. C.; Estroff, L. A.; Kriebel, J. K.; Nuzzo, R. G.; Whitesides, G. M. *Chem. Rev.* **2005**, *105*, 1103-1169.

51. Schilardi, P. L.; et al. *Chem.-Eur. J.* **2005**, *12*, 38-49.

52. Li, H. Y.; Park, S. H.; Reif, J. H.; Labean, T. H.; Yan, H. *J. Am. Chem. Soc.* **2004**, *126*, 418-419.

53. Xiao, S. J.; et al. *J. Nanopart. Res.* **2002**, *4*, 313-317.

54. Park, S. H.; Barish, R.; Li, H.; Reif, J. H.; Finkelstein, G.; Yan, H.; LaBean, T. H. *Nano Lett.* **2005**, *5*, 693-696.

55. Yan, H.; Park, S. H.; Finkelstein, G.; Reif, J. H.; Labean, T. H. *Science* **2003**, *301*, 1882-1884.

56. Pinto, Y. Y.; Le, J. D.; Seeman, N. C.; Musier-Forsyth, K.; Taton, T. A.; Kiehl, R. A. *Nano Lett.* **2005**, *5*, 2399-2402.

57. Seeman, N. C. *Chem. Biol.* **2003**, *10*, 1151-1159.

58. Zhang, R. Y.; Pang, D.-W.; Zhang, Z.-L.; Yan, J.-W.; Tian, Z.-Q.; Yao, J.-L.; Mao, B.-W.; Sun, S.-G. *J. Phys. Chem. B* **2002**, *106*, 11233-11239.

59. Yau, H. C. M.; Chan, H. L.; Sui, S. F.; Yang, M. S. *Thin Solid Films* **2002**, *413*, 218-223.

60. Pang, D. W.; Abruna, H. D. *Anal. Chem.* **2000**, *72*, 4700-4706.

61. Levicky, R.; Herne, T. M.; Tarlov, M. J.; Satija, S. K. *J. Am. Chem. Soc.* **1998**, *120*, 9787-9792.

62. Bietsch, A.; Hegner, M.; Lang, H. P.; Gerber, C. *Langmuir* **2004**, *20*, 5119-5122.

63. Ahmadi, T. S.; Wang, Z. L.; Henglein, A.; El-Sayed, M. A. *Chem. Mater.* **1996**, *8*, 1161-1164.

64. Kirkland, A. I.; et al. *Proc. R. Soc. London A* **1993**, *440*, 589-609.

65. Manna, L.; Scher, E. C.; Alivisatos, A. P. *J. Cluster Sci.* **2002**, *13*, 521-532.

66. Puntes, V. F.; Krishnan, K.; Alivisatos, A. P. *Top. Catal.* **2002**, *19*, 145-148.

67. Puntes, V. F.; Krishnan, K. M.; Alivisatos, A. P. *Science* **2001**, *291*, 2115-2117.

68. Zhang, L.; Sun, L. L.; Cui, Z. Y.; Gottlieb, R. L.; Zhang, B. L. *Bioconjugate Chem.* **2001**, *12*, 939-948.

**69.** Liu, D.; Gugliotti, L. A.; Wu, T.; Dolska, M.; Tkachenko, A. G.; Shipton, M. K.; Eaton, B. E.; Feldheim, D. L. *Langmuir* **2006**, ASAP Article.

# CONCLUSIONS

Biomimetic strategies are useful alternatives for exploring how to control particle growth. In contrast to controlling particle size and shape with surfactant or polymer capping reagents typically used in large excess, biopolymers such as RNA can form highly structured active sites that can dictate the formation of different shaped particles from the same input metal precursors under identical conditions. Many unanswered questions remain regarding how the Pdase RNA structures accomplish the assembly of relatively large particles rapidly with a high degree of shape control. Clearly we now know that the ligand bound to the metal is more important to the control of shape in this process than an isoelectronic metal from the same group of the periodic table. However, metal-ligand bond strengths cannot be ignored as they undoubtedly influence the rate of particle formation. Using *in vitro* selection to explore the catalytic landscape of RNA for the assembly of inorganic materials has revealed new possibilities for the creation of previously unknown Pd and Pt particle shapes, and there is much to learn about this process.

By the process of *in vitro* selection it is possible to test a hypothesis about a range of metal colloids or metal ion compositions under varying conditions that could lead to important new materials or catalysts. In contrast to all other materials discovery methods, RNA mediated materials synthesis can reveal the benefits of evolution. Even if extremely rare, materials composition, crystal type and physical properties can evolve in response to selection pressures.

Overall, this research highlights the remarkable ability of RNA to catalyze the formation of solid-state materials under mild conditions, and to control materials size and shape. To truly have an impact in the field of materials discovery will require surveying a vast number of inorganic compositions under varying conditions. Combining the power of *in vitro* selection and microarray technologies will provide unprecedented capability in materials discovery. Future projects have now been devised to advance RNA-mediated evolutionary materials chemistry to fit within microarrays so it may be used as a method for high-throughput materials discovery.

# APPENDIX

## A.1. RNA sequences that can mediate the formation of hexagonal and cubic palladium containing particles from 400 µM [$Pd_2(DBA)_3$] precursor.

Conserved regions are outlined in boxes. Regions in common between families are highlighted in color. Sequences highlighted in bold text were chosen as representative of the different families, and their ability to form particles was investigated by TEM (Table A.1, p. 91).

Family 1 (14 members, 56%)

**Pd_017** **5′-CCCUUUCUAUCCUCAAUGUACCAACAAAAAAUGUAUUCC-3′**
Pd_021 5′-CUCUUCCUAUCCUCAAAGUACCAACUAAAAAUGUACGCCC-3′
Pd_024 5′-CCCUUUCUAUCUUCAAUGUACCAACUAAAAAUGUAUUCCC-3′
Pd_025 5′-CCCUUUCUAUCCUCAAUGUACCAACUAAAAAUGUAUUCCC-3′
Pd_028 5′-CCCUUCCUAUUUCCAAUGUCCCAACAAAAAAUGUAUUCCC-3′
Pd_029 5′-CCCUUUCUAUCCUCAAUGUACCAACAAAAAAUGUAUUCCC-3′
Pd_031 5′-CCCUUCCUAUUUCCAAUGUCCCAACAAAAAAUGUAUUCCC-3′
Pd_032 5′-CCCUUCCUAUUUCCAAUGUCCCAACAAAAAAUGUAUUCCC-3′
Pd_082 5′-CCCUUCCUAUCUCCAAUGUCCCAACAAAAAAUGUAUUCCC-3′
Pd_085 5′-CCCUUUCUAUCCUCAAUGUACCAACUAAAAAUGUAUGCCC-3′
Pd_086 5′-CCCUUUCUAUUCUCAAUGUACCAACUAAAAAUGUAUUCCC-3′
Pd_090 5′-CCCUUCCUAUCUUCAAUGUCCCAACUAAAAAUGUAUUCCC-3′
Pd_093 5′-CCCUUCCUAUCCCCAAUGUCCCAACAAAAAAUGUAUCCCC-3′
Pd_094 5′-CCCUUCCUAUUUCCAAUGUCCCAACAAAAAAUGUAUUCCC-3′

Family 2 (6 members, 24%)

**Pd_019** **5′-CUCCUUAAUACCUCAAAAUACCCCAUCUUUACGUACGUUA-3′**
Pd_022 5′-CUCCUUAAUACCUUUUAAUACCCCAUCUUUCGUAACGUUA-3′
Pd_026 5′-CUCCUUAAUACCUUAAAAUACCCCAUCUUUAUGUAACGUUA-3′
Pd_027 5′-CUCCUUAAUACCUUAUAAUACCCCAUCUUUACGAACGUUA-3′
Pd_030 5′-CUCCUUAAUACCUUUUAAUACCCCAUCUUUCGUAACGUUA-3′
Pd_092 5′-CUCCUUAAUACCUUUUAAUACCCCAUCUUUCGUAACGUUA-3′

Family 3 (2 members, 8%)

**Pd_020** **5′-CUCUUUAUUUCCUUAAAAUACCAAAUCUUAAUGAAUCCCC-3′**
Pd_091 5′-CUCCUUAUUUCCUUUAUAGUACCCCCUCUUAUUGUAUCGCC-3′

Family 4 (2 members, 8%)

**Pd_081** **5′-CCCCUCAAUACCUUUUAAUACCCCAUCUUUCGUACGUCUA-3′**

Pd_089 5′-CCCCUUCAAUCUUCAAUGUACCAACUAUAAAUGAACGCCC-3′

Orphans

Pd_033 5′-UCACCAACUCAGUAUUCUAGCCUUCCAACACACCUCAAC-3′

**Pd_034** **5′-UCCAACAUCUUUUAAUUUUGUGGCGUCCACAUAUCAUCCA-3′**

**Pd_084** **5′-CCCUUUCUUUUUUCAAAGUACCCCCUAUUAUUGUAUUUCA-3′**

**Table A.1.** Shape and Size Distribution of Pd Containing Particles Formed by Individual Cycle 8 RNA Isolates

| RNA Isolate | Particle Shape* | No. Particles Counted | Size (μm) |
|---|---|---|---|
| 17 | hexagonal | 101 | 1.24 ± 0.57 |
| 19 | hexagonal | ** | ** |
| 20 | hexagonal | ** | ** |
| 34 | cubic | 124 | 0.10 ± 0.05 × 0.07 ± 0.02 |
| 81 | hexagonal | ** | ** |
| 84 | hexagonal | ** | ** |

* The entire TEM grid was examined for all types of materials formed.

** Size distributions for the particles observed were not determined for these isolates.

## A.2. RNA sequences that can mediate the formation of hexagonal, cubic and spherical platinum containing particles from 400 µM [$Pt_2(DBA)_3$] precursor.

Conserved regions are outlined in boxes. Copy numbers for sequences are denoted in brackets immediately following the sequence name. Copy numbers for sequences are listed only if they are greater than one. Sequences highlighted in bold text were chosen as representative of the different families, and their ability to form particles was investigated by TEM (Table A.2, p. 94).

Family 1 (4 members, 5 %)

Pt_003 [2] 5′-UUGCCAGCAUGAUGGUGGGUGAGGGUAUGGUGCCCGCUGU-3′
Pt_007 5′-AUAAGGAUUAGGUACAGGGCUUAAGUACACAGGGGUAUGUUU-3′
Pt_006 5′-AUAGGAUUCGGGUCAGGGCUUAAGUCCACAGGGGUAUGUUU-3′
Pt_008 5′-AUAGGAUUCGAGGUACUGGGCUUAAGUCAUCAGGGGUAUGUUU-3′

Family 2 (3 members, 3 %)

Pt_001 5′-GGGACUAGGAUCUAUGGGUAUGUCGCGGCCGUCGAGAUGCC-′3
**Pt_002 5′-CUCAAGGUUCUAGCGUUCUAUGGGUAUGUCGCUGCCGUCG-3′**
Pt_013 5′-UGCAAAGGGGCAAUACGGCAACCGUUGUCUAUGGGUAAC-3′

Family 3 (5 members, 7 %)

Pt_040 5′-CUAUGAAGGUACACAGCGAUCACUCCAGUCCCCCGGUGAU-3′
Pt_048 5′-UCUUGUGUAGGUAAAUCCGGAUGCACUACGACAGUUUUGG-3′
Pt_049 [3] 5′-UGUAGGUAAUUCGAUGGUAGAGCACCGAAGUCCCCAUAUAA-3′
Pt_110 5′-UGUAGGCAACCAAGUGUGUAUAGCCCAGCGGCCAUCU-3′
Pt_076 5′-UUUCGACAGACUGAUGUAUGAAAUUUCUCACUUCCGAGCU-3′

Family 4 (2 members, 3 %)

Pt_083 5′-CUAUUCGUCAUAGUUGCAAACCCAUCUUUCUUCAUC-3′
Pt_084 [2] 5′-GCAUUCUGCAUUGGCUUUGGGACCGGCGUAGAAGACAUGG-3′

Family 5 (2 members, 2 %)

Pt_086 5′-UUUCAAUCGCGGCUAUGUCGUCCUUUAAGUUAUUACUCG-3′
Pt_087 5′-CUAGACUACCUCCUCCACUGCUGAGAUUGUAUUCCUUUAA-3′

Family 6 (6 members, 6 %)

**Pt_012 5′-GAUUACGUACAACCGUGUACCUUCCCAGCCCACCAAGAUC-3′**
Pt_014 5′-UAAGGCCCAGUGUCCCUCGCUUACUCAACCGUUUUGUGCAA-3′
Pt_015 5′-GUAGUUCGGGAAGACUCCGCGGCUGCGUAACCGUACUCAGCAU-3′

Subfamily 6a

**Pt_018 5′-UAGGCGAUGGUAACCGUUCCCCCGAGUUAACGUCCGCGGC-3′**

Pt_019 5′-ACUUUCUGAGUGGUAGGCGAAUGGUAAUGUAGUGUUGUGUGU-3′
Pt_020 5′-AUGUUCGAAGUGUGUGCAUCAGUGGGCGAGUGUUCAAU-3′

Family 7 (5 members, 8 %)
**Pt_032 5′-CGCAAUGCAUAGGGUUUAGGGUUGGAAAUCGUGGUGAACCU-3′**
Pt_033 5′-UGGCCUGCCAAUGGACGUGUGCUAAGAUUCCACUCGAUAU-3′
Pt_034 5′-CCAUACCCGCAAUGAUACAGACUGGGCCUCAUGUGGUCUG-3′
Pt_035 [3] 5′-GCAAAGCAUAACGCGUACGCAAUGAACGCGGACAUUCAUC-3′
Pt_038 [2] 5′-UAGUGUUAACAGCGGAGCCCCAGGGCCAAUGUCAGUUUUC-3′

Family 8 (2 members, 2 %)
Pt_093 5′-GCUGGUGAGUGUUACAAGGAUAAUCACCACCUAUAAUGUA-3′
Pt_094 5′-ACGACCGAUCCAGCUAAGAUUUGUCAAGUGAGUGCGUGA-3′

Family 9 (3 members, 4 %)
Pt_054 [2] 5′-GCCUGUUGGACGUACUGGAGGAUGGAGUAGAACUACCCUGU-3′
Pt_058 5′-UUAUGGCGUGUCGGUGUACAGUUGGACGUUUAGACUGGGA-3′
Pt_059 5′-UACAGGAUUAUCACUGGAUUGUUGGACAUGAUGAGUGGUC-3′

Family 10 (3 members, 3 %)
Pt_060 5′-ACGCUUGGCAUUCAGGAAGAGAUUGUCGUGAUAUGGGGGU-3′
Pt_061 5′-CGGUAUGUGGCUUGGCAUUUCGCUUACUGCCGGUAUAACCA-3′
Pt_062 5′-UAUGCCCGUGGCCGGAGUUGUUCAUUGGCAUAAUAAGCCA-3′

Orphans
Pt_009 5′-GGGUAAUCUGAUGGCACCGCGUCGUGGAAGUUGUAAUUC-3′
Pt_010 5′-GGGGGGGUAGGAGCUGACGUUUCCAGUGGUCUAGGGUCUGU-3′
Pt_011 5′-UCAAAUCGGUCGGGGUAUAACCUAGUGGCUUCUUGCUCUCA-3′
Pt_016 5′-UGUAUAAGCCUUCUAUUGCGUUCCACCACAUUUAACGAU-3′
Pt_017 5′-CUUGACGCGAUCCGACAUUAAACACGAUCGCCACCCUCCA-3′
**Pt_021 5′-CACCCACUAGGACCCAUGUAGUGCUACCUUUUGCCAGA-3′**
Pt_022 5′-CACCCAUCUAGGACCAUGGAGAAUUACCUUUCGAACCAGUC-3′
Pt_023 5′-UGCACCAGGUGGGGUGCCUUCCGCGUGUAGCACCAUCCUUUCCCC-3′
Pt_024 5′-CUAAGCUGGAUGGGGUGACCUCAACGGUUGGUGGGCC-3′
Pt_025 5′-UCAACUAAGCUGGAUGGGGUGACCUCAACGGUUGGUGGGCC-3′
Pt_027 5′-CUAGCUUGAGAUUAAUCUGAUGGGGUGGCGGUCGUAUCUC-3′
Pt_028 5′-AUGAGUUAAUACGGCGGGUACACCAUGGCAUUGGGAGUCUUG-3′
Pt_029 5′-UACCCGAAUCAUGCUGCUAGUCAGUCAAGCUGGGAGUCUU-3′
Pt_030 5′-CUAAUCCCCGGUUGUAUUAGGAACCAUAUCUUGGGAGUGUA-3′
Pt_031 5′-UCCGAUUAGACGAUUCGAUUUAGUUGUUACGAUGGGAGAA-3′
Pt_041 5′-GUAAGGCGAAGGGGGCAGGGAUUACCUUCAUCCGCUUAGG-3′
Pt_042 5′-CAGACUCAUAGAAGGCCCCCGCCUCCAACCACCGUCCGU-3′
Pt_043 [2] 5′-UACGGUUAUGGCUGCCGCGUAACGAAGGCCAAAACGAAUU-3′
Pt_044 5′-ACUGCCGGAAGGGGUCUGUGCACCGAAGGCGGGGGGGUA-3′
Pt_046 5′-ACCAUGGUCGCCUGAGUACAGAAUUUUGAAGGUUGGUCGA-3′
Pt_047 5′-CGGGGGAACGACUAGCUCGGGGUCCACAUCAGAGAAGCAA-3′
Pt_052 5′-CGUGGUAGGGCUUUAGGGGGUGUAUUAAAACCGGCUCAAAU-3′
Pt_053 5′-CCUCUAGGUGCGGAGUAAUUGAACCAGGCCUCGGAGGUAG-3′
Pt_056 5′-GGUUAUGGAGCUAACCAAGCGUUGGCACUCCCUUCGGGCU-3′
Pt_057 5′-AGUAAAACUGAAUGCCACUGCGUUGGGGAUCGUGUGAUUG-3′
Pt_063 5′-GUGCUCUGGUUAACGCCGCCCGGAAUACAUUAAGCCCCGUA-3′
Pt_064 5′-ACGGUGAGCAUCAAUCCCUUUUUGCCGGUUAUGGUUGCUU-3′

Pt_065 5′-UGGAAGAAUCCUAGACUUCUUCGUGCAUAACCUCUUAUUC-3′
Pt_067 5′-UCGCUUCCUUGUAUCUAGAACUCUCCCUGUUAUUCCGCUU-3′
Pt_068 5′-CACCUUCAGUUAUUCAGAUGAAUCGUUUGUCCACGGUCGU-3′
Pt_069 5′-UGGGCGUAUUACAGACGCUCAUCAGUCCGGGCGUUGAAUC-3′
Pt_070 5′-ACCUCGAGUCAUAGGAGGAUAGGGGCUGACUAAUCCAUUC-3′
Pt_071 5′-GUCUUCGAGUAGCCCCACUAUCACAGGCAUGACUACUUCCC-3′
Pt_072 5′-GAACGCUAAGGUACCCCGAGUUCUAUCACAGUCUAGAGUG-3′
Pt_074 5′-CCAUGAUGGCGCAUUGAGACCACAUCGAGAUUGAGCGCAU-3′
Pt_075 5′-GUGGCUGAUAAUGUUGUGAGGCUGAUCAUCAUACGUACUU-3′
Pt_077 5′-CAUCCAUUAGGCGGCUCUUGUGCUGAUGUCGAGUCAUGA-3′
Pt_078 5′-GAUAAAGAUAGCAGAACUUGACCCUCGAGACUGAUCGGAC-3′
Pt_079 5′-UGAGUACCCUGCAUUCCAUACGGGUCACGUAAAGAUGGA-3′
Pt_080 5′-GUCAGGGUGGACAUACCCUGCGAUAACACGUCUAGUGCCC-3′
Pt_081 5′-UGCACAUCCCUGCUAUCCCGACACAAAACUAUAGGGAGUGA-3′
Pt_082 5′-GCUUCGAGUAGAAUAAUGCUCCCCCUGGACUAAAGAUCGU-3′
Pt_088 5′-GAUCUCAUAUGGGCCAGGUGGCUUUAAAUUAUGGACUCUG-3′
Pt_089 5′-AGAGAUCCAGACUGGUUAUCACGCUGUCACUUUGCGGCUU-3′
Pt_090 5′-GCUUAAGGUAUCCAGGUAUAUUCUCAUAACCCUUGACAGG-3′
Pt_091 [2] 5′-UCAGGGCAUCCGAAUUGUUGAAAGGAUGUUUGUCCAGGUG-3′
Pt_092 5′-UCAGGGCAUCCGAAUUGUUGAAAGGAUGUUUGUCCAGGUG-3′
Pt_095 5′-CGCAUGCUCAGAUUACAGCCGAAGUCCUAGCCUCACGGAA-3′
Pt_096 5′-CUCAUCGCCACACACUGUCCCAUAUUGCCUCAUUAUAGGGA-3′
Pt_097 5′-GUUGGGGACCGAUAUAAGUUCCAACAAGCGAGGUUUGCCG-3′
Pt_098 5′-CCAAACGCCUUACAAAGAUGGAUGGUAAACAACAUUCACA-3′
Pt_099 5′-AUCAUCGAUACACCUGGCCGAUAAUGCCCAUUAUCAGGA-3′
Pt_100 5′-CGUGAGUCAAUCCUAUCAUGUAUGCGGUCCUUAAGGGGG-3′
Pt_101 5′-ACCCCAUUCAUCCUGCAACCCAGAUAAUAUGGCACGAUGC-3′
Pt_102 5′-CGAUACAUCGGAUGGGGAGCUUGGUUUGCCUAAAACCGCG-3′
Pt_103 5′-AGGCGGACAAUUAAGUAAUUCACCCCGUCCCUCUCGCUC-3′
Pt_104 5′-UAAGAACAGCUGGUCGUGCCACAUUUUAGGUUCGUAGUCC-3′
Pt_105 5′-GAUGAAGAAAGAUGGGUUUGCAACUAUGACGAAUAGUUAG-3′
Pt_106 5′-GGGCCUCUAUCGUUGAAGCUGUAACCACCAGGCCAAGG-3′
Pt_107 5′-GUCUAGGUGGGUCGCGAGGAUUCUCGAUCGUUUUAUC-3′
Pt_108 5′-ACCCCGUCUGCAUUCUAAACGGCUUGUUUGCGUGUGC-3′
Pt_109 5′-AGGUGGACUUAGGUAAUUAGCUGUGGUCACGUGUCU-3′

**Table A.2.** Shape and Size Distribution of Pt Containing Particles Formed by Individual Cycle 6 RNA Isolates

| RNA Isolate | Particle Shape | No. Particles Counted | Size (μm) | % Population* |
|---|---|---|---|---|
| 2 | hexagonal | 121 | 0.14 ± 0.05 | 100 |
| 12 | hexagonal | 113 | 0.16 ± 0.08 | 100 |
| 18 | spherical | 282 | 0.023 ± 0.008 | 73 |
| | hexagonal | 65 | 0.22 ± 0.14 | 17 |
| | cubic | 39 | 0.07 ± 0.02 × 0.10 ± 0.03 | 10 |
| 21 | hexagonal | 118 | 0.13 ± 0.04 | 100 |
| 32 | hexagonal | 129 | 0.18 ± 0.09 | 100 |

* The entire TEM grid was examined for all types of materials formed. Percentages represent the amount of these materials observed on the grid from the total population.

## A.3. RNA sequences that can mediate the formation of spherical palladium containing particles from 400 μM [$Pd(PPh_3)_4$] precursor.

Conserved regions are outlined in boxes. Copy numbers for sequences are denoted in brackets immediately following the sequence name. Copy numbers for sequences are listed only if they are greater than one. Sequences highlighted in bold text were chosen as representative of the different families, and their ability to form particles was investigated by TEM (Table A.3, p. 96).

Family 1 (4 members, 16 %)

Pd_S004 5′-AAGCUAGUAGGCGGUAUUUCAGGCGGACAUGACUGACUCCUUA-3′

**Pd_S002 [4] 5′-AAGCAGUAGGUGGAUUUCAGGCAGACGAUGCUGACUCCUU-3′**

Pd_S005 5′-AAGCAGUAGGUGGCAUUUCAGGCAGACGAUGCUGACUCCUU-3′

Pd_S006 5′-AAGCAGUAGGUGGUAUUUCAGCGCUAGCACGAUGCUGACUCCUUA-3′

Family 2 (2 members, 13 %)

Pd_S007 5′-GAUGCCUGUCGAGCAUGCUGUAGUUAGAUGCCUGUCGAGCAUAGCUGUAGAU-3′

Pd_S008 5′-GAUGCCUGUCGAGCAUGCUGUAGAGAUGCCUGUCGAGCAUGCUGUAA-3′

Family 3 (2 members, 13 %)

Pd_S030 5′-GGUGGGAAGUUUAAACGUGAAAGAGUCGAUUGUGAAUCCC-3′

**Pd_S031 5′-UCUCAACGGUGUCACGUAGCGCGAAAGACGCCUGCAACCC-3′**

Family 4 (2 members, 13 %)

Pd_S032 5′-GCAUCUAGCUACAAAGCUUUUUUCUAUUUGAUUCCUUCU-3′

Pd_S033 5′-GCCAUCCCCCCGGUAGCUACAUGAGCGAAGUCUCUACGC-3′

Orphans

Pd_S010 5′-CGGUGUGUGGCCGCAUGCGUACAAACGCGCUGCAAGGUUA-3′

Pd_S011 [3] 5′-UACGAAUGCGGUUUAAACAAUGCAUAAGGGCCGAUGUCCGA-3′

Pd_S014 [2] 5′-CUUAUGUCAGGCGGUUUGAAGCUCCAAGCUCGAAGACGUC-3′

Pd_S016 5′-CAGGAACGCUACAUCGGAGUUUGGUGCUUGUCGAUUGCC-3′

Pd_S017 [2] 5′-UAACUAGUCGCGAAGAGAAGCGUAUUAUUCUCAUCGGUUC-3′

Pd_S019 5′-CGCUACGACUCGGGAAGGGGUCCGUCGUGACAGUCGCUAUGUUC-3′

Pd_S020 5′-UAAAUCUCACAGAUGUUACUAGGUACCUCAUGAAGCUCGG-3′

Pd_S021 5′-CGCACGACUCGGAAGGGGUCCGUCAGUGACGAGCGCAUGUUC-3′

Pd_S022 5′-CGGGUCUUUCAGGACUGAGGCGGGAAUUAGGCAAUGAUGCA-3′

Pd_S023 5′-AUGCCGCUUGGUACAGACUUUGGAUAAAUAUGCAAUGGGU-3′

Pd_S024 5′-UGAUGCUUAGUAAACAGACGUCUAACUUUUGCCCACCACA-3′

Pd_S025 5′-GAAUGUAGCCAAACUUGGGUGUUGCCGCUUUGUGCCAAGC-3′

Pd_S026 5′-GAAGCAUGUAUUUAGUAGGAAUCAUCCUACCCGUCGUGCUUUGC-3′

Pd_S027 5′-GUUUUGAUUCAGGAGGGGUAACUGCCGGCGCUAAUGGUU-3′

| | |
|---|---|
| Pd_S028 | 5′-CACCGACCCAUGAGGGCUUACUGUUCAAUGAAUACACCAU-3′ |
| Pd_S029 | 5′-CACGAACUGGACAUGGGAGGCAAUACCGGUCUCCGCAUGAA-3′ |
| Pd_S034 | 5′-UUCUCUGGUCUUCGACCGCCCGCGCGGGGGGCACUACGC-3′ |
| Pd_S035 | 5′-UUUAGCCCACGAUAAUCCAAGCAGGAUAUGCCCGCUCCCA-3′ |
| Pd_S036 | 5′-AGCAGCGCGCAGAACAUUGACAUGUUAAGCAGACUACCCGGC-3′ |
| Pd_S037 | 5′-GCAGCCGCGCAGACAUUGACAUGUUAAGCAGACUCCCGGC-3′ |
| Pd_S038 | 5′-UUACCAUUACGAGUUAUUACCAGUCACUUCGUCCCGACAUCU-3′ |
| Pd_S039 | 5′-UUACCAUUACGAGAUUAUUACUCAGGUCACUGUCCUCGC-3′ |
| Pd_S040 | 5′-AACUCUAGCACCAAUCAAAGGUCUGCGUGAGACCAACAUC-3′ |
| Pd_S041 | 5′-AAGCAACAUUGGAAGUUAGUUCGGACAGAUUGACC-3′ |

**Table A.3.** Shape and Size Distribution of Pd Containing Particles Formed by Individual Cycle 10 RNA Isolates

| Sample | Particle Shape* | No. Particles Counted | Size (μm) |
|---|---|---|---|
| Isolate Pd_S002 | Spherical | 179 | 0.025 μm ± 0.008 μm |
| Isolate Pd_S031 | Spherical | 194 | 0.027 μm ± 0.009 μm |

* The entire TEM grid was examined for all types of materials formed.

## A.4. RNA sequences that can mediate the formation of spherical platinum containing particles from 100 μM [$Pt(PPh_3)_4$] precursor.

Conserved regions are outlined in boxes. Copy numbers for sequences are denoted in brackets immediately following the sequence name. Copy numbers for sequences are listed only if they are greater than one. Sequences highlighted in bold text were chosen as representative of the different families, and their ability to form particles was investigated by TEM (Table A.4, p. 97).

Family 1 (3 members, 27 %)

**Pt_S049** **5′-UCCCAUCGCUACUUAUUCUAUUUUGAUACCUCGUUAUCUA-3′**
Pt_S060 5′-UCCCAUCGAAUACUUAUUCUAUUUUUGAUCCUCGCCCUC-3′
Pt_S004 5′-UACCUACAAACAAUCUUAUUGUAUCUUACCUCCACCUCC-3′

Orphans

Pt_S058 5′-AUUUUUCAUACAUCACUCUAGCUGCUAUUAUUCUUAAUUG-3′
**Pt_S069 [4]** **5′-UCAUCAUCACUUACCCAUUCAACACCCCUCCUCAAAAAAC-3′**
Pt_S090 5′-AUAGAUACACAUCCUCUAUCAUCCAUUAUCACAAAACAU-3′
Pt_S074 5′-GUGGAAUAAGCCUAUGAGUAGCCCUUUGGAGCCCGACGC-3′
Pt_S057 5′-CAACCACAUAACUCCCUCACAAAUACCCUGUCCCCUCUAUA-3′

**Table A.4.** Shape and Size Distribution of Pt Containing Particles Formed by Individual Cycle 8 RNA Isolates

| Sample | Particle Shape* | No. Particles Counted | Size (μm) |
|---|---|---|---|
| Isolate Pt_S049 | Spherical | 263 | 0.04 μm ± 0.02 μm |
| Isolate Pt_S069 | Spherical | 218 | 0.06 μm ± 0.03 μm |

* The entire TEM grid was examined for all types of materials formed.

**A.5. Comparison of RNA isolates selected to mediate the formation of palladium and platinum containing particles from the organometallic precursors [$Pd_2(DBA)_3$] and [$Pt_2(DBA)_3$], respectively.**

Regions of sequence similarity are outlined in boxes. Isolates that mediate the formation of particles from [$Pd_2(DBA)_3$] are highlighted in red. Isolates that mediate the formation of particles from [$Pt_2(DBA)_3$] are highlighted in green. Copy numbers for sequences are denoted in brackets immediately following the sequence name. Copy numbers for sequences are listed only if they are greater than one.

Pt_083 5′-CUAUUCGUCAUAGUUGCAAACCCAUCUUUCUUCAUC-3′
Pd_019 5′-CUCCUUAAUACCUCAAAAUACCCCAUCUUUACGUACGUUA-3′
Pd_084 5′-CCCUUUCUUUUUUCAAAGUACCCCCUAUUAUUGUAUUUCA-3′
Pd_022 5′-CUCCUUAAUACCUUUUAAUACCCCAUCUUUCGUAACGUUA-3′
Pd_026 5′-CUCCUUAAUACCUUAAAAUACCCCAUCUUUAUGUAACGUUA-3′
Pd_020 5′-CUCUUUAUUUCCUUAAAAUACCAAAUCUUAAUGAAUCCCC-3′
Pd_081 5′-CCCCUCAAUACCUUUUAAUACCCCAUCUUUCGUACGUCUA-3′

Pt_095 5′-CGCAUGCUCAGAUUACAGCCGAAGUCCUAGCCUCACGGAA-3′
Pd_017 5′-CCCUUUCUAUCCUCAAUGUACCAACAAAAAAUGUAUUCC-3′
Pd_021 5′-CUCUUCCUAUCCUCAAAGUCCAACUAAAAAUGUACGCCC-3′
Pd_029 5′-CCCUUUCUAUCCUCAAUGUACCAACAAAAAAUGUAUUCCC-3′
Pd_090 5′-CCCUUCCUAUCUUCAAUGUCCCAACUAAAAAUGUAUUCCC-3′
Pd_093 5′-CCCUUCCUAUCCCCAAUGUCCCAACAAAAAAUGUAUCCCC-3′

Pt_033 5′-UGGCCUGCCAAUGGACGUGUGCUAAGAUUCCACUCGAUAU-3′
Pt_035 [3] 5′-GCAAAGCAUAACGCGUACGCAAUGAACGCGGACAUUCAUC-3′
Pt_037 5′-GCAAAGCAUAACGCGUUACGCAAUGAACGCGGACAUUCAUC-3′
Pt_043 [2] 5′-UACGGUUAUGGCUGCCGCGUAACGAAGGCCAAAACGAAUU-3′
Pt_057 5′-AGUAAAACUGAAUGCCACUGCGUUGGGGAUCGUGUGAUUG-3′
Pt_074 5′-CCAUGAUGGCGCAUUGAGACCACAUCGAGAUUGAGCGCAU-3′
Pd_089 5′-CCCCUUCAAUCUUCAAUGUACCAACUAUAAAUGAACGCCC-3′

**A.6. Comparison of RNA isolates selected to mediate the formation of palladium and platinum containing particles from the organometallic precursors [$Pd(PPh_3)_4$] and [$Pt(PPh_3)_4$], respectively.**

Regions of sequence similarity are outlined in boxes. Isolates that mediate the formation of particles from [$Pd(PPh_3)_4$] are highlighted in orange. Isolates that mediate the formation of particles from [$Pt(PPh_3)_4$] are highlighted in blue. Copy numbers for sequences are denoted in brackets immediately following the sequence name. Copy numbers for sequences are listed only if they are greater than one.

| | |
|---|---|
| Pd_S017 [2] | 5′-UAACUAGUCGCGAAGAGAAGCGUAUUAUUCUCAUCGGUUC-3′ |
| Pd_S032 | 5′-GCAUCUAGCUACAAAGCUUUUUUCUAUUUGAUUCCUUCU-3′ |
| Pt_S049 | 5′-UCCCAUCGCUACUUAUUCUAUUUUGAUACCUCGUUAUCUA-3′ |
| Pt_S060 | 5′-UCCCAUCGAAUACUUAUUCUAUUUUUGAUCCUCGCCCUC-3′ |
| Pt_S004 | 5′-UACCUACAAACAAUCUUAUUGUAUCUUACCUCCACCUCC-3′ |
| Pt_S058 | 5′-AUUUUUCAUACAUCACUCUAGCUGCUAUUAUUCUUAAUUG-3′ |

**A.7. Comparison of RNA isolates selected to mediate the formation of palladium and platinum containing particles from the organometallic precursors $[Pd_2(DBA)_3]$, $[Pd(PPh_3)_4]$, $[Pt_2(DBA)_3]$ and $[Pt(PPh_3)_4]$, respectively.**

Regions of sequence similarity are outlined in boxes. Isolates that mediate the formation of particles from $[Pd_2(DBA)_3]$ are highlighted in red. Isolates that mediate the formation of particles from $[Pd(PPh_3)_4]$ are highlighted in orange. Isolates that mediate the formation of particles from $[Pt_2(DBA)_3]$ are highlighted in green. Isolates that mediate the formation of particles from $[Pt(PPh_3)_4]$ are highlighted in blue.

Pt_S074 5′-GUGGAAUAAGCCUAUGAGUAGCCCUUUGGAGCCCGACGC-3′
Pt_001 5′-GGGACUAGGAUCUAUGGGUAUGUCGCGGCCGUCGAGAUGCC-3′
Pt_002 5′-UCAAGGUUCUAGCGUUCUAUGGGUAUGUCGCUGCCGUCG-3′
Pt_013 5′-UGCAAAGGGGCAAUACGGCAACCGUUGUCUAUGGGUAAC-3′

Pd_S019 5′-CGCUACGACUCGGGAAGGGGUCCGUCGUGACAGUCGCUAUGUUC-3′
Pd_S021 5′-CGCACGACUCGGAAGGGGUCCGUCAGUGACGAGCGCAUGUUC-3′
Pt_041 5′-GUAAGGCGAAGGGGGCAGGGAUUACCUUCAUCCGCUUAGG-3′
Pt_044 5′-ACUGCCGGAAGGGGUCUGUGCACCGAAGGCGGGGGGGUA-3′

Pd_089 5′-CCCCUUCAAUCUUCAAUGUACCAACUAUAAAUGAACGCCC-3′
Pt_S090 5′-AUAGAUACACAUCCUCUAUCAUCCAUUAUCACAAAACAU-3′